

# The Geometric Mechanics of Contrastive Representation Learning: Alignment Potentials, Entropic Dispersion, and Cross-Modal Divergence

Yichao Cai<sup>1</sup> Zhen Zhang<sup>1</sup> Yuhang Liu<sup>1</sup> Javen Qinfeng Shi<sup>1</sup>

## Abstract

While InfoNCE powers modern contrastive learning, its geometric mechanisms remain undercharacterized beyond the canonical alignment-uniformity decomposition. We present a measure-theoretic framework that models learning as the evolution of representation measures on a fixed embedding manifold. By establishing value and gradient consistency in the large-batch limit, we bridge the stochastic objective to explicit deterministic energy landscapes, uncovering a fundamental geometric bifurcation between the unimodal and multimodal regimes. In the unimodal setting, the intrinsic landscape is strictly convex with a unique Gibbs equilibrium; here, entropy acts merely as a tie-breaker, clarifying “uniformity” as a constrained expansion within the alignment basin. In contrast, the symmetric multimodal objective contains a persistent negative symmetric divergence term that remains even after kernel sharpening. We show that this term induces barrier-driven co-adaptation, enforcing a population-level modality gap as a structural geometric necessity rather than an initialization artifact. Our results shift the analytical lens from pointwise discrimination to population geometry, offering a principled basis for diagnosing and controlling distributional misalignment.

## 1. Introduction

Contrastive representation learning has evolved from classical noise-contrastive and density-ratio estimation principles (Gutmann & Hyvärinen, 2010; Mnih & Teh, 2012) into a central workhorse for modern self-supervised and multimodal representation learning. InfoNCE-style objectives were popularized by contrastive predictive coding and related mutual-information surrogates (Oord et al., 2018;

<sup>1</sup>Australian Institute for Machine Learning (AIML), Adelaide University, South Australia 5000, Australia. Correspondence to: Yichao Cai <yichao.cai@adelaide.edu.au>.

Preprint. January 28, 2026.

Poole et al., 2019; Tschannen et al., 2020), and today underpin multimodal foundation models such as CLIP and ALIGN (Radford et al., 2021; Jia et al., 2021). While empirical capabilities have scaled rapidly, a fundamental mechanistic question remains:

*What geometry does the unimodal/multimodal InfoNCE objective impose on the representation space, and how does it govern the configuration of the induced measures?*

Existing theoretical lenses leave key aspects of this question open. The density-ratio viewpoint (Gutmann & Hyvärinen, 2010; Oord et al., 2018) clarifies that the optimal critic approximates pointwise mutual information, yet it remains silent on the deterministic descent directions driven by the softmax gradient. Similarly, while the seminal alignment-uniformity framework (Wang & Isola, 2020) characterizes the asymptotic equilibria, it offers a decompose of the objective that abstracts away the gradient flows driving the coupled evolution of the representation measures. In parallel, identifiability studies establish recovery guarantees under explicit generative assumptions (Zimmermann et al., 2021; Von Kügelgen et al., 2021); however, these results address what is learnable in principle, rather than how the objective’s geometric gradients drive the population. These gaps are particularly acute in multimodal contrastive learning, where strong pointwise alignment coexists with a persistent population-level modality gap (Liang et al., 2022)—a structural feature lacking a mechanistic geometric derivation.

In this work, we develop a measure-theoretic framework that analyzes contrastive learning directly on the representation manifold. Motivated by the ubiquitous feature-normalization regime, we treat the embedding space  $\mathcal{Z}$  as a fixed compact geometric container equipped with its volume measure  $\mu$ . Encoders act by pushing the data distribution forward onto  $\mathcal{Z}$ , inducing representation laws and encoded positive-pair laws in unimodal and multimodal settings. Under the standard exponential similarity kernel, the InfoNCE denominator is a Monte Carlo estimate of a population *partition field*, a kernel-averaged summary of the current representation law. This perspective turns contrastive learning into a geometric process: training evolves probability mass within a fixed manifold according to kernel-induced fields, shifting the analytical lens from opaque parameter updates

to intrinsic population geometry.

We first establish a deterministic bridge from the stochastic InfoNCE loss to an explicit energy landscape. Under mild regularity, gradients are uniformly bounded, and in the large-batch regime unimodal InfoNCE becomes value- and gradient-consistent with a closed-form parametric energy. The softmax denominator thus converges to a population partition field, ensuring that gradient descent tracks a deterministic descent direction on representation measures. This limiting energy separates two forces: potential attraction from positive pairs and entropic dispersion from negatives. To disentangle geometry from parametrization, we further lift the analysis to an *intrinsic* variational functional over distributions on  $\mathcal{Z}$ . This reveals a strictly convex unimodal landscape with a unique stable equilibrium. At low temperatures, the equilibrium concentrates on low-potential (high-alignment) regions, while entropy governs how mass spreads *within* the aligned basin. In turn, the practical parametric energy inherits this intrinsic geometry under encoder expressiveness, redefining “uniformity” not as a competing objective, but as an entropic tie-breaker that dictates mass dispersion solely within the alignment basin.

The multimodal case is qualitatively different. For symmetric CLIP-style training (Radford et al., 2021), we again obtain stability and a deterministic large-batch limit, but the induced geometry is cross-coupled and *directional*: since heterogeneous modalities generally induce distinct conditional laws, they generate mismatched alignment fields that prevent a single shared potential. In the intrinsic variational formulation, we prove the objective contains a persistent *negative* symmetric divergence term that survives even under kernel sharpening. This term functions as a structural wedge that erects a repulsive logarithmic barrier within each modality’s effective field, driving the optimization toward non-Gibbs, boundary-seeking co-adaptation. Consequently, exact matching of representation marginals becomes a knife-edge compatibility condition that is structurally unstable for heterogeneous data. This offers a mechanistic account of the “Mind the Gap” phenomenon (Liang et al., 2022): a population-level modality gap is not merely an artifact of initialization or sampling, but a barrier-driven geometric equilibrium of the objective itself. Our framework thus pivots the analysis from pointwise discrimination to population geometry, implying that bridging the gap requires explicitly regularizing this cross-modal divergence.

**Contribution.** Our main contributions are: (i) the establishment of large-batch value and gradient consistency within a measure-theoretic framework, proving that stochastic optimization tracks deterministic energy landscapes (Thms. 3.1 and 4.1); (ii) a characterization of the unimodal geometry as strictly convex with a unique Gibbs equilibrium, redefining uniformity as a secondary entropic tie-breaker (Thm. 3.2 and Props. 3.2 and 3.3); (iii) the discovery of a

persistent negative symmetric divergence in the multimodal objective that drives barrier-driven co-adaptation, establishing the modality gap as a structural geometric necessity (Thm. 4.2 and Prop. 4.2); and (iv) a derivation of parametric inheritance conditions, proving that under sufficient encoder expressiveness, the learned representations inherit these intrinsic geometric properties (Cors. 3.1 and 4.1). Finally, we position our work within the broader literature in App. A, and provide numerical validations in App. D.

## 2. Setup and Preliminaries

We study unimodal and multimodal contrastive learning within a measure-theoretic framework, characterizing the geometry of learned representations directly on the embedding manifold. In this section, we establish the following setup for our subsequent theoretical analysis.

**Data and distributions.** We model training data as samples from a joint distribution of positive pairs. For unimodal contrastive learning, let  $\mathcal{X}$  be a measurable space and let  $r_{\text{um}}$  denote a joint distribution over pairs  $(\mathbf{x}, \tilde{\mathbf{x}}) \in \mathcal{X} \times \mathcal{X}$ . Let  $p_{\mathbf{x}}$  be its marginal (in standard unimodal setups, both first and second marginals coincide with  $p_{\mathbf{x}}$ ). For multimodal learning, let  $\mathcal{Y}$  be a measurable space and let  $r_{\text{mm}}$  denote a joint distribution over pairs  $(\mathbf{x}, \mathbf{y}) \in \mathcal{X} \times \mathcal{Y}$ , with marginals  $p_{\mathbf{x}}$  and  $p_{\mathbf{y}}$  defined by projection. For notational simplicity, we write sums in the discrete case and integrals in the general case; all subsequent definitions apply to either.

**Encoders and representation measures.** We consider two encoder families  $\{f_{\theta}\}_{\theta \in \Theta}$  and  $\{g_{\phi}\}_{\phi \in \Phi}$  with compact parameter spaces  $\Theta$  and  $\Phi$ . The encoders  $f_{\theta} : \mathcal{X} \rightarrow \mathcal{Z}$  and  $g_{\phi} : \mathcal{Y} \rightarrow \mathcal{Z}$  map observations into a common ambient representation space  $\mathcal{Z} \subset \mathbb{R}^d$ . We model  $\mathcal{Z}$  as a compact Riemannian manifold (e.g., the unit hypersphere  $\mathbb{S}^{d-1}$ ), equipped with its Riemannian volume measure  $\mu$ . This abstraction captures the ubiquitous “feature normalization” regime: the geometry of the embedding space is fixed, and learning acts by reshaping the induced feature distributions. Accordingly, the objects that govern the optimization dynamics are the pushforward measures of the data laws onto  $\mathcal{Z}$  and  $\mathcal{Z} \times \mathcal{Z}$ :

$$\begin{aligned} q_{\theta} &:= (f_{\theta})\# p_{\mathbf{x}}, & q_{\phi} &:= (g_{\phi})\# p_{\mathbf{y}}, \\ \pi_{\theta\theta} &:= (f_{\theta} \times f_{\theta})\# r_{\text{um}}, & \pi_{\theta\phi} &:= (f_{\theta} \times g_{\phi})\# r_{\text{mm}}. \end{aligned}$$

Here  $q_{\theta}$  and  $q_{\phi}$  are the marginal representation laws, while  $\pi_{\theta\theta}$  and  $\pi_{\theta\phi}$  are the encoded joint laws induced by the unimodal and multimodal positive-pair distributions, respectively. We use the same symbol (e.g.,  $q_{\theta}$ ) to denote either a probability measure or, when it exists, its density with respect to the reference measure  $\mu$ . Concretely, if  $q_{\theta} \ll \mu$  we write  $q_{\theta}(\mathbf{z}) := d\mathbf{q}_{\theta}/d\mu(\mathbf{z})$ , so that  $\int g d\mathbf{q}_{\theta} = \int g(\mathbf{z}) q_{\theta}(\mathbf{z}) d\mu(\mathbf{z})$ . Likewise, when  $\pi_{\theta\theta} \ll \mu \otimes \mu$  we write

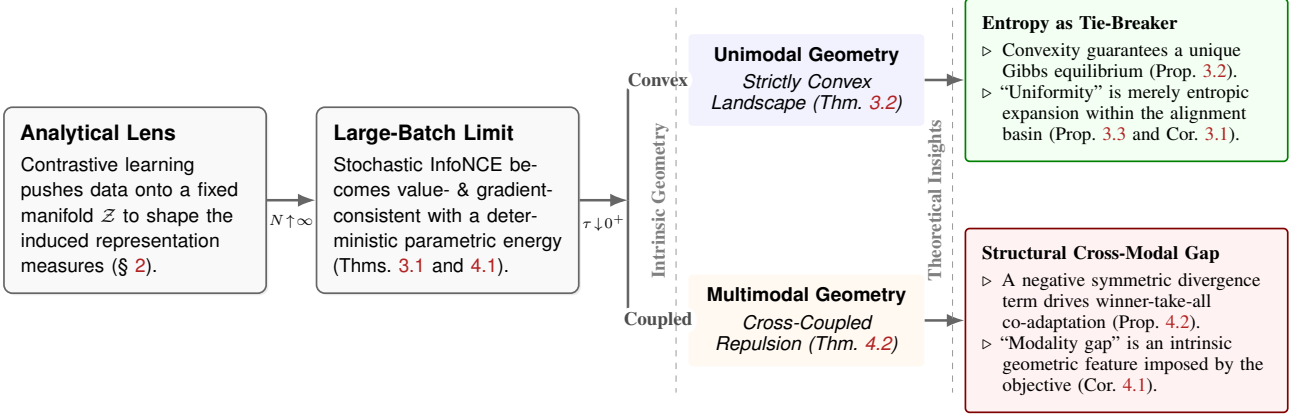


**Figure 1. The geometric bifurcation of contrastive representation learning.** We unify unimodal and multimodal analysis under a measure-theoretic framework. Via a shared analytical path, we bridge the stochastic objective to a deterministic energy landscape in the large-batch limit ( $N \rightarrow \infty$ ). However, at the intrinsic limit ( $\tau \downarrow 0^+$ ), the geometries bifurcate. The unimodal landscape is governed by a strictly convex functional where entropy acts as a unique tie-breaker. Conversely, the multimodal landscape is structurally coupled by a negative symmetric divergence; this erects repulsive barriers that enforce the “modality gap” as a necessary geometric state.

$\pi_{\theta\theta}(\mathbf{z}, \mathbf{w}) := d\pi_{\theta\theta}/d(\mu \otimes \mu)(\mathbf{z}, \mathbf{w})$ , and analogously for  $q_\phi$  and  $\pi_{\theta\phi}$ . Whenever we write pointwise quantities such as  $q_\theta(\mathbf{z})$  or  $\pi_{\theta\phi}(\mathbf{z}, \mathbf{w})$ , we are in the regime of absolute continuity with respect to the corresponding reference measure.

**Unimodal and multimodal learning objectives.** We analyze the standard InfoNCE family using the exponential kernel  $\kappa_\tau(\mathbf{z}, \mathbf{w}) = \kappa_\tau(\mathbf{w}, \mathbf{z}) := \exp(s(\mathbf{z}, \mathbf{w})/\tau)$ , where  $s$  is a similarity critic and  $\tau > 0$  is the temperature.

**Unimodal InfoNCE.** In unimodal contrastive learning, we analyze the directional InfoNCE objective. Given a training batch  $\mathcal{B}$  composed of a positive pair  $(\mathbf{x}, \tilde{\mathbf{x}}) \sim r_{\text{um}}$  and  $N$  negative samples  $\{\mathbf{x}'_j\}_{j=1}^N \stackrel{i.i.d.}{\sim} p_{\mathbf{x}}$ , the empirical loss<sup>1</sup> is:

$$\mathcal{L}_{\text{nce}}(\theta) := \mathbb{E}_{\mathcal{B}} \left[ -\log \frac{\kappa_\tau(f_\theta(\mathbf{x}), f_\theta(\tilde{\mathbf{x}}))}{\kappa_\tau(f_\theta(\mathbf{x}), f_\theta(\tilde{\mathbf{x}})) + \sum_{j=1}^N \kappa_\tau(f_\theta(\mathbf{x}), f_\theta(\mathbf{x}'_j))} \right]. \quad (1)$$

**Symmetric multimodal InfoNCE.** Given a positive pair  $(\mathbf{x}, \mathbf{y}) \sim r_{\text{mm}}$  and  $N$  i.i.d. negatives sampled from the marginal  $p_{\mathbf{y}}$ , we form the directional batch  $\mathcal{B}_{\theta \rightarrow \phi} := \{\mathbf{x}, \mathbf{y}, \mathbf{y}'_1, \dots, \mathbf{y}'_N\}$  with  $\mathbf{y}'_j \stackrel{i.i.d.}{\sim} p_{\mathbf{y}}$ , and define the directional  $\theta \rightarrow \phi$  objective

$$\mathcal{L}_{\text{nce}}^{\theta \rightarrow \phi}(\theta, \phi) := \mathbb{E}_{\mathcal{B}_{\theta \rightarrow \phi}} \left[ -\log \frac{\kappa_\tau(f_\theta(\mathbf{x}), g_\phi(\mathbf{y}))}{\kappa_\tau(f_\theta(\mathbf{x}), g_\phi(\mathbf{y})) + \sum_{j=1}^N \kappa_\tau(f_\theta(\mathbf{x}), g_\phi(\mathbf{y}'_j))} \right].$$

and analogously  $\mathcal{L}_{\text{nce}}^{\phi \rightarrow \theta}(\phi, \theta)$  by swapping modalities. The

<sup>1</sup>We analyze the population objective under i.i.d. sampling. Although in-batch sampling introduces finite-sample dependencies, the estimator remains consistent, and the theoretical properties converge to the i.i.d. setting in the large-batch regime ( $N \rightarrow \infty$ ).

symmetric CLIP-style loss is

$$\mathcal{L}_{\text{mm}}(\theta, \phi) := \frac{1}{2} (\mathcal{L}_{\text{nce}}^{\theta \rightarrow \phi}(\theta, \phi) + \mathcal{L}_{\text{nce}}^{\phi \rightarrow \theta}(\phi, \theta)). \quad (2)$$

**Kernel-induced quantities.** We now introduce the kernel-induced state variables that parameterize the resulting representation geometry. To make the analysis well-posed, we first impose a global assumption on the ambient representation space  $\mathcal{Z}$ , the fixed “container” in which the induced representation measures evolve.

**Assumption 2.1** (Constant kernel volume). The ambient representation space  $\mathcal{Z}$  is compact with  $\mu(\mathcal{Z}) < \infty$ . For each  $\tau > 0$ , there exists  $V_\kappa(\tau) \in (0, \infty)$  such that<sup>2</sup>

$$\int \kappa_\tau(\mathbf{z}, \mathbf{w}) d\mu(\mathbf{w}) \equiv V_\kappa(\tau), \quad \forall \mathbf{z} \in \mathcal{Z}.$$

**Remark 2.1** (Generality of Asm. 2.1). A sufficient condition for Asm. 2.1 is that  $\mathcal{Z}$  is a compact homogeneous manifold,  $\mu$  is the invariant volume, and the kernel is isotropic in the sense that  $\kappa_\tau(\mathbf{z}, \mathbf{w}) = h_\tau(d(\mathbf{z}, \mathbf{w}))$ , where  $d$  is the geodesic distance. In this case, invariance implies that  $V_\kappa(\tau, \mathbf{z}) := \int \kappa_\tau(\mathbf{z}, \mathbf{w}) d\mu(\mathbf{w})$  is independent of  $\mathbf{z}$ . More generally, on a compact manifold without boundary, standard short-time asymptotics for heat-type kernels yield an expansion of the form  $V_\kappa(\tau, \mathbf{z}) = V_0(\tau)(1 + O(\tau))$  uniformly in  $\mathcal{Z}$ , for some scalar function  $V_0(\tau) > 0$ . Thus, on non-homogeneous spaces, Asm. 2.1 holds up to a  $O(\tau)$  perturbation, which vanishes in the  $\tau \downarrow 0^+$  regime central to our analysis.

**Definition 2.1** (Population partition function). Define the population partition functions for the generic encoders  $f_\theta$  and  $g_\phi$  respectively as  $\Gamma_{\theta, \tau}(\mathbf{z}) := \int \kappa_\tau(\mathbf{z}, \mathbf{w}) q_\theta(d\mathbf{w})$  and  $\Gamma_{\phi, \tau}(\mathbf{z}) := \int \kappa_\tau(\mathbf{z}, \mathbf{w}) q_\phi(d\mathbf{w})$ .

<sup>2</sup>Unless otherwise specified, all integrals are taken over the representation manifold  $\mathcal{Z}$ , i.e.,  $\int \cdot d\mu \equiv \int_{\mathcal{Z}} \cdot d\mu$ .

**Definition 2.2** (Smoothed representation density). Define the smoothed representation densities  $\tilde{q}_{\theta,\tau}, \tilde{q}_{\phi,\tau} : \mathcal{Z} \rightarrow \mathbb{R}_+$ :

$$\tilde{q}_{\theta,\tau}(\mathbf{z}) := \Gamma_{\theta,\tau}(\mathbf{z})/V_{\kappa}(\tau), \quad \tilde{q}_{\phi,\tau}(\mathbf{z}) := \Gamma_{\phi,\tau}(\mathbf{z})/V_{\kappa}(\tau).$$

Note that  $\tilde{q}_{\theta,\tau}$  is a valid probability density with respect to the reference measure  $\mu$  by Asm. 2.1.

**Connection to optimization mechanics.** These definitions bridge the empirical objective and representation geometry: the InfoNCE denominator is a Monte Carlo estimator of the population partition function, and the softmax gradients induce stochastic updates of the induced fields  $(\Gamma_{\theta,\tau}, \Gamma_{\phi,\tau})$  and densities  $(\tilde{q}_{\theta,\tau}, \tilde{q}_{\phi,\tau})$ . In the large-batch limit, we will show that the gradient dynamics can be written as the gradient flow of an explicit parametric energy functional over  $\mathcal{Z}$ . Crucially, the analysis depends only on observable properties, avoiding strong assumptions about latent data-generating mechanisms common in prior identifiability work (Zimmermann et al., 2021; Liu et al., 2024).

### 3. Mechanistic Basis of Unimodal InfoNCE

In this section, we characterize the mechanisms driving geometric alignment in unimodal InfoNCE (Eq. (1)). We first establish uniform gradient bounds that guarantee stable optimization, and then derive the large-batch parametric energy whose gradient governs the asymptotic learning dynamics.

**Stable optimization and large-batch dynamics.** Under standard regularity assumptions on the encoder and critic, the InfoNCE gradient is uniformly bounded over  $\Theta$ , ensuring stability of gradient-based training. We then take the large-batch limit  $N \rightarrow \infty$ , where the empirical partition term concentrates and the objective becomes value- and gradient-consistent with an explicit parametric energy, yielding a deterministic descent direction on the induced representation measures.

**Assumption 3.1** (Optimization regularity). We assume the following conditions hold uniformly over the compact parameter space  $\Theta$ :

i) (Encoder regularity). For every  $\mathbf{x} \in \mathcal{X}$ , the map  $\theta \mapsto f_{\theta}(\mathbf{x})$  is  $C^1$  on  $\Theta$ , and its parameter Jacobian is uniformly bounded:  $\sup_{\theta \in \Theta} \sup_{\mathbf{x} \in \mathcal{X}} \|J_{\theta} f_{\theta}(\mathbf{x})\| < \infty$ .

ii) (Critic regularity). The critic  $s$  is  $C^1$  on an open neighborhood of  $\mathcal{Z} \times \mathcal{Z}$ , and its input gradient is uniformly bounded on  $\mathcal{Z} \times \mathcal{Z}$ :  $\sup_{(\mathbf{z}, \mathbf{w}) \in \mathcal{Z} \times \mathcal{Z}} \|\nabla s(\mathbf{z}, \mathbf{w})\| < \infty$ .

These conditions formalize standard engineering practices; see App. B.1 for a justification. Under this regularity, we establish the stability of the gradient-based optimization.

**Proposition 3.1** (Stable unimodal optimization). Assume

Asm. 3.1. Fix any temperature  $\tau > 0$  and any batch size<sup>3</sup>  $N \in \mathbb{N}_+$ . Then the unimodal InfoNCE objective defined in Eq. (1) has a uniformly bounded gradient over the parameter space  $\Theta$ . Formally, there exists a constant  $C(\tau) < \infty$ , depending only on  $\tau$ , such that  $\|\nabla_{\theta} \mathcal{L}_{\text{nce}}\| \leq C(\tau)$ , uniformly for all  $\theta \in \Theta$ .<sup>4</sup>

*Proof.* See App. C.1 for the full proof.  $\square$

We now connect the practical unimodal InfoNCE objective to the geometric functional induced by the kernel-smoothed representation field. The key step is to take the large-batch limit  $N \rightarrow \infty$ , which isolates the Monte Carlo concentration of the empirical partition function for any fixed temperature  $\tau > 0$ . This yields both *value* and *gradient* consistency, establishing that optimization of InfoNCE follows a well-defined geometric descent direction.

**Definition 3.1** (Unimodal alignment potential field). Let  $\nu_{\theta, \mathbf{z}}$  denote the conditional law of  $\mathbf{w}$  given  $\mathbf{z}$  under  $\pi_{\theta\theta}$ , i.e.,  $\pi_{\theta\theta}(d\mathbf{z}, d\mathbf{w}) = q_{\theta}(d\mathbf{z})\nu_{\theta, \mathbf{z}}(d\mathbf{w})$ . Define the alignment potential field at anchor  $\mathbf{z}$  under this conditional law:

$$U_{\theta}(\mathbf{z}) := - \int s(\mathbf{z}, \mathbf{w}) \nu_{\theta, \mathbf{z}}(d\mathbf{w}), \quad \text{for } q_{\theta}\text{-a.e. } \mathbf{z}.$$

**Definition 3.2** (Unimodal parametric energy). Fix  $\tau > 0$ . Define the unimodal parametric energy  $\mathcal{J}_{\tau} : \Theta \rightarrow \mathbb{R}$  by

$$\mathcal{J}_{\tau}(\theta) := \frac{1}{\tau} \mathcal{U}(q_{\theta}) - H_{\times}(q_{\theta}, \tilde{q}_{\theta, \tau}), \quad (3)$$

where  $H_{\times}(q_{\theta}, \tilde{q}_{\theta, \tau}) := - \int \log \tilde{q}_{\theta, \tau} d\mathbf{z}$  is the cross-entropy of the representation against the smoothed field, and  $\mathcal{U}(q_{\theta}) := \int U_{\theta}(\mathbf{z}) q_{\theta}(d\mathbf{z})$  is the expected binding energy of the representation, with the potential  $U_{\theta}$  defined in Def. 3.1.

**Theorem 3.1** (Large-batch unimodal dynamics). Consider the unimodal InfoNCE objective  $\mathcal{L}_{\text{nce}}(\theta)$  in Eq. (1) and the parametric energy  $\mathcal{J}_{\tau}(\theta)$  in Def. 3.2. Assume Asms. 2.1 and 3.1. For any fixed  $\tau > 0$ , as  $N \rightarrow \infty$ :

$$|\mathcal{L}_{\text{nce}}(\theta) - \mathcal{J}_{\tau}(\theta) - \log(NV_{\kappa}(\tau))| \rightarrow 0, \quad (4)$$

$$\|\nabla_{\theta} \mathcal{L}_{\text{nce}}(\theta) - \nabla_{\theta} \mathcal{J}_{\tau}(\theta)\| \rightarrow 0, \quad (5)$$

for each fixed  $\theta \in \Theta$ . Thus, in the large-batch regime, gradient-based optimization of  $\mathcal{L}_{\text{nce}}$  asymptotically follows the descent direction of the parametric energy  $\mathcal{J}_{\tau}$ .

*Proof.* See App. C.2 for the full proof.  $\square$

**Remark 3.1** (From alignment-uniformity to representation geometry). The alignment-uniformity view (Wang & Isola, 2020) is largely a *value-level* account, most often stated for hyperspherical embeddings and cosine/von Mises–Fisher similarities. Our framework is *geometric* and *dynamic*: it

<sup>3</sup>Throughout, we refer to  $N$  as the batch size (strictly  $N + 1$ ) for clarity; none of the analytic results depend on this convention.

<sup>4</sup>Unless otherwise specified,  $\|\cdot\|$  denotes the  $\ell_2$  norm.

extends to compact manifolds under the constant kernel-volume condition (Asm. 2.1), covers general exponential kernels induced by smooth critics, and crucially proves *gradient consistency* (Thm. 3.1), so that large-batch InfoNCE optimization follows the descent direction of the explicit energy  $\mathcal{J}_\tau$  up to vanishing error. This turns a descriptive principle about optima into a mechanistic statement, enabling a direct landscape analysis of representation measures on  $\mathcal{Z}$ , rather than parameter-space heuristics.

### Intrinsic landscape and low-temperature consistency.

The parametric energy remains nonconvex in parameters because  $\theta \mapsto q_\theta$  is implicit. To expose the geometry induced on  $\mathcal{Z}$ , we lift the analysis to an intrinsic functional over  $\rho \in \mathcal{P}(\mathcal{Z})$  with a fixed potential field. This surrogate is strictly convex with a unique Gibbs equilibrium and admits ground-state concentration as  $\tau \downarrow 0^+$ . Moreover, in the sharp-kernel regime, the parametric energy is value-close to the intrinsic functional up to a vanishing KDE mismatch, so the learning landscape inherits the intrinsic geometry.

**Definition 3.3** (Unimodal representation functional). For each fixed  $\tau > 0$  and a potential field  $U : \mathcal{Z} \rightarrow \mathbb{R}$ , define the intrinsic unimodal representation functional  $\mathcal{F}_{\tau,U}(\rho)$  over probability densities  $\rho \in \mathcal{P}(\mathcal{Z}) := \{\rho \in L^1(\mathcal{Z}) : \rho \geq 0 \text{ } \mu\text{-a.e.}, \int \rho d\mu = 1\}$  by:

$$\mathcal{F}_{\tau,U}(\rho) := \frac{1}{\tau} \mathcal{U}(\rho) - H(\rho), \quad (6)$$

where  $\mathcal{U}(\rho) := \int U(\mathbf{z}) \rho(\mathbf{z}) d\mu(\mathbf{z})$  is the expected binding energy under density  $\rho$ , and  $H(\rho)$  is the differential entropy.

*Remark 3.2* (Well-posedness). We adopt the convention  $0 \log 0 := 0$  throughout, and define  $H(\rho) := -\int \rho \log \rho d\mu \in [-\infty, \infty)$ . We view  $\mathcal{F}_{\tau,U}$  as an extended-real functional on  $\mathcal{P}(\mathcal{Z})$ , setting  $\mathcal{F}_{\tau,U}(\rho) = +\infty$  whenever  $\int \rho \log \rho d\mu = +\infty$  or  $\int U \rho d\mu = +\infty$ .

**Definition 3.4** (KDE approximation error). For each fixed  $\tau > 0$  and  $\theta \in \Theta$ , define the KDE approximation error  $\varepsilon_{\text{kde}}^{(\theta)}(\tau)$  between the density  $q_\theta$  and the kernel-smoothed version  $\tilde{q}_{\theta,\tau}$  by  $\varepsilon_{\text{kde}}^{(\theta)}(\tau) := \|\tilde{q}_{\theta,\tau} - q_\theta\|_\infty$ .

**Assumption 3.2** (Sharp diagonal peak). Assume Asm. 2.1. Let  $d(\cdot, \cdot)$  denote the geodesic distance on  $\mathcal{Z}$ . There exist constants  $r > 0$  and  $0 < m_1 \leq m_2 < \infty$  such that for all  $\mathbf{z} \in \mathcal{Z}$  and all  $\mathbf{w} \in \{\mathbf{w} : d(\mathbf{z}, \mathbf{w}) < r\}$ ,

$$-m_2 d(\mathbf{z}, \mathbf{w})^2 \leq s(\mathbf{z}, \mathbf{w}) - s(\mathbf{z}, \mathbf{z}) \leq -m_1 d(\mathbf{z}, \mathbf{w})^2. \quad (7)$$

Moreover, the map  $\mathbf{w} \mapsto s(\mathbf{z}, \mathbf{w})$  attains its unique maximum at  $\mathbf{w} = \mathbf{z}$ , for each  $\mathbf{z} \in \mathcal{Z}$ .

*Remark 3.3.* Asm. 3.2 is a uniform nondegeneracy condition: for each  $\mathbf{z}$ , the map  $s(\mathbf{z}, \cdot)$  attains an isolated, locally quadratic maximum at  $\mathbf{w} = \mathbf{z}$ . With the exponential kernel  $\kappa_\tau(\mathbf{z}, \mathbf{w}) = \exp(s(\mathbf{z}, \mathbf{w})/\tau)$ , this entails that the

normalized kernel mass concentrates in a geodesic neighborhood of the diagonal of radius  $O(\sqrt{\tau})$ . This holds exactly for the RBF family: if  $s(\mathbf{z}, \mathbf{w}) = -\|\mathbf{z} - \mathbf{w}\|^2$ , then  $s(\mathbf{z}, \mathbf{w}) - s(\mathbf{z}, \mathbf{z}) = -\|\mathbf{z} - \mathbf{w}\|^2$ , matching the quadratic bounds with equality. On the hypersphere, cosine similarity is locally quadratic as well: for nearby points,  $1 - \langle \mathbf{z}, \mathbf{w} \rangle \asymp d_S(\mathbf{z}, \mathbf{w})^2$ , so the same bounds hold locally with uniform constants, corresponding to the von Mises–Fisher family.

**Theorem 3.2** (Low-temperature functional consistency). *Assume Asms. 2.1, 3.1 and 3.2 hold. Fix  $\theta \in \Theta$  and assume that  $q_\theta$  admits a continuous  $\mu$ -density bounded away from zero, i.e.,  $\inf_{\mathbf{z}} q_\theta(\mathbf{z}) \geq \underline{q}_\theta > 0$ . Then, there exists  $\tau_0(\theta) > 0$  such that for all  $0 < \tau \leq \tau_0(\theta)$ , the parametric energy converges to the intrinsic functional at a rate controlled by the KDE approximation error:*

$$|\mathcal{J}_\tau(\theta) - \mathcal{F}_{\tau,U_\theta}(q_\theta)| \leq 2 \varepsilon_{\text{kde}}^{(\theta)}(\tau) / \underline{q}_\theta,$$

where  $\mathcal{F}_{\tau,U_\theta}(q_\theta)$  (Def. 3.3) is evaluated at the density  $q_\theta$  and potential field  $U_\theta$ , and  $\varepsilon_{\text{kde}}^{(\theta)}(\tau)$  is the KDE approximation error (Def. 3.4). Moreover, as  $\tau \downarrow 0^+$ ,  $|\mathcal{J}_\tau(\theta) - \mathcal{F}_{\tau,U_\theta}(q_\theta)| \rightarrow 0$  for any such  $\theta$ .

*Proof.* See App. C.3 for the full proof.  $\square$

*Remark 3.4* (Low-temperature regimes and geometric lens). The limit  $\tau \downarrow 0^+$  is used only to control the KDE mismatch between  $q_\theta$  and its smoothing  $\tilde{q}_{\theta,\tau}$ . In this regime the cross-entropy term appearing in the large-batch expansion becomes an accurate proxy for the true entropy of  $q_\theta$ , so the parametric energy  $\mathcal{J}_\tau(\theta)$  is value-close to the intrinsic surrogate  $\mathcal{F}_{\tau,U_\theta}(q_\theta)$  (Thm. 3.2). Hence, in this low-temperature regime the parametric landscape inherits the geometry of  $\mathcal{F}_{\tau,U_\theta}$ , even though  $\tau$  is fixed and nonzero in practice.

We next connect the intrinsic variational landscape to the parametric learning problem. First, we characterize the unique minimizer of  $\mathcal{F}_{\tau,U}$  for each  $\tau > 0$ , defining an ideal geometric equilibrium that the encoder family may approximate. We then formalize an expressivity condition under which minimizers of the practical objective inherit ground-state concentration in the low-temperature regime.

**Proposition 3.2** (Unique Gibbs equilibrium). *Assume  $\mathcal{Z}$  is compact with  $\mu(\mathcal{Z}) < \infty$ . Fix  $\tau > 0$  and let  $U : \mathcal{Z} \rightarrow \mathbb{R}$  be Borel measurable and bounded below  $\mu$ -a.e. Then,  $\mathcal{F}_{\tau,U}$  (Def. 3.3) is strictly convex over  $\mathcal{P}(\mathcal{Z})$  and admits a unique minimizer  $\rho^* \in \mathcal{P}(\mathcal{Z})$ <sup>5</sup>, given by the Gibbs equilibrium*

$$\rho^*(\mathbf{z}) = \frac{\exp(-U(\mathbf{z})/\tau)}{Z_\tau}, \quad Z_\tau := \int \exp\left(\frac{-U(\mathbf{z})}{\tau}\right) d\mu(\mathbf{z}).$$

*Proof.* See App. C.4 for the full proof.  $\square$

<sup>5</sup>Here,  $\rho^*$  denotes  $\rho_\tau^*$ ; we suppress the explicit  $\tau$ -dependence throughout to keep notation light.

**Proposition 3.3** (Low-temperature concentration). *Assume the setting of Prop. 3.2. Fix sufficiently small  $\sigma > 0$ , define the  $\sigma$ -sublevel set  $\mathcal{W}^\sigma := \{\mathbf{z} \in \mathcal{Z} : U(\mathbf{z}) \leq \text{ess inf}_\mu U + \sigma\}$ . Then, as  $\tau \downarrow 0^+$ , the equilibrium measure  $\rho^* \mu$  concentrates on  $\mathcal{W}^\sigma$  in the sense that for every open  $\mathcal{O} \subset \mathcal{Z}$  with  $\mathcal{O} \supset \mathcal{W}^\sigma$ ,  $(\rho^* \mu)(\mathcal{Z} \setminus \mathcal{O}) \rightarrow 0$ .*

*Proof.* See App. C.5 for the full proof.  $\square$

**Remark 3.5** (Ground state under continuous  $U$ ). If  $U : \mathcal{Z} \rightarrow \mathbb{R}$  is continuous, then on compact  $\mathcal{Z}$  the minimizer set  $\mathcal{W} := \arg \min_{\mathbf{z} \in \mathcal{Z}} U(\mathbf{z})$  is nonempty. Consequently, the low-temperature concentration statement in Prop. 3.3 strengthens to concentration on  $\mathcal{W}$  as  $\tau \downarrow 0^+$ .

**Remark 3.6** (Mechanistic forces: potential attraction vs entropic expansion). The functional  $\mathcal{F}_{\tau, U}(\rho) = \frac{1}{\tau} \mathcal{U}(\rho) - H(\rho)$  exposes two competing forces: the potential term  $\frac{1}{\tau} \mathcal{U}(\rho)$  attracts mass toward low-energy regions (strong alignment), while the entropy  $H(\rho)$  repels mass and favors internally dispersed configurations. The temperature  $\tau$  controls their relative strength: as  $\tau$  decreases, the potential term dominates and the landscape becomes increasingly ground-state driven, with entropy acting primarily as a tie-breaker among near-minimizing configurations.

**Corollary 3.1** (Unimodal parametric inheritance under expressiveness). *Assume the setting of Thm. 3.2. For each  $\theta \in \Theta$  and  $\tau > 0$ , define the equilibrium of  $\mathcal{F}_{\tau, U_\theta}$  by  $\rho_\theta^*(\mathbf{z}) := \frac{1}{Z_{\theta, \tau}} \exp(-U_\theta(\mathbf{z})/\tau)$  with  $Z_{\theta, \tau} := \int \exp(-U_\theta(\mathbf{z})/\tau) d\mu(\mathbf{z})$  as the normalization constant. Let  $\hat{\theta} \in \arg \min_{\theta \in \Theta} (-\log Z_{\theta, \tau})$ .<sup>6</sup> Assume the encoder family  $\{f_\theta\}_{\Theta}$  is sufficiently expressive in the sense that*

$$\exists \varepsilon_{\text{real}}(\tau) \xrightarrow{\tau \downarrow 0^+} 0 \text{ s.t. } \mathcal{F}_{\tau, U_{\hat{\theta}}}(\rho_{\hat{\theta}}) + \log Z_{\hat{\theta}, \tau} \leq \varepsilon_{\text{real}}(\tau). \quad (8)$$

Let  $\theta^* \in \arg \min_{\theta \in \Theta} \mathcal{J}_\tau(\theta)$ . Fix sufficiently small  $\sigma > 0$ , define the  $\sigma$ -ground-state set of the induced  $U_{\theta^*}$  by

$$\mathcal{W}_{\theta^*}^\sigma := \{\mathbf{z} \in \mathcal{Z} : U_{\theta^*}(\mathbf{z}) \leq \text{ess inf}_\mu U_{\theta^*} + \sigma\}.$$

Then, as  $\tau \downarrow 0^+$ ,  $q_{\theta^*}$  concentrates on  $\mathcal{W}_{\theta^*}^\sigma$  such that for every open  $\mathcal{O} \subset \mathcal{Z}$  with  $\mathcal{O} \supset \mathcal{W}_{\theta^*}^\sigma$ ,  $(q_{\theta^*} \mu)(\mathcal{Z} \setminus \mathcal{O}) \rightarrow 0$ .

*Proof.* See App. C.6 for the full proof.  $\square$

**Remark 3.7** (Emergence of intrinsic “uniformity”). Conditional on the encoder family  $\{f_\theta\}_{\Theta}$  being able to realize multiple distributions with comparable potential energy (i.e., multiple near-ground-state  $q_\theta$ ), the entropic term favors those that are maximally dispersed subject to the induced potential constraint. In this sense, uniformity is not a global objective (Wang & Isola, 2020), but a robust principle—maximal dispersion *within* the semantically aligned set realizable under the induced alignment potential.

<sup>6</sup>Equivalently,  $\hat{\theta}$  attains the lowest representation energy level among potentials  $U_\theta$  induced by the model family.

## 4. Mechanistic Basis of Multimodal InfoNCE

We analyze the symmetric multimodal InfoNCE objective used in CLIP-style training (Eq. (2)). Unlike the unimodal setting, the geometry is *cross-coupled*: each modality induces the effective field seen by the other. This coupling yields qualitatively different landscapes and permits population-level modality gaps.

**Stable optimization and large-batch dynamics.** Under multimodal regularity conditions, the symmetric objective has uniformly bounded gradients. As  $N \rightarrow \infty$ , the stochastic loss becomes value- and gradient-consistent with a coupled parametric energy, following a deterministic descent direction governed by cross-modal fields.

**Assumption 4.1** (Multimodal optimization regularity). Assume encoder regularity condition in Asm. 3.1 i) holds for  $\{f_\theta\}_{\theta \in \Theta}$  and for  $\{g_\phi\}_{\phi \in \Phi}$ , and the critic  $s$  satisfies the same condition in Asm. 3.1 ii) on  $\mathcal{Z} \times \mathcal{Z}$ , uniformly over  $\Theta \times \Phi$ .

**Proposition 4.1** (Stable multimodal optimization). *Under Asms. 2.1 and 4.1, for any batch size  $N \in \mathbb{N}_+$  and temperature  $\tau > 0$ , the gradient of the symmetric InfoNCE loss (Eq. (2)) is uniformly bounded. Formally, there exists a constant  $C < \infty$  such that the joint gradient satisfies  $\|\nabla_{(\theta, \phi)} \mathcal{L}_{\text{mm}}(\theta, \phi)\| \leq C$ , uniformly over  $\Theta \times \Phi$ .*

*Proof.* See App. C.7 for the full proof.  $\square$

**Definition 4.1** (Directional alignment potential field). By disintegration, there exists Markov kernels  $\{\nu_{\theta \rightarrow \phi, \mathbf{z}}\}_{\mathbf{z} \in \mathcal{Z}}$  and  $\{\nu_{\phi \rightarrow \theta, \mathbf{w}}\}_{\mathbf{w} \in \mathcal{Z}}$  such that

$$\pi_{\theta \phi}(\mathbf{d}\mathbf{z}, \mathbf{d}\mathbf{w}) = q_\theta(\mathbf{d}\mathbf{z}) \nu_{\theta \rightarrow \phi, \mathbf{z}}(\mathbf{d}\mathbf{w}) = q_\phi(\mathbf{d}\mathbf{w}) \nu_{\phi \rightarrow \theta, \mathbf{z}}(\mathbf{d}\mathbf{z}).$$

Define the cross-modal alignment potential fields on  $\mathcal{Z}$  by

$$\begin{aligned} U_{\theta \rightarrow \phi}(\mathbf{z}) &:= - \int s(\mathbf{z}, \mathbf{w}) \nu_{\theta \rightarrow \phi, \mathbf{z}}(\mathbf{d}\mathbf{w}), & q_\theta\text{-a.e. } \mathbf{z}, \\ U_{\phi \rightarrow \theta}(\mathbf{w}) &:= - \int s(\mathbf{z}, \mathbf{w}) \nu_{\phi \rightarrow \theta, \mathbf{w}}(\mathbf{d}\mathbf{z}), & q_\phi\text{-a.e. } \mathbf{w}. \end{aligned}$$

**Definition 4.2** (Multimodal parametric energy). Define the multimodal parametric energy  $\mathcal{J}_\tau^{\text{mm}} : \Theta \times \Phi \rightarrow \mathbb{R}$  by

$$\mathcal{J}_\tau^{\text{mm}}(\theta, \phi) := \frac{1}{2} (\mathcal{J}_\tau^{\theta \rightarrow \phi}(\theta, \phi) + \mathcal{J}_\tau^{\phi \rightarrow \theta}(\theta, \phi)), \quad (9)$$

where the directional energies are

$$\begin{aligned} \mathcal{J}_\tau^{\theta \rightarrow \phi}(\theta, \phi) &:= \frac{1}{\tau} \mathcal{U}^{\theta \rightarrow \phi}(q_\theta) - H_\times(q_\theta, \tilde{q}_{\phi, \tau}), \\ \mathcal{J}_\tau^{\phi \rightarrow \theta}(\theta, \phi) &:= \frac{1}{\tau} \mathcal{U}^{\phi \rightarrow \theta}(q_\phi) - H_\times(q_\phi, \tilde{q}_{\theta, \tau}). \end{aligned}$$

Here  $\mathcal{U}^{\theta \rightarrow \phi}(q_\theta) := \int U_{\theta \rightarrow \phi}(\mathbf{z}) q_\theta(\mathbf{d}\mathbf{z})$  and  $\mathcal{U}^{\phi \rightarrow \theta}(q_\phi) := \int U_{\phi \rightarrow \theta}(\mathbf{w}) q_\phi(\mathbf{d}\mathbf{w})$  are the expected binding energies induced by the potential fields  $U_{\theta \rightarrow \phi}$  and  $U_{\phi \rightarrow \theta}$  from Def. 4.1, and  $H_\times(q, \tilde{q}) := - \int \log \tilde{q} dq$  is the cross-entropy.

**Remark 4.1** (Directional asymmetry). In the multimodal setting, the two disintegrations  $q_\theta(dz)\nu_{\theta\rightarrow\phi,z}(dw)$  and  $q_\phi(dw)\nu_{\phi\rightarrow\theta,w}(dz)$  generally induce different conditional laws, yielding distinct anchor-dependent potentials  $U_{\theta\rightarrow\phi}$  and  $U_{\phi\rightarrow\theta}$ . Collapsing them into a single potential field would require an additional symmetry assumption (i.e., that conditional laws are identical), which is typically unjustified for heterogeneous modalities like images and text.

**Theorem 4.1** (Large-batch multimodal dynamics). *Consider the multimodal InfoNCE objective  $\mathcal{L}_{\text{mm}}(\theta, \phi)$  in Eq. (2) and the parametric energy  $\mathcal{J}_\tau^{\text{mm}}(\theta, \phi)$  in Def. 4.2. Assume Asms. 2.1 and 4.1. For any fixed  $\tau > 0$ , as  $N \rightarrow \infty$ :*

$$|\mathcal{L}_{\text{mm}}(\theta, \phi) - \mathcal{J}_\tau^{\text{mm}}(\theta, \phi) - \log(NV_\kappa(\tau))| \rightarrow 0, \quad (10)$$

$$\|\nabla_{(\theta, \phi)} \mathcal{L}_{\text{mm}}(\theta, \phi) - \nabla_{(\theta, \phi)} \mathcal{J}_\tau^{\text{mm}}(\theta, \phi)\| \rightarrow 0, \quad (11)$$

for each pair  $(\theta, \phi) \in \Theta \times \Phi$ . Thus, in the large-batch regime, gradient-based optimization of  $\mathcal{L}_{\text{mm}}$  asymptotically follows the descent direction of the parametric energy  $\mathcal{J}_\tau^{\text{mm}}$ .

*Proof.* See App. C.8 for the full proof.  $\square$

**Intrinsic geometry and divergence-driven coupling.** To interpret the induced landscape, we lift the parametric energy to an intrinsic functional over modality densities. In the low-temperature regime, a *negative* symmetric divergence term persists, implying that kernel sharpening does not force marginal matching. This term inverts coordinate-wise curvature, driving non-Gibbs responses where each modality effectively erects a barrier against the other.

**Definition 4.3** (Multimodal representation functional). Fix  $\tau > 0$ . Let  $U_{1\rightarrow 2}, U_{2\rightarrow 1} : \mathcal{Z} \rightarrow \mathbb{R}$  be Borel measurable potential fields, and write  $\mathbf{U}_{1,2} := (U_{1\rightarrow 2}, U_{2\rightarrow 1})$ . Let  $\mathcal{P}_+(\mathcal{Z}) := \{\rho \in L^1(\mathcal{Z}) : \rho \geq \underline{\rho} \mu\text{-a.e.}, \int \rho d\mu = 1\}$  for some fixed  $\underline{\rho} > 0$ . For  $(\rho_1, \rho_2) \in \mathcal{P}_+(\mathcal{Z}) \times \mathcal{P}_+(\mathcal{Z})$ , define the multimodal representation functional as

$$\mathcal{F}_{\tau, \mathbf{U}_{1,2}}^{\text{mm}}(\rho_1, \rho_2) := \frac{\mathcal{F}_{\tau, U_{1\rightarrow 2}}(\rho_1) + \mathcal{F}_{\tau, U_{2\rightarrow 1}}(\rho_2)}{2} - D_S(\rho_1, \rho_2),$$

where  $\mathcal{F}_{\tau, U_{i\rightarrow j}}$  are representation functionals defined as in Def. 3.3, and  $D_S(\rho_1, \rho_2) := \frac{1}{2}(D_{\text{KL}}(\rho_1\|\rho_2) + D_{\text{KL}}(\rho_2\|\rho_1))$  is the symmetric KL-divergence.

The density floor  $\underline{\rho} > 0$  is a technical device ensuring the multimodal variational problem is well-posed; see App. B.2 for discussion and practical interpretation.

**Theorem 4.2** (Low-temperature multimodal functional consistency). *Assume Asms. 2.1, 3.2 and 4.1 hold. Fix any  $(\theta, \phi) \in \Theta \times \Phi$ . Assume that  $q_\theta, q_\phi$  admit continuous  $\mu$ -densities bounded below:  $\inf_{\mathbf{z}} q_\theta(\mathbf{z}) \geq \underline{q}_\theta > 0$ ,  $\inf_{\mathbf{z}} q_\phi(\mathbf{z}) \geq \underline{q}_\phi > 0$ . Then, there exists  $\tau_0(\theta, \phi) > 0$  such that for all  $0 < \tau \leq \tau_0(\theta, \phi)$ :*

$$|\mathcal{J}_\tau^{\text{mm}}(\theta, \phi) - \mathcal{F}_{\tau, \mathbf{U}_{\theta, \phi}}^{\text{mm}}(q_\theta, q_\phi)| \leq \frac{\varepsilon_{\text{kde}}^{(\theta)}(\tau) + \varepsilon_{\text{kde}}^{(\phi)}(\tau)}{\min\{q_\theta, q_\phi\}},$$

where  $\varepsilon_{\text{kde}}^{(\theta)}(\tau), \varepsilon_{\text{kde}}^{(\phi)}(\tau)$  are the KDE approximation errors regarding  $q_\theta$  and  $q_\phi$  respectively (Def. 3.4), and  $\mathcal{F}_{\tau, \mathbf{U}_{\theta, \phi}}^{\text{mm}}(q_\theta, q_\phi)$  is the multimodal representation functional (Def. 4.3) evaluated at the densities  $q_\theta, q_\phi$  and the potential fields  $\mathbf{U}_{\theta, \phi} := (U_{\theta\rightarrow\phi}, U_{\phi\rightarrow\theta})$  (Def. 4.1).

Moreover, as  $\tau \downarrow 0^+$ ,  $|\mathcal{J}_\tau^{\text{mm}}(\theta, \phi) - \mathcal{F}_{\tau, \mathbf{U}_{\theta, \phi}}^{\text{mm}}(q_\theta, q_\phi)| \rightarrow 0$  for any pair  $(\theta, \phi) \in \Theta \times \Phi$ .

*Proof.* See App. C.9 for the full proof.  $\square$

**Remark 4.2** (The persistence of the negative divergence). Crucially, the limit  $\tau \downarrow 0^+$  only removes the KDE smoothing error (driving  $\tilde{q} \rightarrow q$ ). It does not affect the symmetric divergence  $D_S(q_\theta, q_\phi)$ . With its *negative* sign, this term penalizes similarity between the marginals, favoring solutions where  $q_\theta$  and  $q_\phi$  remain distinct. This provides a geometric reason for the persistence of population-level gaps.

**Proposition 4.2** (Coordinate-wise extremal collapse). *Assume  $\mathcal{Z}$  is compact with  $\mu(\mathcal{Z}) < \infty$ . Fix a density floor  $\underline{\rho} > 0$  such that  $\underline{\rho}\mu(\mathcal{Z}) < 1$ , and let  $\mathcal{P}_+(\mathcal{Z}) := \{\rho \in L^1(\mathcal{Z}) : \rho \geq \underline{\rho} \mu\text{-a.e.}, \int \rho d\mu = 1\}$  be the set of feasible densities. Let  $\mathcal{F}_{\tau, \mathbf{U}_{1,2}}^{\text{mm}}$  be defined as in Def. 4.3, with  $U_{1\rightarrow 2}, U_{2\rightarrow 1}$  that are Borel measurable and bounded below. Let  $M_{\text{ex}} := 1 - \underline{\rho}\mu(\mathcal{Z})$  be the excess probability mass.*

*Fix  $\rho_2 \in \mathcal{P}_+(\mathcal{Z})$  and define the effective potential field  $V_{1|2}(\mathbf{z}) := \frac{1}{\tau}U_{1\rightarrow 2}(\mathbf{z}) + \log \rho_2(\mathbf{z})$ . The coordinate map  $\rho_1 \mapsto \mathcal{F}_{\tau, \mathbf{U}_{1,2}}^{\text{mm}}(\rho_1, \rho_2)$  is concave, thus the infimum is approached by boundary solutions concentrating on the minima of  $V_{1|2}$ . Specifically, for a sufficiently small  $\sigma > 0$ , let  $\mathcal{W}_1^\sigma := \{\mathbf{z} \in \mathcal{Z} : V_{1|2}(\mathbf{z}) \leq \text{ess inf}_\mu V_{1|2} + \sigma\}$  be the sublevel set. Define the  $\sigma$ -approximate density  $\rho_1^{(\sigma)}$  by concentrating the excess mass on a shrinking set  $\mathcal{S}_1^\sigma \subseteq \mathcal{W}_1^\sigma$ :<sup>7</sup>*

$$\rho_1^{(\sigma)}(\mathbf{z}) = \underline{\rho} + \mathbb{1}_{\mathcal{S}_1^\sigma}(\mathbf{z}) \frac{M_{\text{ex}}}{\mu(\mathcal{S}_1^\sigma)}, \quad \text{with } \lim_{\sigma \downarrow 0} \mu(\mathcal{S}_1^\sigma) = 0. \quad (12)$$

As  $\sigma \downarrow 0$ , the energy of  $\rho_1^{(\sigma)}$  converges to the infimum:

$$\lim_{\sigma \downarrow 0} \mathcal{F}_{\tau, \mathbf{U}_{1,2}}^{\text{mm}}(\rho_1^{(\sigma)}, \rho_2) = \inf_{\rho_1 \in \mathcal{P}_+(\mathcal{Z})} \mathcal{F}_{\tau, \mathbf{U}_{1,2}}^{\text{mm}}(\rho_1, \rho_2).$$

Analogous statements hold for  $\rho_2^{(\sigma)}$  with respect to the dual effective potential field  $V_{2|1}(\mathbf{z}) := \frac{1}{\tau}U_{2\rightarrow 1}(\mathbf{z}) + \log \rho_1(\mathbf{z})$ .

*Proof.* See App. C.10 for the full proof.  $\square$

**Remark 4.3** (Coordinate collapse and effective barriers). Prop. 4.2 reveals that coordinate minimization in the multimodal setting is *not* Gibbs-like. Because the coordinate map is concave, the best response does not spread mass smoothly; instead, it pushes the entire excess budget  $M_{\text{ex}}$  onto approximate minimizers of the effective potential  $V_{1|2}$ , leaving only

<sup>7</sup>In the generic case of a sharp minimum, one simply takes  $\mathcal{S}_1^\sigma = \mathcal{W}_1^\sigma$ ; for a flat minimum, any vanishing  $\mathcal{S}_1^\sigma \subset \mathcal{W}_1^\sigma$  suffices.

the hard floor  $\rho$  elsewhere. The term  $\log \rho_2$  acts as a *population barrier* erected by the other modality: even if the alignment potential  $U_{1 \rightarrow 2}$  is low in a region, a low density  $\rho_2$  there raises the effective potential  $V_{1|2}$  and diverts mass away. Thus, the optimizer implements a *winner-take-all* co-adaptation: each modality reshapes the other's landscape, driving concentration into disjoint sets. This stands in sharp contrast to the unimodal setting (Prop. 3.2), where strict convexity precludes boundary concentration and ensures unique, smooth minimizers.

**Corollary 4.1** (Multimodal parametric inheritance under expressiveness). *Assume the setting of Thm. 4.2. Fix a peer encoder  $\phi \in \Phi$  and, for each  $\tau > 0$ , let  $\theta^* \in \arg \min_{\theta \in \Theta} \mathcal{J}_\tau^{\text{mm}}(\theta, \phi)$ . Write the density floors parameterized by  $\theta^*$  as  $\underline{q}_{\theta^*}$  with  $\underline{q}_{\theta^*} \mu(\mathcal{Z}) < 1$ , and define  $\mathcal{P}_+^{(\theta^*)}(\mathcal{Z}) := \{\rho \in L^1(\mathcal{Z}) : \rho \geq \underline{q}_{\theta^*} \mu\text{-a.e.}, \int \rho d\mu = 1\}$  and the excess mass  $M_{\text{ex}}^{(\theta^*)} := 1 - \underline{q}_{\theta^*} \mu(\mathcal{Z})$ . Define the normalized excess density as  $\bar{q}_{\theta^*}(\mathbf{z}) := (q_{\theta^*}(\mathbf{z}) - \underline{q}_{\theta^*}) / M_{\text{ex}}^{(\theta^*)}$ . Assume the encoder family  $\{f_\theta\}_{\Theta}$  is sufficiently expressive:  $\exists \varepsilon_{\text{real}}(\tau) \rightarrow 0$  as  $\tau \downarrow 0^+$  such that*

$$\mathcal{F}_{\tau, \mathbf{U}_{\theta^*, \phi}}^{\text{mm}}(q_{\theta^*}, q_\phi) \leq \inf_{\rho \in \mathcal{P}_+^{(\theta^*)}(\mathcal{Z})} \mathcal{F}_{\tau, \mathbf{U}_{\theta^*, \phi}}^{\text{mm}}(\rho, q_\phi) + \varepsilon_{\text{real}}(\tau). \quad (13)$$

Let  $V_{\theta^*|\phi}(\mathbf{z}) := \frac{1}{\tau} U_{\theta^* \rightarrow \phi}(\mathbf{z}) + \log q_\phi(\mathbf{z})$ . For  $\sigma > 0$ , define  $\mathcal{W}_{\theta^*}^\sigma := \{\mathbf{z} \in \mathcal{Z} : V_{\theta^*|\phi}(\mathbf{z}) \leq \text{ess inf}_\mu V_{\theta^*|\phi} + \sigma\}$ . Then for every  $\sigma > 0$ ,

$$(\bar{q}_{\theta^*} \mu)(\mathcal{Z} \setminus \mathcal{W}_{\theta^*}^\sigma) \leq 2 \varepsilon_{\text{real}}(\tau) / (M_{\text{ex}}^{(\theta^*)} \sigma). \quad (14)$$

In particular, for any  $\sigma \downarrow 0$  satisfying  $\varepsilon_{\text{real}}(\tau) / \sigma \rightarrow 0$ , we have  $(\bar{q}_{\theta^*} \mu)(\mathcal{Z} \setminus \mathcal{W}_{\theta^*}^\sigma) \rightarrow 0$  as  $\tau \downarrow 0^+$ . A symmetric statement holds for optimizing in  $\phi$  with  $\theta$  fixed.

*Proof.* See App. C.11 for the full proof.  $\square$

**Remark 4.4** (Mechanism of the modality gap). The concentration of  $q_{\theta^*}$  and  $q_\phi$  depends on effective potentials  $V_{\theta^*|\phi^*}$  and  $V_{\phi^*|\theta^*}$  that contain different conditional terms.  $q_{\theta^*} = q_\phi$  is a *knife-edge compatibility condition* that requires these distinct effective potentials to coincide  $\mu$ -almost everywhere. Given the inherent underspecification of heterogeneous data (e.g., noisy image-text pairs, many-to-many matches), this coincidence is generically unlikely. Thus, the objective naturally favors a persistent population-level separation—a mechanistic explanation for the “Mind the Gap” phenomenon (Liang et al., 2022).

## 5. Limitation and Future Directions

Our theoretical framework targets specific geometric regimes to keep the analysis tractable and isolate core mechanisms. These assumptions bound the derivations but at the same time naturally suggest the following extensions. See also App. E for a broader discussion.

**Finite-temperature and finite-batch corrections.** Our results leverage low-temperature ( $\tau \downarrow 0^+$ ) and large-batch limits ( $N \rightarrow \infty$ ) to derive deterministic landscapes. Practical training operates with finite batches and moderate temperatures, introducing stochasticity and entropic smoothing that may soften the predicted modality barriers or permit “tunneling” between metastable states. Characterizing the interplay between batch noise and barrier crossing is a key direction for sharpening practical predictions.

**Singularities and boundary behavior.** In the multimodal formulation, we impose a strict density floor (Prop. 4.2) to regularize the log-barrier singularity at the boundary of the probability simplex. Removing this technical constraint requires analyzing the singular geometry of the KL divergence on the open simplex, which is essential for understanding singular measures—distributions that collapse entirely onto lower-dimensional manifolds or discrete points without strictly positive support.

**Geometric homogeneity.** We assume the embedding space is a fixed, compact manifold with constant kernel volume (Asm. 2.1). Extending our measure-theoretic analysis to unnormalized or heterogeneous geometries, where the local kernel volume  $V_\kappa(\mathbf{z})$  varies, could bridge to unnormalized contrastive objectives (Bardes et al., 2022), hyperbolic contrastive learning (Desai et al., 2023), and non-contrastive predictive frameworks (Assran et al., 2023).

**Geometry vs. dynamics.** We describe the geometry of the objective, not the trajectory of the algorithm. Understanding how stochastic optimization (Robbins & Monroe, 1951) explores this barrier-ridden landscape, and whether it provably finds the specific “knife-edge” solutions, remains the critical frontier connecting geometric analysis to learning theory.

## 6. Conclusion

This work establishes a measure-theoretic framework for contrastive learning, bridging the stochastic InfoNCE objective to deterministic energy landscapes. Our analysis reveals a bifurcation between unimodal and multimodal regimes. We prove unimodal learning is well-behaved, governed by a convex Gibbs landscape where uniformity acts as an entropic tie-breaker. In contrast, we show the modality gap is not an artifact of initialization or sampling, but a structural necessity of the symmetric InfoNCE objective. It arises from a persistent negative symmetric divergence that induces repulsive, barrier-driven co-adaptation and systematic marginal separation across modalities. By isolating this pathology, our framework shifts focus from parameter-level heuristics to population-level geometry, laying the groundwork for next-generation objectives that bridge the gap at its source while preserving desirable unimodal behavior. Numerical validations are provided in App. D.

## Impact Statement

This paper presents work whose goal is to advance the field of Machine Learning. There are many potential societal consequences of our work, none which we feel must be specifically highlighted here.

## References

Arora, S., Khandeparkar, H., Khodak, M., Plevrakis, O., and Saunshi, N. A theoretical analysis of contrastive unsupervised representation learning. In *36th International Conference on Machine Learning, ICML 2019*, pp. 9904–9923, 2019. <https://arxiv.org/pdf/1902.09229.pdf>.

Assran, M., Duval, Q., Misra, I., Bojanowski, P., Vincent, P., Rabbat, M., LeCun, Y., and Ballas, N. Self-supervised learning from images with a joint-embedding predictive architecture. In *Proceedings of the IEEE/CVF Conference on Computer Vision and Pattern Recognition*, pp. 15619–15629, 2023. <https://doi.org/10.1109/CVPR52729.2023.01499>.

Bardes, A., Ponce, J., and LeCun, Y. VICReg: Variance-invariance-covariance regularization for self-supervised learning. In *International Conference on Learning Representations*, 2022. <https://openreview.net/forum?id=xm6YD62D1Ub>.

Boyd, S. and Vandenberghe, L. *Convex optimization*. Cambridge university press, 2004. [https://stanford.edu/~boyd/cvxbook/bv\\_cvxbook.pdf](https://stanford.edu/~boyd/cvxbook/bv_cvxbook.pdf).

Cai, Y., Liu, Y., Gao, E., Jiang, T., Zhang, Z., van den Hengel, A., and Shi, J. Q. On the value of cross-modal misalignment in multimodal representation learning. In *Advances in Neural Information Processing Systems*, 2025. <https://openreview.net/pdf?id=3KtPujOw5z>.

Chen, T., Kornblith, S., Norouzi, M., and Hinton, G. A simple framework for contrastive learning of visual representations. In *International conference on machine learning*, pp. 1597–1607. PMLR, 2020. <https://proceedings.mlr.press/v119/chen20j/chen20j.pdf>.

Chen, T., Luo, C., and Li, L. Intriguing properties of contrastive losses. *Advances in Neural Information Processing Systems*, 34:11834–11845, 2021. <https://dl.acm.org/doi/10.5555/3540261.3541166>.

Chuang, C.-Y., Robinson, J., Yen-Chen, L., Torralba, A., and Jegelka, S. Debiased contrastive learning. In *NeurIPS*, 2020. <https://dl.acm.org/doi/10.5555/3495724.3496459>.

Daunhawer, I., Bizeul, A., Palumbo, E., Marx, A., and Vogt, J. E. Identifiability results for multimodal contrastive learning. In *The Eleventh International Conference on Learning Representations*, 2023. [https://openreview.net/forum?id=U\\_2kuqoTcB](https://openreview.net/forum?id=U_2kuqoTcB).

Desai, K., Nickel, M., Rajpurohit, T., Johnson, J., and Vedantam, S. R. Hyperbolic image-text representations. In *International Conference on Machine Learning*, pp. 7694–7731. PMLR, 2023. <https://proceedings.mlr.press/v202/desai23a/desai23a.pdf>.

Elfwing, S., Uchibe, E., and Doya, K. Sigmoid-weighted linear units for neural network function approximation in reinforcement learning. *Neural networks*, 107:3–11, 2018. <https://doi.org/10.1016/j.neunet.2017.12.012>.

Gretton, A., Borgwardt, K. M., Rasch, M. J., Schölkopf, B., and Smola, A. A kernel two-sample test. *The journal of machine learning research*, 13(1):723–773, 2012. <https://www.jmlr.org/papers/volume13/gretton12a/gretton12a.pdf>.

Gutmann, M. U. and Hyvärinen, A. Noise-contrastive estimation: A new estimation principle for unnormalized statistical models. In Teh, Y. W. and Titterington, M. (eds.), *Proceedings of the 13th International Conference on Artificial Intelligence and Statistics (AISTATS 2010)*, volume 9 of *Proceedings of Machine Learning Research*, pp. 297–304, Sardinia, Italy, 2010. PMLR. <https://proceedings.mlr.press/v9/gutmann10a/gutmann10a.pdf>.

HaoChen, J. Z. and Ma, T. A theoretical study of inductive biases in contrastive learning. In *The Eleventh International Conference on Learning Representations*, 2023. <https://openreview.net/forum?id=AuEgNlEAmed>.

Hendrycks, D. Gaussian error linear units (gelus). *arXiv preprint arXiv:1606.08415*, 2016. <https://arxiv.org/pdf/1606.08415.pdf>.

Hyvarinen, A. and Morioka, H. Unsupervised feature extraction by time-contrastive learning and nonlinear ica. *Advances in neural information processing systems*, 29, 2016. <https://dl.acm.org/doi/abs/10.5555/3157382.3157519>.

Ji, W., Deng, Z., Nakada, R., Zou, J., and Zhang, L. The power of contrast for feature learning: A theoretical analysis. *Journal of Machine Learning Research*, 24(330):1–78, 2023. <https://jmlr.org/papers/volume24/21-1501/21-1501.pdf>.

Jia, C., Yang, Y., Xia, Y., Chen, Y.-T., Parekh, Z., Pham, H., Le, Q., Sung, Y.-H., Li, Z., and Duerig, T. Scaling up visual and vision-language representation learning with noisy text supervision. In *International conference on machine learning*, pp. 4904–4916. PMLR, 2021. <https://proceedings.mlr.press/v139/jia21b/jia21b.pdf>.

Kingma, D. P. and Ba, J. Adam: A method for stochastic optimization. In *3rd International Conference on Learning Representations (ICLR)*, 2015. <https://arxiv.org/pdf/1412.6980>.

Kornblith, S., Norouzi, M., Lee, H., and Hinton, G. Similarity of neural network representations revisited. In *International conference on machine learning*, pp. 3519–3529. PMLR, 2019. <https://proceedings.mlr.press/v97/kornblith19a/kornblith19a.pdf>.

Lei, Y. and Ying, Y. Fine-grained analysis of stability and generalization for stochastic gradient descent. In *International Conference on Machine Learning*, pp. 5809–5819. PMLR, 2020. <https://proceedings.mlr.press/v119/lei20c/lei20c.pdf>.

Liang, V. W., Zhang, Y., Kwon, Y., Yeung, S., and Zou, J. Y. Mind the gap: Understanding the modality gap in multi-modal contrastive representation learning. *Advances in Neural Information Processing Systems*, 35: 17612–17625, 2022. <https://openreview.net/forum?id=S7Evzt9uit3>.

Liu, Q. and Wang, D. Stein variational gradient descent: A general purpose bayesian inference algorithm. *Advances in neural information processing systems*, 29, 2016. [https://papers.nips.cc/paper\\_files/paper/2016/file/b3ba8f1bee1238a2f37603d90b58898d-Paper.pdf](https://papers.nips.cc/paper_files/paper/2016/file/b3ba8f1bee1238a2f37603d90b58898d-Paper.pdf).

Liu, Y., Zhang, Z., Gong, D., Gao, E., Huang, B., Gong, M., Hengel, A. v. d., Zhang, K., and Shi, J. Q. Beyond dags: A latent partial causal model for multimodal learning. *arXiv preprint arXiv:2402.06223*, 2024. <https://arxiv.org/pdf/2402.06223>.

Loshchilov, I. and Hutter, F. Decoupled weight decay regularization. In *International Conference on Learning Representations*, 2019. <https://openreview.net/forum?id=Bkg6RiCqY7>.

Miyato, T., Kataoka, T., Koyama, M., and Yoshida, Y. Spectral normalization for generative adversarial networks. In *International Conference on Learning Representations*, 2018. <https://openreview.net/forum?id=B1QRgziT->.

Mnih, A. and Teh, Y. W. A fast and simple algorithm for training neural probabilistic language models. In *29th International Conference on Machine Learning, ICML 2012*, 2012. <https://icml.cc/2012/papers/855.pdf>.

Oord, A. v. d., Li, Y., and Vinyals, O. Representation learning with contrastive predictive coding. *arXiv preprint arXiv:1807.03748*, 2018. <https://arxiv.org/abs/1807.03748>.

Poole, B., Ozair, S., van den Oord, A., Alemi, A. A., and Tucker, G. On variational bounds of mutual information. In *Proceedings of the 36th International Conference on Machine Learning*, volume 97, pp. 5171–5180. PMLR, 2019. <https://proceedings.mlr.press/v97/poole19a.html>.

Radford, A., Kim, J. W., Hallacy, C., Ramesh, A., Goh, G., Agarwal, S., Sastry, G., Askell, A., Mishkin, P., Clark, J., et al. Learning transferable visual models from natural language supervision. In *International conference on machine learning*, pp. 8748–8763. PMLR, 2021. <https://proceedings.mlr.press/v139/radford21a/radford21a.pdf>.

Reizinger, P., Guo, S., Huszár, F., Schölkopf, B., and Brendel, W. Identifiable exchangeable mechanisms for causal structure and representation learning. In *The Thirteenth International Conference on Learning Representations*, 2025. <https://openreview.net/forum?id=k03mB41vyM>.

Robbins, H. and Monro, S. A stochastic approximation method. *The annals of mathematical statistics*, pp. 400–407, 1951. <https://www.columbia.edu/~ww2040/8100F16/RM51.pdf>.

Saunshi, N., Ash, J., Goel, S., Misra, D., Zhang, C., Arora, S., Kakade, S., and Krishnamurthy, A. Understanding contrastive learning requires incorporating inductive biases. In *International Conference on Machine Learning*, pp. 19250–19286. PMLR, 2022. <https://proceedings.mlr.press/v162/saunshi22a/saunshi22a.pdf>.

Shi, P., Welle, M. C., Björkman, M., and Krägic, D. Towards understanding the modality gap in clip. In *ICLR 2023 workshop on multimodal representation learning: perks and pitfalls*, 2023. <https://openreview.net/pdf?id=8W3KGzw7fNI>.

Sriperumbudur, B. K., Fukumizu, K., Gretton, A., Schölkopf, B., and Lanckriet, G. R. On integral probability metrics,  $\phi$ -divergences and binary classification. *arXiv preprint arXiv:0901.2698*, 2009. <https://arxiv.org/pdf/0901.2698>.

Székely, G. J. and Rizzo, M. L. Energy statistics: A class of statistics based on distances. *Journal of statistical planning and inference*, 143(8):1249–1272, 2013. <https://doi.org/10.1016/j.jspi.2013.03.018>.

Tian, Y., Krishnan, D., and Isola, P. Contrastive multiview coding. In *European conference on computer vision*, pp. 776–794. Springer, 2020. [https://www.ecva.net/papers/eccv\\_2020/papers\\_ECCV/papers/123560749.pdf](https://www.ecva.net/papers/eccv_2020/papers_ECCV/papers/123560749.pdf).

Tschannen, M., Djolonga, J., Rubenstein, P., Gelly, S., and Lucic, M. On mutual information maximization for representation learning. In *Eighth International Conference on Learning Representations*. OpenReview.net, 2020. <https://openreview.net/forum?id=rkxoh24FPH>.

Udandarao, V., Gupta, A., and Albanie, S. Sus-x: Training-free name-only transfer of vision-language models. In *Proceedings of the IEEE/CVF International Conference on Computer Vision*, pp. 2725–2736, 2023. <https://doi.org/10.1109/ICCV51070.2023.00257>.

Uesaka, T., Suzuki, T., Takida, Y., Lai, C.-H., Murata, N., and Mitsufuji, Y. Weighted point set embedding for multimodal contrastive learning toward optimal similarity metric. In *The Thirteenth International Conference on Learning Representations*, 2025. <https://openreview.net/forum?id=uSz2K30RRd>.

Von Kügelgen, J., Sharma, Y., Greselle, L., Brendel, W., Schölkopf, B., Besserve, M., and Locatello, F. Self-supervised learning with data augmentations provably isolates content from style. *Advances in neural information processing systems*, 34:16451–16467, 2021. [https://openreview.net/forum?id=4pf\\_p0o0Dt](https://openreview.net/forum?id=4pf_p0o0Dt).

Wang, F. and Liu, H. Understanding the behaviour of contrastive loss. In *Proceedings of the IEEE/CVF conference on computer vision and pattern recognition*, pp. 2495–2504, 2021. [https://openaccess.thecvf.com/content/CVPR2021/papers/Wang\\_Understanding\\_the\\_Behaviour\\_of\\_Contrastive\\_Loss\\_CVPR\\_2021\\_paper.pdf](https://openaccess.thecvf.com/content/CVPR2021/papers/Wang_Understanding_the_Behaviour_of_Contrastive_Loss_CVPR_2021_paper.pdf).

Wang, T. and Isola, P. Understanding contrastive representation learning through alignment and uniformity on the hypersphere. In *International conference on machine learning*, pp. 9929–9939. PMLR, 2020. <https://dl.acm.org/doi/10.5555/3524938.3525859>.

Welling, M. and Teh, Y. W. Bayesian learning via stochastic gradient langevin dynamics. In *Proceedings of the 28th international conference on machine learning (ICML-11)*, pp. 681–688, 2011. <https://www.stats.ox.ac.uk/~teh/research/compstats/WelTeh2011a.pdf>.

Yao, D., Xu, D., Lachapelle, S., Magliacane, S., Taslakian, P., Martius, G., von Kügelgen, J., and Locatello, F. Multi-view causal representation learning with partial observability. In *The Twelfth International Conference on Learning Representations*, 2024. <https://openreview.net/forum?id=OGtnhKQJms>.

Yoshida, N., Hayakawa, S., Takida, Y., Uesaka, T., Wakaki, H., and Mitsufuji, Y. Theoretical refinement of clip by utilizing linear structure of optimal similarity. *arXiv preprint arXiv:2510.15508*, 2025. <https://arxiv.org/pdf/2510.15508.pdf>.

Zhang, G., Wang, C., Xu, B., and Grosse, R. Three mechanisms of weight decay regularization. In *International Conference on Learning Representations*, 2019. <https://openreview.net/forum?id=B11z-3Rct7>.

Zimmermann, R. S., Sharma, Y., Schneider, S., Bethge, M., and Brendel, W. Contrastive learning inverts the data generating process. In *International conference on machine learning*, pp. 12979–12990. PMLR, 2021. <https://proceedings.mlr.press/v139/zimmermann21a/zimmermann21a.pdf>.

# Appendix

## Contents

A. Related Work .....	12
B. Justification of Assumptions .....	13
B.1. Justification of Optimization Regularity .....	13
B.2. On the Density Floor in the Multimodal Functional .....	14
C. Proofs of Formal Statements .....	14
C.1. Proof of Prop. 3.1 .....	14
C.2. Proof of Thm. 3.1 .....	16
C.3. Proof of Thm. 3.2 .....	19
C.4. Proof of Prop. 3.2 .....	22
C.5. Proof of Prop. 3.3 .....	23
C.6. Proof of Cor. 3.1 .....	24
C.7. Proof of Prop. 4.1 .....	26
C.8. Proof of Thm. 4.1 .....	27
C.9. Proof of Thm. 4.2 .....	30
C.10. Proof of Prop. 4.2 .....	32
C.11. Proof of Cor. 4.1 .....	34
D. Numerical Validations .....	36
D.1. Large-Batch Gradient Consistency Across Critics .....	36
D.2. Unimodal Gibbs Equilibrium and Low-Temperature Concentration .....	37
D.3. Multimodal Structural Gap under Controlled Misalignment .....	38
E. Broader Implications and Discussion .....	42

## A. Related Work

**Contrastive objectives and density-ratio viewpoints.** InfoNCE is a modern instance of noise-contrastive density-ratio estimation: a positive pair is distinguished from negatives drawn from a background marginal through a softmax normalization, inheriting a long line of NCE-style principles and neural approximations (Gutmann & Hyvärinen, 2010; Mnih & Teh, 2012). In representation learning, InfoNCE was popularized by contrastive predictive coding and is widely used as a scalable surrogate for mutual-information-style criteria (Oord et al., 2018; Poole et al., 2019; Tschanne et al., 2020). Multimodal foundation models such as CLIP (Radford et al., 2021) and ALIGN (Jia et al., 2021) adopt the symmetric (bidirectional) InfoNCE objective as the core pretraining loss.

**Geometric interpretations of contrastive learning.** A prominent theoretical lens studies the *population* landscape induced by InfoNCE, most notably via the alignment–uniformity decomposition on hyperspherical embeddings (Wang & Isola, 2020; Wang & Liu, 2021; Chen et al., 2021). While these works characterize the static properties of the loss minimizers, our contribution focuses on the *optimization dynamics*. By proving large-batch *value and gradient consistency*, we bridge the gap between the stochastic empirical loss and the deterministic energy landscape. This allows us to rigorously analyze the descent directions on the embedding manifold, extending geometric insights beyond the hypersphere to general compact domains.

**Learning-theoretic analyses and objective design.** A separate line develops learning-theoretic guarantees for contrastive representations under stylized data models (e.g., latent-class assumptions) and analyzes how negative sampling, false

negatives, and objective variants affect downstream transfer (Arora et al., 2019; Saunshi et al., 2022; Chuang et al., 2020). Other work analyzes multiview contrastive formulations and the inductive biases of contrastive objectives under simplified model classes (Tian et al., 2020; HaoChen & Ma, 2023; Ji et al., 2023). Recent analyses of CLIP-style training also characterize the structure of optimal similarities, often tied to pointwise mutual information, proposing refinements that better exploit this structure (Uesaka et al., 2025; Yoshida et al., 2025). Our results are orthogonal in emphasis: rather than imposing a specific latent generative model, we characterize the *objective-induced* geometry in a distribution-agnostic, measure-theoretic framework.

**Multimodal contrastive learning and modality gaps.** Multimodal contrastive pretraining has been scaled successfully in CLIP-style systems (Radford et al., 2021; Jia et al., 2021), yet empirical work reports that strong pointwise alignment can coexist with a persistent population-level modality gap (Liang et al., 2022; Udandarao et al., 2023). Our multimodal decomposition provides a mechanistic account of this phenomenon that is absent in unimodal theories: we show that the symmetric objective induces *cross-modal coupling* where each modality’s density shapes the other’s effective field via a *negative* symmetric divergence term. Consequently, we establish that the gap is not merely an initialization artifact, but a structural necessity of the bidirectional loss landscape.

**Orthogonal identifiability analyses.** A related but distinct line of inquiry examines when contrastive objectives identify latent factors under explicit generative assumptions—such as invertible mixing or conditional independence. These studies establish recovery guarantees up to admissible ambiguities (Hyvarinen & Morioka, 2016; Zimmermann et al., 2021; Von Kügelgen et al., 2021; Daunhawer et al., 2023; Yao et al., 2024; Liu et al., 2024; Cai et al., 2025). While these works target *identifiability* (what can be recovered given a data-generating mechanism), our focus lies on the *optimization geometry* (what representation distributions the loss enforces). We view these perspectives as complementary: identifiability results specify when aligned representations are theoretically meaningful, while our mechanistic analysis explains how optimization dynamics realize (or systematically deviate from) those ideal solutions (Reizinger et al., 2025).

## B. Justification of Assumptions

### B.1. Justification of Optimization Regularity

We argue that the regularity conditions in Asm. 3.1 are fully compatible with standard practice in representation learning. We focus on two dominant geometric regimes: the spherical regime used in modern contrastive learning (e.g., CLIP (Radford et al., 2021), SimCLR (Chen et al., 2020)) and the Euclidean regime common in classical kernel methods. Both admit the generalized exponential form  $\kappa_\tau(\mathbf{z}, \mathbf{w}) := \exp(s(\mathbf{z}, \mathbf{w})/\tau)$ .

- *Spherical regime (von Mises–Fisher kernel).* Representations are constrained to the hypersphere  $\mathbb{S}^{d-1}$  via  $\ell_2$  normalization, and the critic is the cosine similarity  $s(\mathbf{z}, \mathbf{w}) = \langle \mathbf{z}, \mathbf{w} \rangle$ :

$$\kappa_{\text{vmf}}(\mathbf{z}, \mathbf{w}) := \exp\left(\frac{\langle \mathbf{z}, \mathbf{w} \rangle}{\tau}\right), \quad \forall \mathbf{z}, \mathbf{w} \in \mathbb{S}^{d-1}. \quad (15)$$

- *Euclidean regime (RBF kernel).* The representations lie in a compact subset of  $\mathbb{R}^d$ , and the critic is the negative squared Euclidean distance  $s(\mathbf{z}, \mathbf{w}) = -\|\mathbf{z} - \mathbf{w}\|^2$ :

$$\kappa_{\text{rbf}}(\mathbf{z}, \mathbf{w}) := \exp\left(-\frac{\|\mathbf{z} - \mathbf{w}\|^2}{\tau}\right). \quad (16)$$

**Encoder regularity.** Condition Asm. 3.1 i) requires that for each  $\mathbf{x}$ , the map  $\theta \mapsto f_\theta(\mathbf{x})$  is  $C^1$  and that its parameter Jacobian is uniformly bounded:  $\sup_{\theta \in \Theta} \sup_{\mathbf{x} \in \mathcal{X}} \|J_\theta f_\theta(\mathbf{x})\| < \infty$ . For standard neural encoders built from differentiable primitives (e.g., linear maps, convolutions, normalization layers) and smooth activations (e.g., GELU (Hendrycks, 2016), SiLU (Elfwing et al., 2018)), the map  $\theta \mapsto f_\theta(\mathbf{x})$  is  $C^1$  (or at least piecewise  $C^1$ , which suffices for almost-everywhere analysis). In practice, uniform Jacobian control is promoted by explicit Lipschitz constraints (e.g., spectral normalization, which bounds layer operator norms and hence the network Jacobian via composition (Miyato et al., 2018)) together with standard norm-regularizing training choices such as weight decay (Loshchilov & Hutter, 2019; Zhang et al., 2019). Accordingly, we interpret compactness of  $\Theta$  as a mild *localization* assumption: although the ambient parameter space

is  $\mathbb{R}^p$ , successful training typically keeps iterates within a bounded region (often formalized as ‘‘SGD iterates belong to a ball’’ in stability analyses (Lei & Ying, 2020)). One may therefore restrict the analysis to a sufficiently large compact subset  $\Theta_R$  containing the training trajectory, or equivalently consider projected updates onto  $\Theta_R$  as standard in constrained optimization (Boyd & Vandenberghe, 2004).

**Critic regularity.** Condition Asm. 3.1 ii) requires that  $s$  is  $C^1$  on an open neighborhood of  $\mathcal{Z} \times \mathcal{Z}$  and that  $\sup_{(\mathbf{z}, \mathbf{w}) \in \mathcal{Z} \times \mathcal{Z}} \|\nabla s(\mathbf{z}, \mathbf{w})\| < \infty$ . In the spherical regime,  $s(\mathbf{z}, \mathbf{w}) = \langle \mathbf{z}, \mathbf{w} \rangle$  is  $C^\infty$  on  $\mathbb{R}^d \times \mathbb{R}^d$  with gradient norms  $\|\nabla_{\mathbf{z}} s\| = \|\mathbf{w}\|$  and  $\|\nabla_{\mathbf{w}} s\| = \|\mathbf{z}\|$ . Since  $\|\mathbf{z}\| = \|\mathbf{w}\| = 1$ , these are uniformly bounded by 1. In the Euclidean regime,  $s(\mathbf{z}, \mathbf{w}) = -\|\mathbf{z} - \mathbf{w}\|^2$  is also  $C^\infty$  with gradients scaling linearly with distance. Thus, provided  $\mathcal{Z}$  is compact (e.g., via bounded activations like  $\tanh$  or explicit clipping),  $\|\nabla s\|$  remains uniformly bounded on  $\mathcal{Z} \times \mathcal{Z}$ .

**Boundedness of the kernel.** For any fixed  $\tau > 0$ , the exponential kernel  $\kappa_\tau = \exp(s/\tau)$  is strictly positive and bounded. For the spherical regime,  $\langle \mathbf{z}, \mathbf{w} \rangle \in [-1, 1]$  implies  $\kappa_{\text{vmf}}(\mathbf{z}, \mathbf{w}) \in [\exp(-1/\tau), \exp(1/\tau)]$ . For the RBF regime on a compact domain with diameter  $D = \text{diam}(\mathcal{Z})$ , we have  $\kappa_{\text{rbf}}(\mathbf{z}, \mathbf{w}) \in [\exp(-D^2/\tau), 1]$ . Crucially, in both cases, the kernel is bounded away from zero ( $\kappa \geq c > 0$ ), ensuring that the logarithmic loss terms are well-defined and Lipschitz continuous.

## B.2. On the Density Floor in the Multimodal Functional

In Def. 4.3 we restrict  $\rho_1, \rho_2$  to  $\mathcal{P}_+(\mathcal{Z}) := \{\rho \in L^1(\mathcal{Z}) : \rho \geq \underline{\rho} \text{ } \mu\text{-a.e.}, \int \rho \, d\mu = 1\}$ . This *density floor* is introduced as a theoretical device to establish the coordinate-collapse statement in Prop. 4.2. The key point is that, for fixed  $\rho_2$ , the coordinate map  $\rho_1 \mapsto \mathcal{F}_{\tau, \mathbf{U}}^{\text{mm}}(\rho_1, \rho_2)$  is concave due to the  $\int \rho_2 \log \rho_1$  term, so minimizing sequences are driven to the boundary of the feasible set. Imposing  $\rho_1 \geq \underline{\rho}$  provides a clean decomposition

$$\rho_1 = \underline{\rho} + \eta, \quad \eta \geq 0, \quad \int \eta \, d\mu =: M_{\text{ex}} = 1 - \underline{\rho} \mu(\mathcal{Z}),$$

which isolates a fixed ‘‘background’’ mass from an ‘‘excess’’ budget  $M_{\text{ex}}$ . This makes the extremal (spike-like) best-response geometry in Prop. 4.2 transparent and quantitatively controllable. The floor also prevents degeneracies intrinsic to the multimodal functional. Because  $\mathcal{F}_{\tau, \mathbf{U}}^{\text{mm}}$  subtracts the symmetric KL term, allowing  $\rho_1$  or  $\rho_2$  to vanish can make  $D_S(\rho_1, \rho_2) = +\infty$  (e.g., if  $\rho_1 = 0$  on a set where  $\rho_2 > 0$ , then  $D_{\text{KL}}(\rho_2 \parallel \rho_1) = +\infty$ ), and hence  $\mathcal{F}_{\tau, \mathbf{U}}^{\text{mm}}(\rho_1, \rho_2) = -\infty$ . In other words, without a positivity constraint the variational problem may become ill-posed and the coordinate minimization problem ceases to describe a meaningful best response.

In the parametric problem, the quantities that enter the large-batch objective are the kernel-smoothed fields  $\tilde{q}_{\theta, \tau}, \tilde{q}_{\phi, \tau}$  (Def. 2.2), rather than the raw pushforwards  $q_\theta, q_\phi$ . Since  $\kappa_\tau(\mathbf{z}, \mathbf{w}) = \exp(s(\mathbf{z}, \mathbf{w})/\tau) > 0$  pointwise, we have

$$\tilde{q}_{\theta, \tau}(\mathbf{z}) = \frac{1}{V_\kappa(\tau)} \int \kappa_\tau(\mathbf{z}, \mathbf{w}) q_\theta(d\mathbf{w}) > 0, \quad \forall \mathbf{z} \in \mathcal{Z},$$

and analogously for  $\tilde{q}_{\phi, \tau}$  for every fixed  $(\theta, \phi)$ . In the sharp-kernel regime  $\tau \downarrow 0^+$ ,  $\tilde{q}_{\theta, \tau}$  approximates  $q_\theta$  in the sense controlled by the KDE error (cf. Thms. 3.2 and 4.2). Thus, the density floor used in the intrinsic best-response analysis is best viewed as a technical device that mirrors the inherent positivity of the effective smoothed quantities at finite  $\tau$ , without requiring a parameter-uniform lower bound over  $\Theta \times \Phi$ .

## C. Proofs of Formal Statements

### C.1. Proof of Prop. 3.1

*Proof.* The proof relies on establishing bounds on the components of the gradient via compactness, then propagating these bounds through the loss structure.

**Step 1: Bounding components in the loss.** Since  $\mathcal{Z}$  is compact, the product  $\mathcal{Z} \times \mathcal{Z}$  is compact. By Asm. 3.1 ii),  $s$  is  $C^1$  on an open neighborhood of  $\mathcal{Z} \times \mathcal{Z}$ , so  $\nabla s$  is continuous on  $\mathcal{Z} \times \mathcal{Z}$  and hence attains its maximum norm on this compact set. For a fixed  $\tau > 0$ , define the temperature-dependent critic sensitivity bound

$$C_s(\tau) := \sup_{(\mathbf{z}, \mathbf{w}) \in \mathcal{Z} \times \mathcal{Z}} \left\| \nabla_{(\mathbf{z}, \mathbf{w})} \left( \frac{1}{\tau} s(\mathbf{z}, \mathbf{w}) \right) \right\| = \frac{1}{\tau} \sup_{(\mathbf{z}, \mathbf{w}) \in \mathcal{Z} \times \mathcal{Z}} \|\nabla s(\mathbf{z}, \mathbf{w})\| < \infty. \quad (17)$$

Next, by Asm. 3.1 i), the encoder Jacobian is uniformly bounded:

$$C_\Theta := \sup_{\theta \in \Theta} \sup_{\mathbf{x} \in \mathcal{X}} \|J_\theta f_\theta(\mathbf{x})\| < \infty. \quad (18)$$

For any  $\mathbf{x}, \mathbf{x}' \in \mathcal{X}$  with representations  $\mathbf{z} = f_\theta(\mathbf{x})$  and  $\mathbf{w} = f_\theta(\mathbf{x}')$ , define  $\alpha_\theta(\mathbf{z}, \mathbf{w}) := \nabla_\theta \left( \frac{1}{\tau} s(\mathbf{z}, \mathbf{w}) \right)$ . By the chain rule,

$$\alpha_\theta(\mathbf{z}, \mathbf{w}) = \nabla_{\mathbf{z}} \left( \frac{1}{\tau} s(\mathbf{z}, \mathbf{w}) \right)^\top J_\theta f_\theta(\mathbf{x}) + \nabla_{\mathbf{w}} \left( \frac{1}{\tau} s(\mathbf{z}, \mathbf{w}) \right)^\top J_\theta f_\theta(\mathbf{x}').$$

Therefore, by the triangle inequality and sub-multiplicativity,

$$\|\alpha_\theta(\mathbf{z}, \mathbf{w})\| \leq \left\| \nabla_{\mathbf{z}} \frac{1}{\tau} s(\mathbf{z}, \mathbf{w}) \right\| \cdot \|J_\theta f_\theta(\mathbf{x})\| + \left\| \nabla_{\mathbf{w}} \frac{1}{\tau} s(\mathbf{z}, \mathbf{w}) \right\| \cdot \|J_\theta f_\theta(\mathbf{x}')\| \leq 2 C_s(\tau) C_\Theta. \quad (19)$$

Thus, the parameter gradient of any pairwise similarity term is uniformly bounded.

**Step 2: Gradient of the empirical partition function.** Fix an anchor  $\mathbf{z} = f_\theta(\mathbf{x})$ , a positive  $\mathbf{v} = f_\theta(\tilde{\mathbf{x}})$ , and negatives  $\{\mathbf{w}_j\}_{j=1}^N$ . Define the contrastive set  $\mathcal{C}(\mathbf{z}) := \{\mathbf{v}\} \cup \{\mathbf{w}_j\}_{j=1}^N$ . The gradient of the log-partition function  $\log Z_{\mathcal{B}}(\mathbf{z}) = \log \sum_{\mathbf{w} \in \mathcal{C}(\mathbf{z})} \exp(s(\mathbf{z}, \mathbf{w})/\tau)$  is given by the softmax-weighted sum of the inner gradients (see e.g. Boyd & Vandenberghe, 2004, p. 74). Since  $\kappa_\tau = \exp(s/\tau) > 0$ , we may differentiate  $\log Z_{\mathcal{B}}$  and write

$$\nabla_\theta \log Z_{\mathcal{B}}(\mathbf{z}) = \sum_{\mathbf{w} \in \mathcal{C}(\mathbf{z})} \sigma_{\mathcal{B}}(\mathbf{w}) \nabla_\theta \log \kappa_\tau(\mathbf{z}, \mathbf{w}) = \sum_{\mathbf{w} \in \mathcal{C}(\mathbf{z})} \sigma_{\mathcal{B}}(\mathbf{w}) \alpha_\theta(\mathbf{z}, \mathbf{w}), \quad (20)$$

where

$$\sigma_{\mathcal{B}}(\mathbf{w}) := \frac{\kappa(\mathbf{z}, \mathbf{w})}{Z_{\mathcal{B}}(\mathbf{z})} \quad \text{satisfies} \quad \sigma_{\mathcal{B}}(\mathbf{w}) \geq 0, \quad \sum_{\mathbf{w} \in \mathcal{C}(\mathbf{z})} \sigma_{\mathcal{B}}(\mathbf{w}) = 1.$$

Therefore, using Eq. (19),

$$\|\nabla_\theta \log Z_{\mathcal{B}}(\mathbf{z})\| \leq \sum_{\mathbf{w} \in \mathcal{C}(\mathbf{z})} \sigma_{\mathcal{B}}(\mathbf{w}) \|\alpha_\theta(\mathbf{z}, \mathbf{w})\| \leq 2 C_s(\tau) C_\Theta \sum_{\mathbf{w} \in \mathcal{C}(\mathbf{z})} \sigma_{\mathcal{B}}(\mathbf{w}) = 2 C_s(\tau) C_\Theta. \quad (21)$$

**Step 3: Bounding the loss gradient.** For a batch  $\mathcal{B}$  and anchor  $\mathbf{z} = f_\theta(\mathbf{x})$ , define the per-batch loss

$$\ell_{\mathcal{B}}(\theta) := -\log \kappa_\tau(\mathbf{z}, \mathbf{v}) + \log Z_{\mathcal{B}}(\mathbf{z}),$$

where  $\mathbf{v} = f_\theta(\tilde{\mathbf{x}})$  is the positive match. Since  $\nabla_\theta \log \kappa_\tau(\mathbf{z}, \mathbf{v}) = \alpha_\theta(\mathbf{z}, \mathbf{v})$ ,

$$\nabla_\theta \ell_{\mathcal{B}}(\theta) = -\alpha_\theta(\mathbf{z}, \mathbf{v}) + \nabla_\theta \log Z_{\mathcal{B}}(\mathbf{z}).$$

By the triangle inequality and Eqs. (19) and (21),

$$\|\nabla_\theta \ell_{\mathcal{B}}(\theta)\| \leq \|\alpha_\theta(\mathbf{z}, \mathbf{v})\| + \|\nabla_\theta \log Z_{\mathcal{B}}(\mathbf{z})\| \leq 2 C_s(\tau) C_\Theta + 2 C_s(\tau) C_\Theta = 4 C_s(\tau) C_\Theta. \quad (22)$$

Finally, the population objective is  $\mathcal{L}_{\text{nce}}(\theta) = \mathbb{E}_{\mathcal{B}}[\ell_{\mathcal{B}}(\theta)]$ . Since  $\ell_{\mathcal{B}}$  is differentiable in  $\theta$  by Asm. 3.1 for each  $\mathcal{B}$  and  $\|\nabla_\theta \ell_{\mathcal{B}}(\theta)\| \leq 4 C_s(\tau) C_\Theta$  provides an integrable dominating function, we may differentiate under the expectation by dominated convergence, obtaining

$$\nabla_\theta \mathcal{L}_{\text{nce}}(\theta) = \mathbb{E}_{\mathcal{B}}[\nabla_\theta \ell_{\mathcal{B}}(\theta)].$$

Taking norms and applying Jensen's inequality yields

$$\|\nabla_\theta \mathcal{L}_{\text{nce}}(\theta)\| \leq \mathbb{E}_{\mathcal{B}}[\|\nabla_\theta \ell_{\mathcal{B}}(\theta)\|] \leq 4 C_s(\tau) C_\Theta.$$

Thus, for each fixed  $\tau > 0$  and any  $N \in \mathbb{N}_+$ , the gradient of unimodal InfoNCE is uniformly bounded over  $\Theta$  by  $C(\tau) := 4 C_s(\tau) C_\Theta$ .  $\square$

## C.2. Proof of Thm. 3.1

*Proof.* Consider a batch  $\mathcal{B}$  consisting of a positive pair and  $N$  independent negative samples. For a specific anchor  $\mathbf{x} \sim p_{\mathbf{x}}$ , the batch is constructed as:

$$\mathcal{B} := \{(\mathbf{x}, \tilde{\mathbf{x}}), \mathbf{x}'_1, \dots, \mathbf{x}'_N\},$$

where the positive partner  $\tilde{\mathbf{x}}$  is sampled from the positive conditional  $r_{\text{um}}(\tilde{\mathbf{x}}|\mathbf{x})$ , and the negative samples  $\{\mathbf{x}'_j\}_{j=1}^N$  are drawn i.i.d. from the marginal observation distribution  $p_{\mathbf{x}}$ . Fix any  $\theta \in \Theta$ , we denote the representations as  $\mathbf{z} = f_{\theta}(\mathbf{x})$ ,  $\mathbf{v} = f_{\theta}(\tilde{\mathbf{x}})$ , and  $\mathbf{w}_j = f_{\theta}(\mathbf{x}'_j)$ . The per-batch unimodal InfoNCE loss  $\ell_{\mathcal{B}}(\theta; \mathbf{x})$  is defined as:

$$\ell_{\mathcal{B}}(\theta; \mathbf{x}) := -\frac{1}{\tau} s(\mathbf{z}, \mathbf{v}) + \log \underbrace{\left( \kappa_{\tau}(\mathbf{z}, \mathbf{v}) + \sum_{j=1}^N \kappa_{\tau}(\mathbf{z}, \mathbf{w}_j) \right)}_{=: Z_{\mathcal{B}}(\mathbf{z})}, \quad (23)$$

where the kernel  $\kappa_{\tau}(\cdot, \cdot) = \exp(s(\cdot, \cdot)/\tau)$  induced by the loss formulation.

**Part (i). Value consistency.** We analyze the asymptotic behavior of the loss as  $N \rightarrow \infty$ .

**Step 1: Isolate the positive bias.** First, we decompose the partition sum  $Z_{\mathcal{B}}$  inside the logarithm into the positive term and the sum over negatives:

$$Z_{\mathcal{B}} = P + S_N, \quad \text{where } P := \kappa_{\tau}(\mathbf{z}, \mathbf{v}), \quad S_N := \sum_{j=1}^N \kappa_{\tau}(\mathbf{z}, \mathbf{w}_j).$$

The logarithmic term  $\log Z_{\mathcal{B}}$  becomes:

$$\log Z_{\mathcal{B}} = \log(S_N + P) = \log S_N + \underbrace{\log(1 + \frac{P}{S_N})}_{=: \epsilon_N}.$$

Fix  $\tau > 0$ . Since  $\mathcal{Z}$  is compact and  $s$  is continuous on  $\mathcal{Z} \times \mathcal{Z}$  by Asm. 3.1 ii), there exist finite constants  $s_{\min}$  and  $s_{\max}$  such that  $s_{\min} \leq s(\mathbf{z}, \mathbf{w}) \leq s_{\max}$  for all  $(\mathbf{z}, \mathbf{w}) \in \mathcal{Z} \times \mathcal{Z}$ . Consequently, the exponential kernel satisfies the bounds

$$0 < m_{\tau} := \exp(s_{\min}/\tau) \leq \kappa_{\tau}(\mathbf{z}, \mathbf{w}) \leq \exp(s_{\max}/\tau) =: M_{\tau} < \infty.$$

Thus,  $m_{\tau} \leq P \leq M_{\tau}$  and  $Nm_{\tau} \leq S_N \leq NM_{\tau}$ . Using  $\log(1 + x) \leq x$  for  $x \geq 0$ ,

$$0 < \epsilon_N = \log\left(1 + \frac{P}{S_N}\right) \leq \frac{P}{S_N} \leq \frac{M_{\tau}}{Nm_{\tau}} = O_{\tau}(N^{-1}).$$

Therefore, for each fixed  $\tau > 0$ ,  $\log Z_{\mathcal{B}} = \log S_N + O_{\tau}(N^{-1})$ .

**Step 2: Concentration of the negative partition sum.** Fix  $\theta$  and an anchor representation  $\mathbf{z} = f_{\theta}(\mathbf{x})$ . For negatives  $\mathbf{x}'_j \stackrel{\text{i.i.d.}}{\sim} p_{\mathbf{x}}$ , define  $\mathbf{w}_j := f_{\theta}(\mathbf{x}'_j)$  and

$$\mathbf{Y}_j(\mathbf{z}) := \kappa_{\tau}(\mathbf{z}, \mathbf{w}_j), \quad S_N(\mathbf{z}) := \sum_{j=1}^N \mathbf{Y}_j(\mathbf{z}).$$

For fixed  $\mathbf{z}$ , the variables  $\{\mathbf{Y}_j(\mathbf{z})\}_{j=1}^N$  are i.i.d. with mean

$$\mu_{\kappa}(\mathbf{z}) := \mathbb{E}[\mathbf{Y}_1(\mathbf{z}) \mid \mathbf{z}] = \int \kappa_{\tau}(\mathbf{z}, \mathbf{w}) d\mathbf{q}_{\theta}(\mathbf{w}) \equiv \Gamma_{\theta, \tau}(\mathbf{z}) \geq m_{\tau},$$

and variance  $\sigma_{\kappa}^2(\mathbf{z}) := \text{Var}(\mathbf{Y}_1(\mathbf{z}) \mid \mathbf{z}) < \infty$ . Moreover, for each fixed  $\tau > 0$ ,  $\kappa_{\tau}$  is bounded on  $\mathcal{Z} \times \mathcal{Z}$ , so  $\mathbf{Y}_j(\mathbf{z})$  is bounded and hence sub-Gaussian. By Hoeffding's inequality, the sample mean concentrates:

$$\frac{S_N(\mathbf{z})}{N} - \mu_{\kappa}(\mathbf{z}) = O_p(N^{-1/2}).$$

Equivalently, writing

$$\frac{S_N(\mathbf{z})}{N\mu_\kappa(\mathbf{z})} = 1 + \Delta_N(\mathbf{z}), \quad \Delta_N(\mathbf{z}) = O_p(N^{-1/2}),$$

and noting  $\mu_\kappa(\mathbf{z}) > 0$  since  $\kappa_\tau > 0$ , we can expand the logarithm with the Taylor expansion  $\log(1 + x) = x + O(x^2)$  and  $\Delta_N(\mathbf{z}) = o_p(1)$ :

$$\log S_N(\mathbf{z}) = \log(N\mu_\kappa(\mathbf{z})) + \log(1 + \Delta_N(\mathbf{z})) = \log N + \log \Gamma_{\theta,\tau}(\mathbf{z}) + O_p(N^{-1/2}),$$

Therefore,

$$\log S_N(\mathbf{z}) = \log N + \log \Gamma_{\theta,\tau}(\mathbf{z}) + O_p(N^{-1/2}).$$

**Step 3: Identification of the induced parametric energy.** Combining Steps 1–2, for an anchor  $\mathbf{z} = f_\theta(\mathbf{x})$  we have

$$\log Z_B(\mathbf{z}) = \log N + \log \Gamma_{\theta,\tau}(\mathbf{z}) + o_p(1),$$

where  $o_p(1)$  denotes a term vanishing in probability as  $N \rightarrow \infty$  (for fixed  $\tau > 0$ ). Substituting into Eq. (23) yields the per-batch expansion

$$\ell_B(\theta; \mathbf{x}) = -\frac{1}{\tau} s(\mathbf{z}, \mathbf{v}) + \log N + \log \Gamma_{\theta,\tau}(\mathbf{z}) + o_p(1). \quad (24)$$

Taking expectations over the batch construction  $(\mathbf{x}, \tilde{\mathbf{x}}) \sim r_{\text{um}}$  and i.i.d. negatives, and using  $\mathcal{L}_{\text{nce}}(\theta) = \mathbb{E}[\ell_B(\theta; \mathbf{x})]$ , we obtain

$$\mathcal{L}_{\text{nce}}(\theta) = \mathbb{E}_{(\mathbf{x}, \tilde{\mathbf{x}})} \left[ -\frac{1}{\tau} s(f_\theta(\mathbf{x}), f_\theta(\tilde{\mathbf{x}})) \right] + \mathbb{E}_{\mathbf{x}} [\log \Gamma_{\theta,\tau}(f_\theta(\mathbf{x}))] + \log N + o(1), \quad (25)$$

where  $o(1) \rightarrow 0$  as  $N \rightarrow \infty$ .

By disintegration of  $\pi_{\theta\theta} = (f_\theta \times f_\theta) \# r_{\text{um}}$ , define  $U_\theta(\mathbf{z}) = -\int s(\mathbf{z}, \mathbf{w}) \nu_{\mathbf{z}}(\mathrm{d}\mathbf{w})$ . Then the law of iterated expectations gives

$$\mathbb{E}_{(\mathbf{x}, \tilde{\mathbf{x}})} \left[ -\frac{1}{\tau} s(\mathbf{z}, \mathbf{v}) \right] = \frac{1}{\tau} \mathbb{E}_{\mathbf{z} \sim q_\theta} [U_\theta(\mathbf{z})] = \frac{1}{\tau} \mathcal{U}(q_\theta). \quad (26)$$

Since  $\mathbf{z} = f_\theta(\mathbf{x}) \sim q_\theta$ , we can rewrite

$$\mathbb{E}_{\mathbf{x}} [\log \Gamma_{\theta,\tau}(f_\theta(\mathbf{x}))] = \mathbb{E}_{\mathbf{z} \sim q_\theta} [\log \Gamma_{\theta,\tau}(\mathbf{z})].$$

Under the constant kernel-volume condition Asm. 2.1,  $\tilde{q}_{\theta,\tau}(\mathbf{z}) = \Gamma_{\theta,\tau}(\mathbf{z})/V_\kappa(\tau)$  (Def. 2.2), hence

$$\mathbb{E}_{\mathbf{z} \sim q_\theta} [\log \Gamma_{\theta,\tau}(\mathbf{z})] = \log V_\kappa(\tau) + \mathbb{E}_{\mathbf{z} \sim q_\theta} [\log \tilde{q}_{\theta,\tau}(\mathbf{z})] = \log V_\kappa(\tau) - H_{\times}(q_\theta, \tilde{q}_{\theta,\tau}), \quad (27)$$

where  $H_{\times}(q_\theta, \tilde{q}_{\theta,\tau}) := -\mathbb{E}_{q_\theta} [\log \tilde{q}_{\theta,\tau}]$  is the cross-entropy.

Substituting Eqs. (26) and (27) into Eq. (25) yields

$$\mathcal{L}_{\text{nce}}(\theta) = \frac{1}{\tau} \mathcal{U}(q_\theta) - H_{\times}(q_\theta, \tilde{q}_{\theta,\tau}) + \log(NV_\kappa(\tau)) + o(1) = \mathcal{J}_\tau(\theta) + \log(NV_\kappa(\tau)) + o(1),$$

where  $\mathcal{J}_\tau(\theta) := \frac{1}{\tau} \mathcal{U}(q_\theta) - H_{\times}(q_\theta, \tilde{q}_{\theta,\tau})$ . Since  $\theta$  is arbitrarily chosen from  $\Theta$  and  $\Theta$  is compact by Asm. 3.1, this proves Eq. (4) of Thm. 3.1 for any fixed  $\theta \in \Theta$ .

**Part (ii). Gradient consistency.** We now analyze the gradient dynamics of the batch loss  $\ell_B(\theta; \mathbf{x})$ . Fix  $\tau > 0$  in the limit of  $N \rightarrow \infty$ . Differentiating Eq. (24) with respect to  $\theta$  yields

$$\nabla_\theta \ell_B(\theta; \mathbf{x}) = -\frac{1}{\tau} \nabla_\theta s(\mathbf{z}, \mathbf{v}) + \nabla_\theta \log Z_B(\mathbf{z}), \quad Z_B(\mathbf{z}) = \mathsf{P} + \mathsf{S}_N, \quad (28)$$

where  $\mathsf{P} := \kappa_\tau(\mathbf{z}, \mathbf{v})$  and  $\mathsf{S}_N := \sum_{j=1}^N \kappa_\tau(\mathbf{z}, \mathbf{w}_j)$ .

**Step 1: Removing the positive term in the log-partition gradient.** Let

$$\mathbf{g}_N(\mathbf{z}) := \nabla_\theta \log(\mathsf{P} + \mathsf{S}_N), \quad \mathbf{r}_N(\mathbf{z}) := \nabla_\theta \log \mathsf{S}_N.$$

Then

$$\begin{aligned}
 \mathbf{g}_N - \mathbf{r}_N &= \nabla_{\theta} \log(\mathbf{P} + \mathbf{S}_N) - \nabla_{\theta} \log \mathbf{S}_N \\
 &= \frac{\nabla_{\theta} \mathbf{P} + \nabla_{\theta} \mathbf{S}_N}{\mathbf{P} + \mathbf{S}_N} - \frac{\nabla_{\theta} \mathbf{S}_N}{\mathbf{S}_N} \\
 &= \frac{\nabla_{\theta} \mathbf{P}}{\mathbf{P} + \mathbf{S}_N} + \nabla_{\theta} \mathbf{S}_N \left( \frac{\mathbf{S}_N - (\mathbf{P} + \mathbf{S}_N)}{\mathbf{S}_N(\mathbf{P} + \mathbf{S}_N)} \right) \\
 &= \frac{\nabla_{\theta} \mathbf{P}}{\mathbf{P} + \mathbf{S}_N} - \frac{\mathbf{P}}{\mathbf{S}_N(\mathbf{P} + \mathbf{S}_N)} \nabla_{\theta} \mathbf{S}_N.
 \end{aligned} \tag{29}$$

Under Asm. 3.1, the continuity of  $s$  on the compact domain  $\mathcal{Z} \times \mathcal{Z}$  ensures the kernel  $\kappa_{\tau}$  is uniformly bounded. Furthermore, expanding  $\nabla_{\theta} \kappa_{\tau}$  via the chain rule yields a product of terms—specifically the kernel, the critic gradient, and the encoder Jacobian—that are all uniformly bounded by assumption. Thus, for any fixed  $\tau > 0$ , there exist finite constants  $M_{\tau}, G_{\tau}$  such that  $0 < \kappa_{\tau} \leq M_{\tau}$  and  $\|\nabla_{\theta} \kappa_{\tau}\| \leq G_{\tau}$ . Moreover, since  $\kappa_{\tau}$  is continuous and strictly positive on the compact  $\mathcal{Z} \times \mathcal{Z}$ , it attains a positive minimum  $m_{\tau} > 0$ . Hence  $\mathbf{P} \leq M_{\tau}$ ,  $\|\nabla_{\theta} \mathbf{P}\| \leq G_{\tau}$ ,  $\mathbf{S}_N \geq Nm_{\tau}$ , and  $\|\nabla_{\theta} \mathbf{S}_N\| \leq NG_{\tau}$ .

Taking norms in Eq. (29) and using these bounds gives

$$\|\mathbf{g}_N - \mathbf{r}_N\| \leq \frac{G_{\tau}}{Nm_{\tau}} + \frac{M_{\tau}}{(Nm_{\tau})^2} \cdot NG_{\tau} = O(N^{-1}).$$

Therefore,

$$\nabla_{\theta} \log Z_{\mathcal{B}}(\mathbf{z}) = \nabla_{\theta} \log \mathbf{S}_N(\mathbf{z}) + O(N^{-1}). \tag{30}$$

**Step 2: Consistency of the negative-sum ratio.** Write

$$\nabla_{\theta} \log \mathbf{S}_N(\mathbf{z}) = \frac{\nabla_{\theta} \mathbf{S}_N(\mathbf{z})}{\mathbf{S}_N(\mathbf{z})} = \frac{\frac{1}{N} \sum_{j=1}^N \nabla_{\theta} \kappa_{\tau}(\mathbf{z}, \mathbf{w}_j)}{\frac{1}{N} \sum_{j=1}^N \kappa_{\tau}(\mathbf{z}, \mathbf{w}_j)}.$$

Conditioning on the anchor  $\mathbf{z}$ , the negatives  $\mathbf{w}_j$  are i.i.d. with law  $q_{\theta}$ , and both  $\kappa_{\tau}(\mathbf{z}, \mathbf{w})$  and  $\nabla_{\theta} \kappa_{\tau}(\mathbf{z}, \mathbf{w})$  are bounded (by Prop. 3.1). Thus by the law of large numbers,

$$\frac{1}{N} \sum_{j=1}^N \kappa_{\tau}(\mathbf{z}, \mathbf{w}_j) \xrightarrow{p} \Gamma_{\theta, \tau}(\mathbf{z}), \quad \frac{1}{N} \sum_{j=1}^N \nabla_{\theta} \kappa_{\tau}(\mathbf{z}, \mathbf{w}_j) \xrightarrow{p} \mathbb{E}_{\mathbf{w} \sim q_{\theta}} [\nabla_{\theta} \kappa_{\tau}(\mathbf{z}, \mathbf{w})].$$

As  $q_{\theta} = (f_{\theta})_{\#} p_{\mathbf{x}}$  and  $\sup_{\theta \in \Theta, \mathbf{x} \in \mathcal{X}} \|\nabla_{\theta} \kappa_{\tau}(\mathbf{z}, f_{\theta}(\mathbf{x}))\| < \infty$  by Asm. 3.1, differentiation under the integral sign is justified (e.g., by dominated convergence). Thus, for each fixed  $\mathbf{z}$ ,

$$\mathbb{E}_{\mathbf{w} \sim q_{\theta}} [\nabla_{\theta} \kappa_{\tau}(\mathbf{z}, \mathbf{w})] = \mathbb{E}_{\mathbf{x} \sim p_{\mathbf{x}}} [\nabla_{\theta} \kappa_{\tau}(\mathbf{z}, f_{\theta}(\mathbf{x}))] = \nabla_{\theta} \mathbb{E}_{\mathbf{x} \sim p_{\mathbf{x}}} [\kappa_{\tau}(\mathbf{z}, f_{\theta}(\mathbf{x}))] = \nabla_{\theta} \mathbb{E}_{\mathbf{w} \sim q_{\theta}} [\kappa_{\tau}(\mathbf{z}, \mathbf{w})] = \nabla_{\theta} \Gamma_{\theta, \tau}(\mathbf{z}).$$

Because  $\|\nabla_{\theta} \kappa_{\tau}\|$  is bounded, we can interchange gradient and expectation:

$$\mathbb{E}_{\mathbf{w} \sim q_{\theta}} [\nabla_{\theta} \kappa_{\tau}(\mathbf{z}, \mathbf{w})] = \nabla_{\theta} \mathbb{E}_{\mathbf{w} \sim q_{\theta}} [\kappa_{\tau}(\mathbf{z}, \mathbf{w})] = \nabla_{\theta} \Gamma_{\theta, \tau}(\mathbf{z}).$$

Since  $\Gamma_{\theta, \tau}(\mathbf{z}) \geq m_{\tau} > 0$ , the continuous mapping theorem yields

$$\nabla_{\theta} \log \mathbf{S}_N(\mathbf{z}) \xrightarrow{p} \frac{\nabla_{\theta} \Gamma_{\theta, \tau}(\mathbf{z})}{\Gamma_{\theta, \tau}(\mathbf{z})} = \nabla_{\theta} \log \Gamma_{\theta, \tau}(\mathbf{z}). \tag{31}$$

Combining Eqs. (30) and (31) gives

$$\nabla_{\theta} \log Z_{\mathcal{B}}(\mathbf{z}) \xrightarrow{p} \nabla_{\theta} \log \Gamma_{\theta, \tau}(\mathbf{z}). \tag{32}$$

**Step 3: Passing to the population objective and identifying  $\nabla_{\theta} \mathcal{J}_{\tau}$ .** Recall  $\mathcal{L}_{\text{nce}}(\theta) = \mathbb{E}_{\mathcal{B}}[\ell_{\mathcal{B}}(\theta; \mathbf{x})]$  and  $\nabla_{\theta} \mathcal{L}_{\text{nce}}(\theta) = \mathbb{E}_{\mathcal{B}}[\nabla_{\theta} \ell_{\mathcal{B}}(\theta; \mathbf{x})]$  by Prop. 3.1. From Eq. (28) and Eq. (32), we have the pointwise (in the batch randomness) convergence

$$\nabla_{\theta} \ell_{\mathcal{B}}(\theta; \mathbf{x}) = -\frac{1}{\tau} \nabla_{\theta} s(\mathbf{z}, \mathbf{v}) + \nabla_{\theta} \log Z_{\mathcal{B}}(\mathbf{z}) \xrightarrow{p} -\frac{1}{\tau} \nabla_{\theta} s(\mathbf{z}, \mathbf{v}) + \nabla_{\theta} \log \Gamma_{\theta, \tau}(\mathbf{z}).$$

Moreover, by Prop. 3.1,  $\|\nabla_\theta \ell_B\|$  is uniformly bounded, so we may use dominated convergence together with Eq. (32) to interchange  $\lim_{N \rightarrow \infty}$  and expectation:

$$\nabla_\theta \mathcal{L}_{\text{nce}}(\theta) = \mathbb{E}_B[\nabla_\theta \ell_B(\theta; \mathbf{x})] \longrightarrow -\frac{1}{\tau} \mathbb{E}_{r_{\text{um}}}[\nabla_\theta s(f_\theta(\mathbf{x}), f_\theta(\tilde{\mathbf{x}}))] + \mathbb{E}_{\mathbf{x} \sim p_{\mathbf{x}}}[\nabla_\theta \log \Gamma_{\theta, \tau}(f_\theta(\mathbf{x}))]. \quad (\star)$$

We now identify the two terms in  $(\star)$  as the gradient of the parametric energy  $\mathcal{J}_\tau(\theta) := \frac{1}{\tau} \mathcal{U}(q_\theta) - H_\times(q_\theta, \tilde{q}_{\theta, \tau})$ .

Define the alignment potential as a function of  $\theta$  by

$$\mathcal{U}(q_\theta) := \mathbb{E}_{(\mathbf{x}, \tilde{\mathbf{x}}) \sim r_{\text{um}}}[-s(f_\theta(\mathbf{x}), f_\theta(\tilde{\mathbf{x}}))].$$

Under Asm. 3.1,  $\nabla_\theta s$  is bounded on the relevant compact set, so we may differentiate under the expectation to obtain

$$\nabla_\theta \mathcal{U}(q_\theta) = -\mathbb{E}_{r_{\text{um}}}[\nabla_\theta s(f_\theta(\mathbf{x}), f_\theta(\tilde{\mathbf{x}}))].$$

Therefore the first term in  $(\star)$  equals  $\frac{1}{\tau} \nabla_\theta \mathcal{U}(q_\theta)$ .

By definition,

$$H_\times(q_\theta, \tilde{q}_{\theta, \tau}) := -\mathbb{E}_{\mathbf{z} \sim q_\theta}[\log \tilde{q}_{\theta, \tau}(\mathbf{z})] = -\mathbb{E}_{\mathbf{x} \sim p_{\mathbf{x}}}[\log \tilde{q}_{\theta, \tau}(f_\theta(\mathbf{x}))].$$

Under Asm. 2.1,  $\tilde{q}_{\theta, \tau}(\mathbf{z}) = \Gamma_{\theta, \tau}(\mathbf{z})/V_\kappa(\tau)$  with  $V_\kappa(\tau)$  constant in  $\theta$  (Def. 2.2). Hence

$$\nabla_\theta H_\times(q_\theta, \tilde{q}_{\theta, \tau}) = -\mathbb{E}_{\mathbf{x}}[\nabla_\theta \log \tilde{q}_{\theta, \tau}(f_\theta(\mathbf{x}))] = -\mathbb{E}_{\mathbf{x}}[\nabla_\theta \log \Gamma_{\theta, \tau}(f_\theta(\mathbf{x}))],$$

where differentiation under the expectation is justified by boundedness of  $\nabla_\theta \log \Gamma_{\theta, \tau}(f_\theta(\mathbf{x}))$ . Thus the second term in  $(\star)$  equals  $-\nabla_\theta H_\times(q_\theta, \tilde{q}_{\theta, \tau})$ . This gives

$$\nabla_\theta \mathcal{L}_{\text{nce}}(\theta) \longrightarrow \frac{1}{\tau} \nabla_\theta \mathcal{U}(q_\theta) - \nabla_\theta H_\times(q_\theta, \tilde{q}_{\theta, \tau}) = \nabla_\theta \mathcal{J}_\tau(\theta),$$

which proves gradient consistency with the cross-entropy-induced energy  $\mathcal{J}_\tau$  for each fixed  $\tau > 0$ . Since  $\theta$  is arbitrarily chosen from  $\Theta$ , this proves Eq. (5) of Thm. 3.1.  $\square$

### C.3. Proof of Thm. 3.2

Before establishing the proof of Thm. 3.2, we introduce the following lemma:

**Lemma C.1** (Vanishing KDE error by sharp-peak smoothing). *Assume Asms. 2.1, 3.1 and 3.2. Fix  $\theta \in \Theta$  and suppose  $q_\theta$  admits a continuous  $\mu$ -density on  $\mathcal{Z}$  that is bounded away from zero, i.e.  $q_\theta := \inf_{\mathbf{z} \in \mathcal{Z}} q_\theta(\mathbf{z}) > 0$ . Let  $\varepsilon_{\text{kde}}^{(\theta)}(\tau) := \|\tilde{q}_{\theta, \tau} - q_\theta\|_\infty$  denote the KDE approximation error in Def. 3.4. Then, as  $\tau \downarrow 0^+$ ,  $\varepsilon_{\text{kde}}^{(\theta)}(\tau) \rightarrow 0$ .*

*Proof.* Fix any  $\theta \in \Theta$ . Let  $d(\cdot, \cdot)$  denote the geodesic distance on the compact Riemannian manifold  $\mathcal{Z}$  as in Asm. 3.2. Since  $\mathcal{Z}$  is compact and  $q_\theta$  is continuous,  $q_\theta$  is bounded. Define the normalized kernel

$$\bar{\kappa}_\tau(\mathbf{z}, \mathbf{w}) := \frac{\kappa_\tau(\mathbf{z}, \mathbf{w})}{V_\kappa(\tau)}.$$

We first show that  $\bar{\kappa}_\tau$  concentrates near the diagonal  $\{\mathbf{z} = \mathbf{w}\}$  as  $\tau \downarrow 0^+$ , and then prove Lem. C.1.

**Step 1: Uniform concentration of  $\bar{\kappa}_\tau$  near the diagonal.** Fix any  $\delta \in (0, r)$ , where  $r$  is from Asm. 3.2, and define

$$\mathcal{A}_\delta := \{(\mathbf{z}, \mathbf{w}) \in \mathcal{Z} \times \mathcal{Z} : d(\mathbf{z}, \mathbf{w}) \geq \delta\}.$$

By compactness of  $\mathcal{Z}$ , the set  $\mathcal{A}_\delta$  is compact. Since  $s$  is continuous by Asm. 3.1, consider the continuous function

$$g(\mathbf{z}, \mathbf{w}) := s(\mathbf{z}, \mathbf{z}) - s(\mathbf{z}, \mathbf{w}).$$

By Asm. 3.2, for each fixed  $\mathbf{z}$  the map  $\mathbf{w} \mapsto s(\mathbf{z}, \mathbf{w})$  has a unique maximizer at  $\mathbf{w} = \mathbf{z}$ ; hence  $g(\mathbf{z}, \mathbf{w}) > 0$  whenever  $d(\mathbf{z}, \mathbf{w}) \geq \delta$ . Therefore  $g$  is strictly positive on  $\mathcal{A}_\delta$ , and by compactness it attains a strictly positive minimum:

$$m_\delta := \min_{(\mathbf{z}, \mathbf{w}) \in \mathcal{A}_\delta} g(\mathbf{z}, \mathbf{w}) > 0.$$

Equivalently, for all  $\mathbf{z} \in \mathcal{Z}$  and all  $\mathbf{w} \in \mathcal{Z}$  with  $d(\mathbf{z}, \mathbf{w}) \geq \delta$ ,

$$s(\mathbf{z}, \mathbf{w}) \leq s(\mathbf{z}, \mathbf{z}) - m_\delta. \quad (33)$$

Fix  $\eta \in (0, \delta)$ . By compactness of  $\mathcal{Z}$ , choose a finite cover  $\mathcal{Z} \subset \bigcup_{i=1}^M B(\mathbf{z}_i, \eta/2)$ . For any  $\mathbf{z} \in \mathcal{Z}$ , pick  $i$  such that  $\mathbf{z} \in B(\mathbf{z}_i, \eta/2)$ ; then  $B(\mathbf{z}_i, \eta/2) \subset B(\mathbf{z}, \eta)$  by the triangle inequality. Hence

$$\mu(B(\mathbf{z}, \eta)) \geq \min_{1 \leq i \leq M} \mu(B(\mathbf{z}_i, \eta/2)) =: b_\eta > 0,$$

where positivity holds because  $\mu$  has full support on the manifold.

Now, let  $\delta \in (0, r)$  be as above and choose  $\eta \in (0, \delta)$  so that

$$m_2 \eta^2 < m_\delta, \quad (34)$$

where  $m_2$  is the constant in Asm. 3.2. This is possible since  $m_\delta > 0$ . Then, for  $\mathbf{w} \in B(\mathbf{z}, \eta) \subset B(\mathbf{z}, r)$ , the lower quadratic bound in Asm. 3.2 gives

$$s(\mathbf{z}, \mathbf{w}) \geq s(\mathbf{z}, \mathbf{z}) - m_2 d(\mathbf{z}, \mathbf{w})^2 \geq s(\mathbf{z}, \mathbf{z}) - m_2 \eta^2,$$

so

$$\kappa_\tau(\mathbf{z}, \mathbf{w}) \geq \exp(s(\mathbf{z}, \mathbf{z})/\tau) \exp(-m_2 \eta^2/\tau).$$

Integrating over  $B(\mathbf{z}, \eta)$  and using  $\mu(B(\mathbf{z}, \eta)) \geq b_\eta$  yields the uniform lower bound

$$V_\kappa(\tau) = \int \kappa_\tau(\mathbf{z}, \mathbf{w}) d\mu(\mathbf{w}) \geq b_\eta \exp(s(\mathbf{z}, \mathbf{z})/\tau) \exp(-m_2 \eta^2/\tau). \quad (35)$$

Here, by Asm. 2.1,  $V_\kappa(\tau)$  is independent of  $\mathbf{z}$ . (The factor  $\exp(s(\mathbf{z}, \mathbf{z})/\tau)$  cancels in the ratio below.)

Next, for  $\mathbf{w} \notin B(\mathbf{z}, \delta)$  we have  $d(\mathbf{z}, \mathbf{w}) \geq \delta$ , so by Eq. (33),

$$\kappa_\tau(\mathbf{z}, \mathbf{w}) = \exp(s(\mathbf{z}, \mathbf{w})/\tau) \leq \exp(s(\mathbf{z}, \mathbf{z})/\tau) \exp(-m_\delta/\tau).$$

Therefore, with  $V_\mu := \mu(\mathcal{Z}) < \infty$ ,

$$\int_{\mathcal{Z} \setminus B(\mathbf{z}, \delta)} \kappa_\tau(\mathbf{z}, \mathbf{w}) d\mu(\mathbf{w}) \leq V_\mu \exp(s(\mathbf{z}, \mathbf{z})/\tau) \exp(-m_\delta/\tau). \quad (36)$$

Dividing Eq. (36) by Eq. (35) and using Eq. (34) yields, uniformly in  $\mathbf{z}$ ,

$$\int_{\mathcal{Z} \setminus B(\mathbf{z}, \delta)} \bar{\kappa}_\tau(\mathbf{z}, \mathbf{w}) d\mu(\mathbf{w}) \leq \frac{V_\mu}{b_\eta} \exp\left(-\frac{m_\delta - m_2 \eta^2}{\tau}\right) \xrightarrow{\tau \downarrow 0^+} 0. \quad (37)$$

**Step 2: Sup-norm convergence of the smoothing.** Fix  $\varepsilon > 0$ . Since  $q_\theta$  is continuous on compact  $\mathcal{Z}$ , it is uniformly continuous. By uniform continuity in  $\mathbf{z}$  of  $q_\theta$  for each fixed  $\theta \in \Theta$ , choose  $\delta \in (0, r)$  such that

$$|q_\theta(\mathbf{w}) - q_\theta(\mathbf{z})| \leq \varepsilon \quad \text{whenever } d(\mathbf{z}, \mathbf{w}) < \delta.$$

For any  $\mathbf{z} \in \mathcal{Z}$ , write

$$\tilde{q}_{\theta, \tau}(\mathbf{z}) - q_\theta(\mathbf{z}) = \int \bar{\kappa}_\tau(\mathbf{z}, \mathbf{w}) (q_\theta(\mathbf{w}) - q_\theta(\mathbf{z})) d\mu(\mathbf{w}),$$

and split the integral over  $B(\mathbf{z}, \delta)$  and its complement. Using  $\int \bar{\kappa}_\tau(\mathbf{z}, \mathbf{w}) d\mu(\mathbf{w}) = 1$ , the bound on  $B(\mathbf{z}, \delta)$ , and  $|q_\theta(\mathbf{w}) - q_\theta(\mathbf{z})| \leq 2\|q_\theta\|_\infty$  everywhere, we obtain

$$|\tilde{q}_{\theta, \tau}(\mathbf{z}) - q_\theta(\mathbf{z})| \leq \varepsilon + 2\|q_\theta\|_\infty \int_{\mathcal{Z} \setminus B(\mathbf{z}, \delta)} \bar{\kappa}_\tau(\mathbf{z}, \mathbf{w}) d\mu(\mathbf{w}).$$

By the boundedness of  $q_\theta$ , taking the supremum over  $\mathbf{z} \in \mathcal{Z}$  and invoking Eq. (37) gives

$$\limsup_{\tau \downarrow 0^+} \|\tilde{q}_{\theta, \tau} - q_\theta\|_\infty \leq \varepsilon.$$

Since  $\varepsilon > 0$  is arbitrary, and by the non-negativity of norm,  $\liminf_{\tau \downarrow 0^+} \|\tilde{q}_{\theta, \tau} - q_\theta\|_\infty \geq 0$ . Therefore, for each fixed  $\theta \in \Theta$ ,

$$\varepsilon_{\text{kde}}^{(\theta)}(\tau) := \|\tilde{q}_{\theta, \tau} - q_\theta\|_\infty \xrightarrow{\tau \downarrow 0^+} 0$$

□

Now, we proceed to prove Thm. 3.2:

*Proof. Step 1: Well-posedness of the alignment potential term.* Fix any  $\theta \in \Theta$ . By disintegration of the positive-pair measure  $\pi_{\theta\theta}$  with respect to its first marginal  $q_\theta$ , there exists a Markov kernel  $\{\nu_{\theta, \mathbf{z}}\}_{\mathbf{z} \in \mathcal{Z}}$  such that

$$\pi_{\theta\theta}(\mathrm{d}\mathbf{z}, \mathrm{d}\mathbf{w}) = q_\theta(\mathrm{d}\mathbf{z}) \nu_{\theta, \mathbf{z}}(\mathrm{d}\mathbf{w}).$$

Recall the definition of the alignment potential (Def. 3.1) for  $q_\theta$ -a.e.  $\mathbf{z}$  by

$$U_\theta(\mathbf{z}) := - \int s(\mathbf{z}, \mathbf{w}) \nu_{\theta, \mathbf{z}}(\mathrm{d}\mathbf{w}).$$

Under Asm. 3.1, the critic  $s$  is bounded and Borel measurable, hence  $U_\theta$  is Borel measurable and bounded, and therefore integrable with respect to  $q_\theta$ . Moreover, the expected potential can be written without any density:

$$\mathcal{U}_\theta(q_\theta) := \int U_\theta(\mathbf{z}) q_\theta(\mathrm{d}\mathbf{z}) = - \iint s(\mathbf{z}, \mathbf{w}) \pi_{\theta\theta}(\mathrm{d}\mathbf{z}, \mathrm{d}\mathbf{w}).$$

Consequently, the intrinsic representation energy (Def. 3.3)

$$\mathcal{F}_{\tau, U_\theta}(q_\theta) := \frac{1}{\tau} \mathcal{U}_\theta(q_\theta) - H(q_\theta)$$

is well-defined for each  $\tau > 0$ .

*Step 2: Difference reduces to a KL divergence.* Recall

$$\mathcal{J}_\tau(\theta) = \frac{1}{\tau} \mathcal{U}_\theta(q_\theta) - H_{\times}(q_\theta, \tilde{q}_{\theta, \tau}).$$

Using  $H_{\times}(q, \tilde{q}) = H(q) + D_{\text{KL}}(q\| \tilde{q})$ , we obtain

$$\mathcal{J}_\tau(\theta) = \frac{1}{\tau} \mathcal{U}_\theta(q_\theta) - H(q_\theta) - D_{\text{KL}}(q_\theta\| \tilde{q}_{\theta, \tau}),$$

and hence

$$\mathcal{F}_{\tau, U_\theta}(q_\theta) - \mathcal{J}_\tau(\theta) = D_{\text{KL}}(q_\theta\| \tilde{q}_{\theta, \tau}). \quad (38)$$

*Step 3: Vanishing KL divergence of the smoothing.* Fix any  $\theta \in \Theta$ . By assumption  $\inf_{\mathbf{z} \in \mathcal{Z}} q_\theta(\mathbf{z}) \geq \underline{q}_\theta > 0$  and Lem. C.1, there exists  $\tau_0(\theta) > 0$  such that for all  $\tau \leq \tau_0(\theta)$ ,

$$\varepsilon_{\text{kde}}^{(\theta)}(\tau) := \|\tilde{q}_{\theta, \tau} - q_\theta\|_\infty \leq \frac{\underline{q}_\theta}{2}.$$

Then for all  $\mathbf{z}$ ,

$$\tilde{q}_{\theta, \tau}(\mathbf{z}) \geq q_\theta(\mathbf{z}) - \frac{\underline{q}_\theta}{2} \geq \frac{\underline{q}_\theta}{2}. \quad (39)$$

On  $[\underline{q}_\theta/2, \infty)$ , the derivative of  $\log x$  is  $1/x \leq 2/\underline{q}_\theta$ . Hence for all  $a, b > \underline{q}_\theta/2$ ,

$$|\log a - \log b| \leq \frac{2}{\underline{q}_\theta} |a - b|.$$

Apply this with  $a = q_\theta(\mathbf{z})$  and  $b = \tilde{q}_{\theta, \tau}(\mathbf{z})$ . Therefore,

$$\left| \log \frac{q_\theta(\mathbf{z})}{\tilde{q}_{\theta, \tau}(\mathbf{z})} \right| = |\log q_\theta(\mathbf{z}) - \log \tilde{q}_{\theta, \tau}(\mathbf{z})| \leq \frac{2}{\underline{q}_\theta} |q_\theta(\mathbf{z}) - \tilde{q}_{\theta, \tau}(\mathbf{z})| \leq \frac{2 \varepsilon_{\text{kde}}^{(\theta)}(\tau)}{\underline{q}_\theta}. \quad (40)$$

Now

$$D_{\text{KL}}(q_{\theta} \| \tilde{q}_{\theta, \tau}) = \int q_{\theta}(\mathbf{z}) \log \frac{q_{\theta}(\mathbf{z})}{\tilde{q}_{\theta, \tau}(\mathbf{z})} d\mu(\mathbf{z}).$$

Using  $\int q_{\theta} d\mu = 1$  and Eq. (40),

$$D_{\text{KL}}(q_{\theta} \| \tilde{q}_{\theta, \tau}) \leq \int q_{\theta}(\mathbf{z}) \left| \log \frac{q_{\theta}(\mathbf{z})}{\tilde{q}_{\theta, \tau}(\mathbf{z})} \right| d\mu(\mathbf{z}) \leq \frac{2 \varepsilon_{\text{kde}}^{(\theta)}(\tau)}{q_{\theta}}. \quad (41)$$

Substituting this to Eq. (38) yields

$$|\mathcal{J}_{\tau}(\theta) - \mathcal{F}_{\tau, U_{\theta}}(q_{\theta})| \leq \frac{2 \varepsilon_{\text{kde}}^{(\theta)}(\tau)}{q_{\theta}}.$$

Moreover, by Lem. C.1,  $\varepsilon_{\text{kde}}^{(\theta)}(\tau) \rightarrow 0$  as  $\tau \downarrow 0^+$ ; thus,  $|\mathcal{J}_{\tau}(\theta) - \mathcal{F}_{\tau, U_{\theta}}(q_{\theta})| \xrightarrow{\tau \downarrow 0^+} 0$ , completing the proof.  $\square$

#### C.4. Proof of Prop. 3.2

*Proof.* We analyze the properties of the functional  $\mathcal{F}_{\tau, U} : \mathcal{P}(\mathcal{Z}) \rightarrow \mathbb{R}$  defined on the space of probability densities  $\mathcal{P}(\mathcal{Z}) = \{\rho \in L^1(\mathcal{Z}) : \rho \geq 0 \text{ } \mu\text{-a.e.}, \int \rho d\mu = 1\}$ . The proof proceeds in three steps: establishing the geometry of the domain, proving the convexity of the energy functional, and deriving the unique minimizer.

**Step 1: Convexity of the domain  $\mathcal{P}(\mathcal{Z})$ .** First, we verify that the optimization domain  $\mathcal{P}(\mathcal{Z})$  is a convex set. Consider any two densities  $\rho_1, \rho_2 \in \mathcal{P}(\mathcal{Z})$  and a mixing coefficient  $\lambda \in (0, 1)$ . Define the interpolation  $\rho_{\lambda} := \lambda \rho_1 + (1 - \lambda) \rho_2$ . We observe that  $\rho_{\lambda}$  satisfies the following two conditions. (i) Non-negativity: Since  $\rho_1, \rho_2 \geq 0$  and  $\lambda \in (0, 1)$  by construction,  $\rho_{\lambda} \geq 0$   $\mu$ -a.e. (ii) Normalization: By the linearity of the integral,  $\int \rho_{\lambda} = \lambda \int \rho_1 d\mu + (1 - \lambda) \int \rho_2 d\mu = 1$ . Therefore,  $\rho_{\lambda} \in \mathcal{P}(\mathcal{Z})$  for any  $\lambda \in (0, 1)$ , confirming that the space of valid densities  $\mathcal{P}(\mathcal{Z})$  is a convex set.

**Step 2: Strict functional convexity.** Let  $\rho_1, \rho_2 \in \mathcal{P}(\mathcal{Z})$  be two distinct densities (i.e.,  $\rho_1 \not\equiv \rho_2$  almost everywhere) and let  $\lambda \in (0, 1)$  be a mixing coefficient. Define the convex combination  $\rho_{\lambda} := \lambda \rho_1 + (1 - \lambda) \rho_2$ . We now analyze the two components of  $\mathcal{F}_{\tau, U}(\rho_{\lambda})$  separately.

In the binding energy term  $\frac{1}{\tau} \mathcal{U}(\rho)$ , since  $U(\mathbf{z})$  acts as a fixed coefficient relative to  $\rho$  for fixed  $\tau > 0$ , the total binding energy  $\frac{1}{\tau} \mathcal{U}(\rho) = \frac{1}{\tau} \int \rho(\mathbf{z}) U(\mathbf{z}) d\mu(\mathbf{z})$  is therefore a linear functional. By the linearity of the Lebesgue integral:

$$\begin{aligned} \frac{1}{\tau} \mathcal{U}(\rho_{\lambda}) &= \frac{1}{\tau} \int (\lambda \rho_1(\mathbf{z}) + (1 - \lambda) \rho_2(\mathbf{z})) U(\mathbf{z}) d\mu(\mathbf{z}) \\ &= \frac{\lambda}{\tau} \int \rho_1(\mathbf{z}) U(\mathbf{z}) d\mu(\mathbf{z}) + \frac{1 - \lambda}{\tau} \int \rho_2(\mathbf{z}) U(\mathbf{z}) d\mu(\mathbf{z}) \\ &= \frac{\lambda}{\tau} \mathcal{U}(\rho_1) + \frac{1 - \lambda}{\tau} \mathcal{U}(\rho_2). \end{aligned}$$

The entropy term is  $-H(\rho) = \int \rho \log \rho d\mu$ , with the convention  $0 \log 0 = 0$ . Since  $\phi(t) = t \log t$  is strictly convex on  $(0, \infty)$  and convex on  $[0, \infty)$ , we have

$$\int \phi(\rho_{\lambda}) d\mu < \lambda \int \phi(\rho_1) d\mu + (1 - \lambda) \int \phi(\rho_2) d\mu$$

whenever  $\rho_1 \not\equiv \rho_2$  (i.e., they differ on a set of positive  $\mu$ -measure). Hence  $-H$  is strictly convex on  $\mathcal{P}(\mathcal{Z})$ . Combining the two parts:

$$\begin{aligned} \mathcal{F}_{\tau, U}(\rho_{\lambda}) &= \frac{1}{\tau} \mathcal{U}(\rho_{\lambda}) - H(\rho_{\lambda}) \\ &< \frac{\lambda}{\tau} \mathcal{U}(\rho_1) + \frac{1 - \lambda}{\tau} \mathcal{U}(\rho_2) + \lambda(-H(\rho_1)) + (1 - \lambda)(-H(\rho_2)) \\ &= \lambda \mathcal{F}_{\tau, U}(\rho_1) + (1 - \lambda) \mathcal{F}_{\tau, U}(\rho_2). \end{aligned}$$

Therefore, the functional  $\mathcal{F}_{\tau, U}(\rho)$  is strictly convex over the space of probability densities  $\mathcal{P}(\mathcal{Z})$ .

**Step 3: Existence and uniqueness of global minimizer.** Since  $\mathcal{F}_{\tau, U}(\rho)$  is strictly convex on the convex domain  $\mathcal{P}(\mathcal{Z})$ , any local minimizer is the unique global minimizer. For fixed  $\tau > 0$ , we solve for the optimal density  $\rho^* \in \mathcal{P}(\mathcal{Z})$  using the

method of Lagrange multipliers. Define the Lagrangian  $\Lambda(\rho, \gamma)$  to enforce the normalization constraint  $\int \rho(\mathbf{z}) d\mu(\mathbf{z}) = 1$ :

$$\Lambda(\rho, \gamma) := \mathcal{F}_{\tau, U}(\rho) + \gamma \left( \int \rho(\mathbf{z}) d\mu(\mathbf{z}) - 1 \right).$$

Taking the functional derivative with respect to  $\rho(\mathbf{z})$  and setting it to zero:

$$\begin{aligned} \frac{\delta \Lambda}{\delta \rho(\mathbf{z})} &= \int \frac{\delta}{\delta \rho(\mathbf{z})} [\rho(\mathbf{w}) (\frac{1}{\tau} U(\mathbf{w}) + \log \rho(\mathbf{w}) + \gamma)] d\mu(\mathbf{w}) \\ &= = \frac{1}{\tau} U(\mathbf{z}) + \log \rho(\mathbf{z}) + 1 + \gamma. \\ &= 0. \end{aligned}$$

Solving for  $\rho^*(\mathbf{z})$ :

$$\log \rho^*(\mathbf{z}) = -\frac{U(\mathbf{z})}{\tau} - \gamma - 1 \implies \rho^*(\mathbf{z}) = \frac{1}{\exp(\gamma + 1)} \exp\left(-\frac{U(\mathbf{z})}{\tau}\right),$$

where the first term of the right-hand side is a constant determined by the normalization constraint. Therefore, the unique minimizer is the Gibbs distribution:

$$\rho^*(\mathbf{z}) = \frac{1}{Z_\tau} \cdot \exp\left(-\frac{U(\mathbf{z})}{\tau}\right), \quad \text{where } Z_\tau = \int \exp\left(-\frac{U(\mathbf{z})}{\tau}\right) d\mu(\mathbf{w}).$$

Since  $\text{ess inf}_\mu U > -\infty$  by assumption, we have  $U(\mathbf{z}) \geq m$  for  $\mu$ -a.e.  $\mathbf{z}$ . Hence

$$0 < Z_\tau = \int_{\mathcal{Z}} e^{-U(\mathbf{z})/\tau} d\mu(\mathbf{z}) \leq e^{-m/\tau} \mu(\mathcal{Z}) < \infty,$$

so  $\rho^*$  is well-defined. This confirms that the system admits a unique Gibbs equilibrium characterized by the potential  $U$ .  $\square$

### C.5. Proof of Prop. 3.3

*Proof.* We analyze the Gibbs-equilibrium measure  $\rho^* \mu$  as  $\tau \downarrow 0^+$ . Let

$$m := \text{ess inf}_\mu U \quad \text{and} \quad \mathcal{W}^\sigma := \left\{ \mathbf{z} \in \mathcal{Z} : U(\mathbf{z}) \leq m + \sigma \right\},$$

for an arbitrarily small but fixed  $\sigma > 0$ .

Consider any open set  $\mathcal{O} \subset \mathcal{Z}$  such that  $\mathcal{O} \supset \mathcal{W}^\sigma$ , and denote  $\mathcal{O}^c := \mathcal{Z} \setminus \mathcal{O}$ . Since  $\mathcal{O}$  contains  $\mathcal{W}^\sigma$ , its complement satisfies

$$\mathcal{O}^c \subset \{ \mathbf{z} \in \mathcal{Z} : U(\mathbf{z}) > m + \sigma \}.$$

Therefore, using  $\rho^*(\mathbf{z}) = \frac{1}{Z_\tau} \exp(-U(\mathbf{z})/\tau)$ ,

$$(\rho^* \mu)(\mathcal{O}^c) = \frac{\int_{\mathcal{O}^c} \exp(-U(\mathbf{z})/\tau) d\mu(\mathbf{z})}{\int_{\mathcal{Z}} \exp(-U(\mathbf{w})/\tau) d\mu(\mathbf{w})}.$$

Multiplying numerator and denominator by  $\exp(m/\tau)$  yields

$$(\rho^* \mu)(\mathcal{O}^c) = \frac{\int_{\mathcal{O}^c} \exp(-(U(\mathbf{z}) - m)/\tau) d\mu(\mathbf{z})}{\int_{\mathcal{Z}} \exp(-(U(\mathbf{w}) - m)/\tau) d\mu(\mathbf{w})}.$$

(i) *Numerator bound.* For all  $\mathbf{z} \in \mathcal{O}^c$  we have  $U(\mathbf{z}) - m \geq \sigma$ , hence

$$\int_{\mathcal{O}^c} \exp\left(-\frac{U(\mathbf{z}) - m}{\tau}\right) d\mu(\mathbf{z}) \leq \int_{\mathcal{O}^c} \exp\left(-\frac{\sigma}{\tau}\right) d\mu(\mathbf{z}) = \mu(\mathcal{O}^c) \exp\left(-\frac{\sigma}{\tau}\right).$$

(ii) *Denominator lower bound.* By the definition of  $m = \text{ess inf}_\mu U$ , for any  $\eta > 0$  the set  $\{\mathbf{z} \in \mathcal{Z} : U(\mathbf{z}) < m + \eta\}$  has strictly positive  $\mu$ -measure. Fix  $\eta := \sigma/2$  and define

$$\mathcal{A} := \left\{ \mathbf{w} \in \mathcal{Z} \mid U(\mathbf{w}) < m + \sigma/2 \right\}, \quad \text{so that} \quad \mu(\mathcal{A}) > 0.$$

On  $\mathcal{A}$  we have  $U(\mathbf{w}) - m < \sigma/2$ , hence

$$\int \exp\left(-\frac{U(\mathbf{w}) - m}{\tau}\right) d\mu(\mathbf{w}) \geq \int_{\mathcal{A}} \exp\left(-\frac{U(\mathbf{w}) - m}{\tau}\right) d\mu(\mathbf{w}) \geq \mu(\mathcal{A}) \exp\left(-\frac{\sigma}{2\tau}\right).$$

Combining the bounds, we obtain

$$(\rho^* \mu)(\mathcal{O}^c) \leq \frac{\mu(\mathcal{O}^c) \exp(-\sigma/\tau)}{\mu(\mathcal{A}) \exp(-\sigma/(2\tau))} = \frac{\mu(\mathcal{O}^c)}{\mu(\mathcal{A})} \exp\left(-\frac{\sigma}{2\tau}\right).$$

Since  $\mu(\mathcal{O}^c) \leq \mu(\mathcal{Z}) < \infty$  and  $\mu(\mathcal{A}) > 0$  is fixed, the right-hand side converges to 0 as  $\tau \downarrow 0^+$ . Hence, for any open neighborhood  $\mathcal{O} \supset \mathcal{W}^\sigma$ , we have  $(\rho^* \mu)(\mathcal{O}^c) \rightarrow 0$ , i.e., the Gibbs measure concentrates in any neighborhood of  $\mathcal{W}^\sigma$ .  $\square$

### C.6. Proof of Cor. 3.1

*Proof. Step 1: Well-defined “best achievable” equilibrium.* We first isolate the intrinsic quantity that governs the “best achievable” equilibrium value at temperature  $\tau$ . Fix any  $\theta \in \Theta$  and  $\tau > 0$ . By Asm. 2.1,  $\mathcal{Z}$  is compact with  $\mu(\mathcal{Z}) < \infty$ ; and by Asm. 3.1,  $s : \mathcal{Z} \times \mathcal{Z} \rightarrow \mathbb{R}$  is continuous. Then, by the extreme value theorem,  $s$  is bounded on  $\mathcal{Z} \times \mathcal{Z}$ :

$$S_{\max} := \max_{\mathbf{z}, \mathbf{w} \in \mathcal{Z}} s(\mathbf{z}, \mathbf{w}) < \infty.$$

The induced alignment potential (Def. 3.1) is  $U_\theta(\mathbf{z}) = - \int s(\mathbf{z}, \mathbf{w}) \nu_{\theta, \mathbf{z}}(d\mathbf{w})$ , hence  $U_\theta(\mathbf{z}) \geq -S_{\max}$  for all  $\mathbf{z}$ . Therefore, for any fixed  $\tau > 0$ ,

$$0 < \exp\left(-\frac{U_\theta(\mathbf{z})}{\tau}\right) \leq \exp\left(\frac{S_{\max}}{\tau}\right) \quad \text{for all } \mathbf{z} \in \mathcal{Z},$$

and thus

$$0 < Z_{\theta, \tau} := \int_{\mathcal{Z}} \exp\left(-\frac{U_\theta(\mathbf{z})}{\tau}\right) d\mu(\mathbf{z}) \leq \mu(\mathcal{Z}) \exp\left(\frac{S_{\max}}{\tau}\right) < \infty.$$

Thus, the representational energy  $\mathcal{F}_{\tau, U_\theta}(\rho) = \frac{1}{\tau} \int U_\theta \rho d\mu - H(\rho)$  admits the unique Gibbs minimizer  $\rho_\theta^* \propto e^{-U_\theta/\tau}$  (Prop. 3.2). The corresponding minimum is

$$\inf_{\rho \in \mathcal{P}(\mathcal{Z})} \mathcal{F}_{\tau, U_\theta}(\rho) = \mathcal{F}_{\tau, U_\theta}(\rho_\theta^*) = -\log Z_{\theta, \tau}, \quad Z_{\theta, \tau} := \int \exp\left(-\frac{U_\theta(\mathbf{z})}{\tau}\right) d\mu(\mathbf{z}). \quad (42)$$

We interpret  $-\log Z_{\theta, \tau}$  as the lowest representation energy level induced by the potential  $U_\theta$ , which is the best intrinsic value attainable by *any* density in  $\mathcal{P}(\mathcal{Z})$  once  $U_\theta$  is fixed.

*Step 2: Representation energy gap equals a KL-divergence.* Fix  $\theta$  and  $\tau$ . Recall that, by Prop. 3.2, the unique Gibbs equilibrium is

$$\rho_\theta^*(\mathbf{z}) = \frac{\exp(-U_\theta(\mathbf{z})/\tau)}{Z_{\theta, \tau}},$$

we have the pointwise identity

$$\log \rho_\theta^*(\mathbf{z}) = -\frac{U_\theta(\mathbf{z})}{\tau} - \log Z_{\theta, \tau}.$$

Define the KL divergence  $D_{\text{KL}}(q_\theta \| \rho_\theta^*)$ . Expanding yields

$$\begin{aligned}
 D_{\text{KL}}(q_\theta \| \rho_\theta^*) &= \int q_\theta(\mathbf{z}) \log \frac{q_\theta(\mathbf{z})}{\rho_\theta^*(\mathbf{z})} d\mu(\mathbf{z}) \\
 &= \int q_\theta \log q_\theta d\mu - \int q_\theta \log \rho_\theta^* d\mu \\
 &= \int q_\theta \log q_\theta d\mu - \int q_\theta \left( -\frac{U_\theta}{\tau} - \log Z_{\theta,\tau} \right) d\mu \\
 &= \frac{1}{\tau} \int U_\theta q_\theta d\mu + \int q_\theta \log q_\theta d\mu + \log Z_{\theta,\tau} \int q_\theta d\mu \\
 &= \mathcal{F}_{\tau,U_\theta}(q_\theta) + \log Z_{\theta,\tau}.
 \end{aligned}$$

Finally, by Eq. (42),  $\inf_{\rho \in \mathcal{P}(\mathcal{Z})} \mathcal{F}_{\tau,U_\theta}(\rho) = \mathcal{F}_{\tau,U_\theta}(\rho^*) = -\log Z_{\theta,\tau}$ , hence

$$\mathcal{F}_{\tau,U_\theta}(q_\theta) - \inf_{\rho \in \mathcal{P}(\mathcal{Z})} \mathcal{F}_{\tau,U_\theta}(\rho) = \mathcal{F}_{\tau,U_\theta}(q_\theta) + \log Z_{\theta,\tau} = D_{\text{KL}}(q_\theta \| \rho_\theta^*). \quad (43)$$

**Step 3: Transfer ground-state concentration to  $q_{\theta^*}$ .** Define the approximation error

$$\eta_\tau(\theta) := |\mathcal{J}_\tau(\theta) - \mathcal{F}_{\tau,U_\theta}(q_\theta)|,$$

which satisfies  $\eta_\tau(\theta) \rightarrow 0$  for each fixed  $\theta \in \Theta$  as  $\tau \downarrow 0^+$ , by Thm. 3.2. Let  $\theta^* \in \arg \min_{\theta \in \Theta} \mathcal{J}_\tau(\theta)$ , and let  $\hat{\theta} \in \arg \min_{\theta \in \Theta} (-\log Z_{\theta,\tau})$  as defined in Cor. 3.1. By optimality,  $\mathcal{J}_\tau(\theta^*) \leq \mathcal{J}_\tau(\hat{\theta})$ , hence

$$\mathcal{F}_{\tau,U_{\theta^*}}(q_{\theta^*}) \leq \mathcal{J}_\tau(\theta^*) + \eta_\tau(\theta^*) \leq \mathcal{J}_\tau(\hat{\theta}) + \eta_\tau(\theta^*) \leq \mathcal{F}_{\tau,U_{\hat{\theta}}}(q_{\hat{\theta}}) + \eta_\tau(\theta^*) + \eta_\tau(\hat{\theta}).$$

Adding  $\log Z_{\theta^*,\tau}$  and using  $\log Z_{\theta^*,\tau} \leq \log Z_{\hat{\theta},\tau}$  by definition of  $\hat{\theta}$ , we obtain

$$\begin{aligned}
 \mathcal{F}_{\tau,U_{\theta^*}}(q_{\theta^*}) + \log Z_{\theta^*,\tau} &\leq \mathcal{F}_{\tau,U_{\hat{\theta}}}(q_{\hat{\theta}}) + \log Z_{\theta^*,\tau} + \eta_\tau(\theta^*) + \eta_\tau(\hat{\theta}) \\
 &\leq \mathcal{F}_{\tau,U_{\hat{\theta}}}(q_{\hat{\theta}}) + \log Z_{\hat{\theta},\tau} + \eta_\tau(\theta^*) + \eta_\tau(\hat{\theta}).
 \end{aligned}$$

Substituting Eq. (8) yields

$$\mathcal{F}_{\tau,U_{\theta^*}}(q_{\theta^*}) + \log Z_{\theta^*,\tau} \leq \varepsilon_{\text{real}}(\tau) + \eta_\tau(\theta^*) + \eta_\tau(\hat{\theta}).$$

Invoking Eq. (43) at  $\theta = \theta^*$  yields

$$D_{\text{KL}}(q_{\theta^*} \| \rho_{\theta^*}^*) \leq \varepsilon_{\text{real}}(\tau) + \eta_\tau(\theta^*) + \eta_\tau(\hat{\theta}) \xrightarrow{\tau \downarrow 0^+} 0.$$

Hence, by Pinsker's inequality,

$$\|q_{\theta^*} - \rho_{\theta^*}^*\|_{\text{TV}} \leq \sqrt{\frac{1}{2} D_{\text{KL}}(q_{\theta^*} \| \rho_{\theta^*}^*)} \xrightarrow{\tau \downarrow 0^+} 0. \quad (44)$$

Now fix any open set  $\mathcal{O} \subset \mathcal{Z}$  with  $\mathcal{O} \supset \mathcal{W}_{\theta^*}^\sigma$ , where  $\mathcal{W}_{\theta^*}^\sigma := \{\mathbf{z} \in \mathcal{Z} \mid U_{\theta^*}(\mathbf{z}) \leq \text{ess inf}_\mu U_{\theta^*} + \sigma\}$  with any fixed  $\sigma > 0$ . Applying Prop. 3.3 to the potential  $U_{\theta^*}$  gives the Gibbs concentration

$$(\rho_{\theta^*}^* \mu)(\mathcal{Z} \setminus \mathcal{O}) \xrightarrow{\tau \downarrow 0^+} 0.$$

Finally, by the variational characterization of total variation, for any measurable  $\mathcal{A}$ ,  $|q_{\theta^*} \mu(\mathcal{A}) - \rho_{\theta^*}^* \mu(\mathcal{A})| \leq \|q_{\theta^*} - \rho_{\theta^*}^*\|_{\text{TV}}$ . Taking  $\mathcal{A} = \mathcal{Z} \setminus \mathcal{O}$  and combining with Eq. (44) yields

$$(q_{\theta^*} \mu)(\mathcal{Z} \setminus \mathcal{O}) \leq (\rho_{\theta^*}^* \mu)(\mathcal{Z} \setminus \mathcal{O}) + \|q_{\theta^*} - \rho_{\theta^*}^*\|_{\text{TV}} \xrightarrow{\tau \downarrow 0^+} 0,$$

which is the desired ground-state concentration.  $\square$

### C.7. Proof of Prop. 4.1

*Proof. Step 1: Uniform bounds on components.* We retain the bound on the similarity critic sensitivity  $C_s(\tau)$  from Eq. (17). For the encoders, we define the uniform bound on the Jacobians over the joint space, which is guaranteed by Asm. 4.1. Let  $C_\Theta$  and  $C_\Phi$  be the maximal sensitivities:

$$C_\Theta := \sup_{\theta \in \Theta} \sup_{\mathbf{x} \in \mathcal{X}} \|J_\theta f_\theta(\mathbf{x})\| < \infty, \quad C_\Phi := \sup_{\phi \in \Phi} \sup_{\mathbf{y} \in \mathcal{Y}} \|J_\phi g_\phi(\mathbf{y})\| < \infty.$$

We define the global encoder constant  $C_{\text{enc}} := \max(C_\Theta, C_\Phi)$ . Consider a generic cross-modal representation pair  $(\mathbf{z}, \mathbf{w})$  where  $\mathbf{z}$  depends on  $\theta$  and  $\mathbf{w}$  depends on  $\phi$ . The gradient of the kernel term  $\kappa_\tau(\mathbf{z}, \mathbf{w})$  with respect to the joint parameter vector  $(\theta, \phi)$  splits into block components. Using Eq. (19), the partial gradients satisfy:

$$\|\nabla_\theta \log \kappa_\tau(\mathbf{z}, \mathbf{w})\| \leq C_s(\tau) C_\Theta \leq C_s(\tau) C_{\text{enc}}, \quad \|\nabla_\phi \log \kappa_\tau(\mathbf{z}, \mathbf{w})\| \leq C_s(\tau) C_\Phi \leq C_s(\tau) C_{\text{enc}}. \quad (45)$$

**Step 2: Bounding directional partial derivatives.** Define a training batch  $\mathcal{B}$  as a collection of  $N + 1$  independent pairs: a primary positive pair  $(\mathbf{x}, \mathbf{y})$  and  $N$  negative keys  $\{\mathbf{y}'_j\}_{j=1}^N$  (and similarly in reverse). The symmetric loss is the average of two directional losses computed on this batch:

$$\ell_S(\mathcal{B}) = \frac{1}{2} (\ell_{\theta \rightarrow \phi}(\mathcal{B}) + \ell_{\phi \rightarrow \theta}(\mathcal{B})).$$

By the triangle inequality, the norm of the joint gradient satisfies:

$$\|\nabla_{(\theta, \phi)} \ell_S\| \leq \frac{1}{2} \|\nabla_{(\theta, \phi)} \ell_{\theta \rightarrow \phi}\| + \frac{1}{2} \|\nabla_{(\theta, \phi)} \ell_{\phi \rightarrow \theta}\|.$$

We first analyze the forward component  $\ell_{\theta \rightarrow \phi}$ . Here,  $\mathbf{x}$  serves as the anchor,  $\mathbf{y}$  as the positive key, and the set  $\{\mathbf{y}'_j\}_{j=1}^N$  as the negative keys. The loss is:

$$\ell_{\theta \rightarrow \phi} := -\log \kappa_\tau(f_\theta(\mathbf{x}), g_\phi(\mathbf{y})) + \log \left( \kappa_\tau(f_\theta(\mathbf{x}), g_\phi(\mathbf{y})) + \sum_{j=1}^N \kappa_\tau(f_\theta(\mathbf{x}), g_\phi(\mathbf{y}'_j)) \right).$$

Crucially, the joint gradient vector is the concatenation  $\nabla_{(\theta, \phi)} \ell_{\theta \rightarrow \phi} = (\nabla_\theta \ell_{\theta \rightarrow \phi}^\top, \nabla_\phi \ell_{\theta \rightarrow \phi}^\top)^\top$ . We bound the partial gradients of  $\ell_{\theta \rightarrow \phi}$  with respect to each parameter block separately. Note that the set of key representations in the batch is  $\mathcal{C}_\phi = \{g_\phi(\mathbf{y})\} \cup \{g_\phi(\mathbf{y}'_j)\}_{j=1}^N$ , and we denote the softmax probability assigned to any key  $\mathbf{v} \in \mathcal{C}_\phi$  as  $\sigma(\mathbf{v})$ .

(i) Gradient with respect to  $\theta$  (anchor sensitivity): In this direction,  $\theta$  governs only the anchor  $f_\theta(\mathbf{x})$ ; the keys  $\mathcal{C}_\phi$  are constant. We expand the gradient of the loss as the alignment term plus the gradient of the log-partition function:

$$\nabla_\theta \ell_{\theta \rightarrow \phi} = -\nabla_\theta \log \kappa_\tau(f_\theta(\mathbf{x}), g_\phi(\mathbf{y})) + \sum_{\mathbf{v} \in \mathcal{C}_\phi} \sigma(\mathbf{v}) \nabla_\theta \log \kappa_\tau(f_\theta(\mathbf{x}), \mathbf{v}).$$

Applying the triangle inequality and the uniform sensitivity bound  $C_s(\tau) C_\Theta$  derived in Eq. (45):

$$\begin{aligned} \|\nabla_\theta \ell_{\theta \rightarrow \phi}\| &\leq \|\nabla_\theta \log \kappa_\tau(f_\theta(\mathbf{x}), g_\phi(\mathbf{y}))\| + \sum_{\mathbf{v} \in \mathcal{C}_\phi} \sigma(\mathbf{v}) \|\nabla_\theta \log \kappa_\tau(f_\theta(\mathbf{x}), \mathbf{v})\| \\ &\leq C_s(\tau) C_\Theta + C_s(\tau) C_\Theta \sum_{\mathbf{v} \in \mathcal{C}_\phi} \sigma(\mathbf{v}) \\ &= 2C_s(\tau) C_\Theta. \quad (\text{Since } \sum_{\mathbf{v} \in \mathcal{C}_\phi} \sigma(\mathbf{v}) = 1) \end{aligned}$$

(ii) Gradient with respect to  $\phi$  (key sensitivity): In this direction,  $\phi$  parametrizes every key in the batch (both positive and negative), while the anchor  $f_\theta(\mathbf{x})$  acts as a constant. The gradient is:

$$\nabla_\phi \ell_{\theta \rightarrow \phi} = -\nabla_\phi \log \kappa_\tau(f_\theta(\mathbf{x}), g_\phi(\mathbf{y})) + \sum_{\mathbf{v} \in \mathcal{C}_\phi} \sigma(\mathbf{v}) \nabla_\phi \log \kappa_\tau(f_\theta(\mathbf{x}), \mathbf{v}).$$

Similarly, applying the triangle inequality and the sensitivity bound  $C_s(\tau)C_\Phi$ :

$$\|\nabla_\phi \ell_{\theta \rightarrow \phi}\| \leq C_s(\tau)C_\Phi + C_s(\tau)C_\Phi \sum_{\mathbf{v} \in \mathcal{C}_\phi} \sigma(\mathbf{v}) = 2C_s(\tau)C_\Phi.$$

**Step 3: Global uniform bound.** Based on the above analysis, the total gradient magnitude for the forward loss is bounded by the vector norm:

$$\|\nabla_{(\theta, \phi)} \ell_{\theta \rightarrow \phi}\| = \sqrt{\|\nabla_\theta \ell_{\theta \rightarrow \phi}\|^2 + \|\nabla_\phi \ell_{\theta \rightarrow \phi}\|^2} \leq \sqrt{(2C_s(\tau)C_\Theta)^2 + (2C_s(\tau)C_\Phi)^2} \leq 2\sqrt{2}C_s(\tau)C_{\text{enc}}.$$

By symmetry, the exact same bound applies to the backward loss  $\ell_{\phi \rightarrow \theta}$ . Therefore, the batch loss gradient is bounded by:

$$\|\nabla_{(\theta, \phi)} \ell_S\| = \frac{1}{2} \|\nabla_{(\theta, \phi)} \ell_{\theta \rightarrow \phi} + \nabla_{(\theta, \phi)} \ell_{\phi \rightarrow \theta}\| \leq \frac{1}{2} (\|\nabla_{(\theta, \phi)} \ell_{\theta \rightarrow \phi}\| + \|\nabla_{(\theta, \phi)} \ell_{\phi \rightarrow \theta}\|) = 2\sqrt{2}C_s(\tau)C_{\text{enc}}.$$

Since  $\|\nabla_{(\theta, \phi)} \ell_S(\mathcal{B})\|$  is uniformly bounded and  $\ell_S$  is differentiable a.e. in  $(\theta, \phi)$ , we may differentiate under the expectation by dominated convergence, yielding

$$\|\nabla_{(\theta, \phi)} \mathcal{L}_{\text{mm}}\| = \|\nabla_{\theta, \phi} \mathbb{E}_{\mathcal{B}}[\ell_S]\| \leq \mathbb{E}_{\mathcal{B}}[\|\nabla \ell_S\|] \leq 2\sqrt{2}C_s(\tau)C_{\text{enc}}.$$

Defining  $C := 2\sqrt{2}C_s(\tau)C_{\text{enc}} < \infty$ , the gradient is uniformly bounded over  $\Theta \times \Phi$ , concluding the proof.  $\square$

### C.8. Proof of Thm. 4.1

*Proof.* Consider a batch  $\mathcal{B}$  consisting of a positive pair  $(\mathbf{x}, \mathbf{y}) \sim r_{\text{mm}}$  together with  $N$  i.i.d. negatives  $\{\mathbf{y}'_j\}_{j=1}^N \stackrel{\text{i.i.d.}}{\sim} p_{\mathbf{y}}$  and  $N$  i.i.d. negatives  $\{\mathbf{x}'_j\}_{j=1}^N \stackrel{\text{i.i.d.}}{\sim} p_{\mathbf{x}}$ , all independent conditional on  $(\mathbf{x}, \mathbf{y})$ . Write the representations

$$\mathbf{z} = f_\theta(\mathbf{x}), \quad \mathbf{w} = g_\phi(\mathbf{y}), \quad \mathbf{w}'_j = g_\phi(\mathbf{y}'_j), \quad \mathbf{z}'_j = f_\theta(\mathbf{x}'_j),$$

and define the exponential kernel  $\kappa_\tau(\cdot, \cdot) = \exp(s(\cdot, \cdot)/\tau)$ . Denote the directional partition sums

$$Z_{\mathcal{B}}^{\theta \rightarrow \phi}(\mathbf{z}) := \kappa_\tau(\mathbf{z}, \mathbf{w}) + \sum_{j=1}^N \kappa_\tau(\mathbf{z}, \mathbf{w}'_j), \quad Z_{\mathcal{B}}^{\phi \rightarrow \theta}(\mathbf{w}) := \kappa_\tau(\mathbf{z}, \mathbf{w}) + \sum_{j=1}^N \kappa_\tau(\mathbf{z}'_j, \mathbf{w}).$$

The symmetric per-batch loss can be written as

$$\ell_{\mathcal{B}}^{\text{sym}}(\theta, \phi) = \frac{1}{2} \underbrace{(-\frac{1}{\tau} s(\mathbf{z}, \mathbf{w}) + \log Z_{\mathcal{B}}^{\theta \rightarrow \phi}(\mathbf{z}))}_{\ell_{\mathcal{B}}^{\theta \rightarrow \phi}(\theta, \phi)} + \frac{1}{2} \underbrace{(-\frac{1}{\tau} s(\mathbf{z}, \mathbf{w}) + \log Z_{\mathcal{B}}^{\phi \rightarrow \theta}(\mathbf{w}))}_{\ell_{\mathcal{B}}^{\phi \rightarrow \theta}(\theta, \phi)}. \quad (46)$$

**Part (i). Value consistency.** Fix any  $\tau > 0$  and  $(\theta, \phi) \in \Theta \times \Phi$ . We analyze the directional loss  $\mathcal{L}_{\text{mm}}^{\theta \rightarrow \phi}(\theta, \phi)$ ; the reverse direction follows by symmetry. From Eq. (46), the corresponding per-batch directional loss is

$$\ell_{\mathcal{B}}^{\theta \rightarrow \phi}(\theta, \phi) := -\frac{1}{\tau} s(\mathbf{z}, \mathbf{w}) + \log Z_{\mathcal{B}}^{\theta \rightarrow \phi}(\mathbf{z}). \quad (47)$$

**Step 1: Bias-variance control of the log-partition term.** The structure of  $Z_{\mathcal{B}}^{\theta \rightarrow \phi}$  is identical to the unimodal partition function (Eq. (23)), except that negatives are drawn from  $q_\phi$  rather than  $q_\theta$ . Under Asm. 4.1,  $\mathcal{Z}$  is compact and  $s$  is continuous, hence  $\kappa_\tau$  is bounded on  $\mathcal{Z} \times \mathcal{Z}$  for each fixed  $\tau > 0$ . Let

$$\mathsf{P} := \kappa_\tau(\mathbf{z}, \mathbf{w}), \quad \mathsf{S}_N^{\theta \rightarrow \phi}(\mathbf{z}) := \sum_{j=1}^N \kappa_\tau(\mathbf{z}, \mathbf{w}'_j), \quad Z_{\mathcal{B}}^{\theta \rightarrow \phi} = \mathsf{P} + \mathsf{S}_N^{\theta \rightarrow \phi}.$$

As in Step 1 of the unimodal proof (Part (i) of Thm. 3.1), the positive contribution induces a vanishing bias:

$$\log(\mathsf{P} + \mathsf{S}_N^{\theta \rightarrow \phi}) = \log \mathsf{S}_N^{\theta \rightarrow \phi} + \log \left(1 + \frac{\mathsf{P}}{\mathsf{S}_N^{\theta \rightarrow \phi}}\right), \quad \log \left(1 + \frac{\mathsf{P}}{\mathsf{S}_N^{\theta \rightarrow \phi}}\right) = O_\tau(N^{-1}).$$

Define the population partition function induced by the target encoder  $\phi$ :

$$\Gamma_{\phi,\tau}(\mathbf{z}) := \mathbb{E}_{\mathbf{w} \sim q_\phi} [\kappa_\tau(\mathbf{z}, \mathbf{w})] = \int \kappa_\tau(\mathbf{z}, \mathbf{w}) q_\phi(d\mathbf{w}).$$

Conditioned on the anchor  $\mathbf{z}$ , the terms  $\kappa_\tau(\mathbf{z}, \mathbf{w}_j')$  are i.i.d. and bounded, hence by concentration (cf. Step 2 in Part (i) of Thm. 3.1)

$$\frac{1}{N} S_N^{\theta \rightarrow \phi}(\mathbf{z}) = \Gamma_{\phi,\tau}(\mathbf{z}) + O_p(N^{-1/2}),$$

which implies, by the same Taylor expansion used in the unimodal proof, that

$$\log S_N^{\theta \rightarrow \phi}(\mathbf{z}) = \log N + \log \Gamma_{\phi,\tau}(\mathbf{z}) + O_p(N^{-1/2}).$$

Combining the above displays yields the asymptotic expansion

$$\ell_{\mathcal{B}}^{\theta \rightarrow \phi}(\theta, \phi) = -\frac{1}{\tau} s(\mathbf{z}, \mathbf{w}) + \log N + \log \Gamma_{\phi,\tau}(\mathbf{z}) + O_p(N^{-1/2}). \quad (48)$$

**Step 2: Identification of the directional energy.** Taking expectation of Eq. (48) over the batch construction gives

$$\mathcal{L}_{\text{mm}}^{\theta \rightarrow \phi}(\theta, \phi) := \mathbb{E}_{\mathcal{B}} [\ell_{\mathcal{B}}^{\theta \rightarrow \phi}(\theta, \phi)] = \mathbb{E} \left[ -\frac{1}{\tau} s(\mathbf{z}, \mathbf{w}) \right] + \mathbb{E} [\log \Gamma_{\phi,\tau}(\mathbf{z})] + \log N + o(1).$$

Here, since  $\kappa_\tau$  is uniformly bounded for fixed  $\tau$ , the reminder term is uniformly integrable, so taking expectations preserves  $o_p(1)$  as  $o(1)$ . Moreover,  $o(1) \rightarrow 0$  as  $N \rightarrow \infty$  for fixed  $\tau > 0$  by boundedness and dominated convergence.

Now, treating  $\mathbf{x}$  (equivalently  $\mathbf{z}$ ) as the anchor and using the disintegration in Def. 4.1, the law of iterated expectation yields

$$\mathbb{E}_{(\mathbf{x}, \mathbf{y}) \sim r_{\text{mm}}} \left[ -\frac{1}{\tau} s(f_\theta(\mathbf{x}), g_\phi(\mathbf{y})) \right] = \frac{1}{\tau} \mathbb{E}_{\mathbf{z} \sim q_\theta} [U_{\theta \rightarrow \phi}(\mathbf{z})] = \frac{1}{\tau} \mathcal{U}^{\theta \rightarrow \phi}(q_\theta).$$

Since  $\mathbf{z} = f_\theta(\mathbf{x}) \sim q_\theta$ , we have

$$\mathbb{E} [\log \Gamma_{\phi,\tau}(\mathbf{z})] = \mathbb{E}_{\mathbf{z} \sim q_\theta} [\log \Gamma_{\phi,\tau}(\mathbf{z})].$$

Under the constant kernel-volume condition Asm. 2.1,  $\tilde{q}_{\phi,\tau}(\mathbf{z}) = \Gamma_{\phi,\tau}(\mathbf{z})/V_\kappa(\tau)$  (Def. 2.2), hence

$$\begin{aligned} \mathbb{E}_{\mathbf{z} \sim q_\theta} [\log \Gamma_{\phi,\tau}(\mathbf{z})] &= \log V_\kappa(\tau) + \mathbb{E}_{\mathbf{z} \sim q_\theta} [\log \tilde{q}_{\phi,\tau}(\mathbf{z})] \\ &= \log V_\kappa(\tau) - H_{\times}(q_\theta, \tilde{q}_{\phi,\tau}). \end{aligned}$$

Substituting into the preceding expansion gives

$$\begin{aligned} \mathcal{L}_{\text{mm}}^{\theta \rightarrow \phi}(\theta, \phi) &= \frac{1}{\tau} \mathcal{U}^{\theta \rightarrow \phi}(q_\theta) - H_{\times}(q_\theta, \tilde{q}_{\phi,\tau}) + \log(N V_\kappa(\tau)) + o(1) \\ &= \mathcal{J}_\tau^{\theta \rightarrow \phi}(\theta, \phi) + \log(N V_\kappa(\tau)) + o(1). \end{aligned}$$

The reverse direction  $\phi \rightarrow \theta$  follows analogously, yielding the same form with  $(\theta, \phi)$  swapped. Averaging the two directional expansions and using the definition Eq. (9) proves Eq. (10) in Thm. 4.1.

**Part (ii): Gradient consistency.** Fix any  $\tau > 0$  and  $(\theta, \phi) \in \Theta \times \Phi$ . Differentiating the batch loss in Eq. (46) gives

$$\nabla \ell_{\mathcal{B}}^{\text{sym}}(\theta, \phi) = -\frac{1}{\tau} \nabla s(\mathbf{z}, \mathbf{w}) + \frac{1}{2} \nabla \log Z_{\mathcal{B}}^{\theta \rightarrow \phi}(\mathbf{z}) + \frac{1}{2} \nabla \log Z_{\mathcal{B}}^{\phi \rightarrow \theta}(\mathbf{w}), \quad (49)$$

where we denote the joint gradient  $\nabla_{(\theta, \phi)}$  as  $\nabla$  for simplicity.

**Step 1: Removing the positive term in each log-partition gradient.** Define

$$\mathbf{g}_N^{\theta \rightarrow \phi} := \nabla \log(\mathbf{P} + S_N^{\theta \rightarrow \phi}), \quad \mathbf{r}_N^{\theta \rightarrow \phi} := \nabla \log S_N^{\theta \rightarrow \phi},$$

and analogously  $(\mathbf{g}_N^{\phi \rightarrow \theta}, \mathbf{r}_N^{\phi \rightarrow \theta})$ . As in Eq. (29), a direct algebraic manipulation yields

$$\mathbf{g}_N^{\theta \rightarrow \phi} - \mathbf{r}_N^{\theta \rightarrow \phi} = \frac{\nabla \mathbf{P}}{\mathbf{P} + S_N^{\theta \rightarrow \phi}} - \frac{\mathbf{P}}{S_N^{\theta \rightarrow \phi}(\mathbf{P} + S_N^{\theta \rightarrow \phi})} \nabla S_N^{\theta \rightarrow \phi},$$

and the same identity holds with  $\theta \rightarrow \phi$  replaced by  $\phi \rightarrow \theta$ .

Under Asm. 4.1,  $\mathcal{Z}$  is compact and  $s$  is  $C^1$  with bounded input gradient. Together with the  $C^1$  encoders with uniformly bounded Jacobians, this implies that for each fixed  $\tau > 0$  there exist finite constants

$$0 < m_\tau \leq \kappa_\tau(\cdot, \cdot) \leq M_\tau < \infty, \quad \sup_{(\theta, \phi) \in \Theta \times \Phi} \sup_{\mathcal{B}} \|\nabla \kappa_\tau\| \leq G_\tau < \infty.$$

Consequently, uniformly over  $(\theta, \phi)$  and batch realizations,

$$P \leq M_\tau, \quad \|\nabla P\| \leq G_\tau, \quad S_N^{\theta \rightarrow \phi} \geq Nm_\tau, \quad \|\nabla S_N^{\theta \rightarrow \phi}\| \leq NG_\tau,$$

and the same bounds hold for  $S_N^{\phi \rightarrow \theta}$ . Taking norms in the identity above gives the uniform bound

$$\|\nabla \log Z_B^{\theta \rightarrow \phi}(\mathbf{z}) - \nabla \log S_N^{\theta \rightarrow \phi}(\mathbf{z})\| = O(N^{-1}), \quad \|\nabla \log Z_B^{\phi \rightarrow \theta}(\mathbf{w}) - \nabla \log S_N^{\phi \rightarrow \theta}(\mathbf{w})\| = O(N^{-1}), \quad (50)$$

where the  $O(N^{-1})$  constants depend on  $\tau$  but are uniform over  $\Theta \times \Phi$ .

**Step 2: Consistency of the negative-sum ratios.** We treat the direction  $\theta \rightarrow \phi$ ; the reverse direction is analogous. Rewrite

$$\nabla \log S_N^{\theta \rightarrow \phi} = \frac{\nabla S_N^{\theta \rightarrow \phi}}{S_N^{\theta \rightarrow \phi}} = \frac{\frac{1}{N} \sum_{j=1}^N \nabla \kappa_\tau(\mathbf{z}, \mathbf{w}'_j)}{\frac{1}{N} \sum_{j=1}^N \kappa_\tau(\mathbf{z}, \mathbf{w}'_j)}.$$

Fix  $(\theta, \phi)$ . Conditioning on  $(\mathbf{x}, \mathbf{y})$ , the anchor representations  $\mathbf{z} = f_\theta(\mathbf{x})$  and  $\mathbf{w} = g_\phi(\mathbf{y})$  are deterministic. The negatives  $\{\mathbf{y}'_j\}_{j=1}^N$  are i.i.d. from  $p_{\mathbf{y}}$ , hence  $\{\mathbf{w}'_j\}_{j=1}^N$  are i.i.d. through the map  $g_\phi$ . Write the kernel-smoothed mass as

$$\Gamma_{\phi, \tau}(\mathbf{z}) = \mathbb{E}_{\mathbf{y}' \sim p_{\mathbf{y}}} [\kappa_\tau(\mathbf{z}, g_\phi(\mathbf{y}'))],$$

which is strictly positive and uniformly bounded:  $\Gamma_{\phi, \tau}(\mathbf{z}) \geq m_\tau$ . By the law of large numbers and boundedness of  $\kappa_\tau$ ,

$$\frac{1}{N} \sum_{j=1}^N \kappa_\tau(\mathbf{z}, \mathbf{w}'_j) \xrightarrow{p} \Gamma_{\phi, \tau}(\mathbf{z}).$$

Similarly, since  $\|\nabla \kappa_\tau\|$  is uniformly bounded,

$$\frac{1}{N} \sum_{j=1}^N \nabla \kappa_\tau(\mathbf{z}, \mathbf{w}'_j) \xrightarrow{p} \mathbb{E}_{\mathbf{y}' \sim p_{\mathbf{y}}} [\nabla \kappa_\tau(\mathbf{z}, g_\phi(\mathbf{y}'))].$$

Since the expectation is taken with respect to the parameter-free distribution  $p_{\mathbf{y}}$  and, by Asm. 4.1,  $\sup_{(\theta, \phi)} \sup_{\mathbf{y}' \in \mathcal{Y}} \|\nabla \kappa_\tau(\mathbf{z}, g_\phi(\mathbf{y}'))\| < \infty$ , differentiation under the expectation is justified (e.g., by dominated convergence). Hence

$$\mathbb{E}_{\mathbf{y}' \sim p_{\mathbf{y}}} [\nabla \kappa_\tau(\mathbf{z}, g_\phi(\mathbf{y}'))] = \nabla \mathbb{E}_{\mathbf{y}' \sim p_{\mathbf{y}}} [\kappa_\tau(\mathbf{z}, g_\phi(\mathbf{y}'))] = \nabla \Gamma_{\phi, \tau}(\mathbf{z}).$$

Since the denominator converges to a strictly positive limit, the continuous mapping theorem yields

$$\nabla \log S_N^{\theta \rightarrow \phi} \xrightarrow{p} \frac{\nabla \Gamma_{\phi, \tau}(\mathbf{z})}{\Gamma_{\phi, \tau}(\mathbf{z})} = \nabla \log \Gamma_{\phi, \tau}(\mathbf{z}). \quad (51)$$

The reverse direction follows identically by defining

$$\Gamma_{\theta, \tau}(\mathbf{w}) := \mathbb{E}_{\mathbf{x}' \sim p_{\mathbf{x}}} [\kappa_\tau(f_\theta(\mathbf{x}'), \mathbf{w})],$$

and obtaining

$$\nabla \log S_N^{\phi \rightarrow \theta} \xrightarrow{p} \nabla \log \Gamma_{\theta, \tau}(\mathbf{w}). \quad (52)$$

Combining Eqs. (50) to (52), we obtain the batch-level limit

$$\nabla \log Z_B^{\theta \rightarrow \phi}(\mathbf{z}) \xrightarrow{p} \nabla \log \Gamma_{\phi, \tau}(\mathbf{z}), \quad \nabla \log Z_B^{\phi \rightarrow \theta}(\mathbf{w}) \xrightarrow{p} \nabla \log \Gamma_{\theta, \tau}(\mathbf{w}). \quad (53)$$

**Step 3: Passing to the population objective and identifying  $\nabla \mathcal{J}_\tau^{\text{mm}}$ .** By Prop. 4.1,  $\|\nabla \ell_{\mathcal{B}}^{\text{sym}}(\theta, \phi)\|$  is uniformly bounded over  $\Theta \times \Phi$  and all  $N$ . Therefore, applying dominated convergence to Eq. (49) together with Eq. (53) yields

$$\nabla \mathcal{L}_{\text{mm}}(\theta, \phi) = \mathbb{E}_{\mathcal{B}}[\nabla \ell_{\mathcal{B}}^{\text{sym}}(\theta, \phi)] \longrightarrow -\frac{1}{\tau} \mathbb{E}_{(\mathbf{z}, \mathbf{w}) \sim \pi_{\theta, \phi}}[\nabla s(\mathbf{z}, \mathbf{w})] + \frac{1}{2} \mathbb{E}_{\mathbf{z} \sim q_\theta}[\nabla \log \Gamma_{\phi, \tau}(\mathbf{z})] + \frac{1}{2} \mathbb{E}_{\mathbf{w} \sim q_\phi}[\nabla \log \Gamma_{\theta, \tau}(\mathbf{w})]. \quad (54)$$

We now identify the right-hand side as  $\nabla \mathcal{J}_\tau^{\text{mm}}(\theta, \phi)$ . First, by the definition of  $\pi_{\theta, \phi} = (f_\theta \times g_\phi)_\# r_{\text{mm}}$  and the law of iterated expectation applied to Def. 4.1,

$$\mathcal{U}^{\theta \rightarrow \phi}(q_\theta) = \int U_{\theta \rightarrow \phi}(\mathbf{z}) q_\theta(d\mathbf{z}) = \mathbb{E}_{(\mathbf{x}, \mathbf{y}) \sim r_{\text{mm}}}[-s(f_\theta(\mathbf{x}), g_\phi(\mathbf{y}))],$$

and similarly  $\mathcal{U}^{\phi \rightarrow \theta}(q_\phi)$  equals the same joint expectation.<sup>8</sup> Under Asm. 4.1, we may differentiate under the expectation to obtain

$$\nabla \mathcal{U}^{\theta \rightarrow \phi}(q_\theta) = -\mathbb{E}_{(\mathbf{z}, \mathbf{w}) \sim \pi_{\theta, \phi}}[\nabla s(\mathbf{z}, \mathbf{w})], \quad \nabla \mathcal{U}^{\phi \rightarrow \theta}(q_\phi) = -\mathbb{E}_{(\mathbf{z}, \mathbf{w}) \sim \pi_{\theta, \phi}}[\nabla s(\mathbf{z}, \mathbf{w})],$$

where  $\pi_{\theta, \phi} := (f_\theta \times g_\phi)_\# r_{\text{mm}}$  and  $(\mathbf{z}, \mathbf{w}) = (f_\theta(\mathbf{x}), g_\phi(\mathbf{y}))$ .

Second, under the constant kernel-volume condition Asm. 2.1, the smoothed densities satisfy

$$\tilde{q}_{\phi, \tau}(\mathbf{z}) = \Gamma_{\phi, \tau}(\mathbf{z}) / V_\kappa(\tau), \quad \tilde{q}_{\theta, \tau}(\mathbf{w}) = \Gamma_{\theta, \tau}(\mathbf{w}) / V_\kappa(\tau),$$

with  $V_\kappa(\tau)$  independent of  $(\theta, \phi)$ , and

$$\Gamma_{\phi, \tau}(\mathbf{z}) := \int \kappa_\tau(\mathbf{z}, \mathbf{w}) q_\phi(d\mathbf{w}), \quad \Gamma_{\theta, \tau}(\mathbf{w}) := \int \kappa_\tau(\mathbf{z}, \mathbf{w}) q_\theta(d\mathbf{z}).$$

Therefore, using  $\log \tilde{q}_{\phi, \tau} = \log \Gamma_{\phi, \tau} - \log V_\kappa(\tau)$  and  $\log \tilde{q}_{\theta, \tau} = \log \Gamma_{\theta, \tau} - \log V_\kappa(\tau)$ , we have

$$\begin{aligned} \nabla H_\times(q_\theta, \tilde{q}_{\phi, \tau}) &= -\nabla \int \log \tilde{q}_{\phi, \tau}(\mathbf{z}) q_\theta(d\mathbf{z}) = -\int \nabla \log \Gamma_{\phi, \tau}(\mathbf{z}) q_\theta(d\mathbf{z}), \\ \nabla H_\times(q_\phi, \tilde{q}_{\theta, \tau}) &= -\nabla \int \log \tilde{q}_{\theta, \tau}(\mathbf{w}) q_\phi(d\mathbf{w}) = -\int \nabla \log \Gamma_{\theta, \tau}(\mathbf{w}) q_\phi(d\mathbf{w}), \end{aligned}$$

where the derivative passes under the integral by dominated convergence, since  $\|\nabla \log \Gamma_{\cdot, \tau}\|$  is uniformly bounded by Asm. 4.1 and Prop. 4.1.

Combining these identities with the definition of  $\mathcal{J}_\tau^{\text{mm}}$  in Def. 4.2 shows that the limit in Eq. (54) equals  $\nabla \mathcal{J}_\tau^{\text{mm}}(\theta, \phi)$ .

Thus, for any fixed  $(\theta, \phi) \in \Theta \times \Phi$ , the  $\theta$ - and  $\phi$ -components of the above argument yield  $\|\nabla_\theta \mathcal{L}_{\text{mm}} - \nabla_\theta \mathcal{J}_\tau^{\text{mm}}\| \rightarrow 0$  and  $\|\nabla_\phi \mathcal{L}_{\text{mm}} - \nabla_\phi \mathcal{J}_\tau^{\text{mm}}\| \rightarrow 0$ . Therefore, for the joint gradient  $\nabla_{(\theta, \phi)} = (\nabla_\theta, \nabla_\phi)$ ,

$$\left\| \nabla_{(\theta, \phi)} \mathcal{L}_{\text{mm}} - \nabla_{(\theta, \phi)} \mathcal{J}_\tau^{\text{mm}} \right\| = \sqrt{\left\| \nabla_\theta \mathcal{L}_{\text{mm}} - \nabla_\theta \mathcal{J}_\tau^{\text{mm}} \right\|^2 + \left\| \nabla_\phi \mathcal{L}_{\text{mm}} - \nabla_\phi \mathcal{J}_\tau^{\text{mm}} \right\|^2} \longrightarrow 0,$$

which proves the gradient consistency claimed in Eq. (11).  $\square$

### C.9. Proof of Thm. 4.2

*Proof.* Fix any  $(\theta, \phi) \in \Theta \times \Phi$ . Under Asm. 4.1,  $s$  is bounded and Borel measurable, hence both cross-modal potentials  $U_{\theta, \phi}$  and  $U_{\phi \rightarrow \theta}$  from Def. 4.1 are Borel measurable and bounded. Therefore the expected binding energies  $\mathcal{U}^{\theta \rightarrow \phi}(q_\theta)$  and  $\mathcal{U}^{\phi \rightarrow \theta}(q_\phi)$  are well-defined. Moreover, Since  $\mathcal{Z}$  is compact and  $q_\theta, q_\phi$  are continuous with  $q_\theta, q_\phi \geq \min\{\underline{q}_\theta, \underline{q}_\phi\} > 0$ , both  $\log q_\theta$  and  $\log q_\phi$  are bounded, hence  $D_{\text{KL}}(q_\theta \| q_\phi)$  and  $D_{\text{KL}}(q_\phi \| q_\theta)$  are finite. Consequently, the multimodal functional  $\mathcal{F}_{\tau, \mathbf{U}_{\theta, \phi}}^{\text{mm}}(q_\theta, q_\phi)$  is well-defined.

**Step 1: Functional discrepancy reduces to log-ratio perturbations.** Recall the directional multimodal parametric energies from Def. 4.2:

$$\mathcal{J}_\tau^{\theta \rightarrow \phi}(\theta, \phi) = \frac{1}{\tau} \mathcal{U}^{\theta \rightarrow \phi}(q_\theta) - H_\times(q_\theta, \tilde{q}_{\phi, \tau}), \quad \mathcal{J}_\tau^{\phi \rightarrow \theta}(\theta, \phi) = \frac{1}{\tau} \mathcal{U}^{\phi \rightarrow \theta}(q_\phi) - H_\times(q_\phi, \tilde{q}_{\theta, \tau}),$$

<sup>8</sup>While the scalar alignment term yields the same joint expectation in both directions, the fields  $U_{\theta \rightarrow \phi}$  and  $U_{\phi \rightarrow \theta}$  differ pointwise. The directionality is instead governed by the  $\log q_\theta$  and  $\log q_\phi$  barrier terms, which we discuss in the subsequent analysis.

and  $\mathcal{J}_\tau^{\text{mm}} = \frac{1}{2}(\mathcal{J}_\tau^{\theta \rightarrow \phi} + \mathcal{J}_\tau^{\phi \rightarrow \theta})$ . Using  $H_\times(p, r) = H(p) + D_{\text{KL}}(p\|r)$ , we can rewrite

$$\begin{aligned}\mathcal{J}_\tau^{\text{mm}}(\theta, \phi) &= \frac{1}{2} \left( \frac{1}{\tau} \mathcal{U}^{\theta \rightarrow \phi}(q_\theta) - H(q_\theta) - D_{\text{KL}}(q_\theta\|\tilde{q}_{\phi,\tau}) + \frac{1}{\tau} \mathcal{U}^{\phi \rightarrow \theta}(q_\phi) - H(q_\phi) - D_{\text{KL}}(q_\phi\|\tilde{q}_{\theta,\tau}) \right) \\ &= \frac{1}{2} \left( \mathcal{F}_{\tau, U_{\theta \rightarrow \phi}}(q_\theta) + \mathcal{F}_{\tau, U_{\phi \rightarrow \theta}}(q_\phi) \right) - \frac{1}{2} \left( D_{\text{KL}}(q_\theta\|\tilde{q}_{\phi,\tau}) + D_{\text{KL}}(q_\phi\|\tilde{q}_{\theta,\tau}) \right).\end{aligned}\quad (55)$$

On the other hand, by Def. 4.3 with  $D_S(q_\theta, q_\phi) = \frac{1}{2}(D_{\text{KL}}(q_\theta\|q_\phi) + D_{\text{KL}}(q_\phi\|q_\theta))$ ,

$$\mathcal{F}_{\tau, U_{\theta \rightarrow \phi}}^{\text{mm}}(q_\theta, q_\phi) = \frac{1}{2}(\mathcal{F}_{\tau, U_{\theta \rightarrow \phi}}(q_\theta) + \mathcal{F}_{\tau, U_{\phi \rightarrow \theta}}(q_\phi)) - D_S(q_\theta, q_\phi). \quad (56)$$

Subtracting Eq. (56) from Eq. (55), the potential and entropy terms cancel, giving the exact identity

$$\mathcal{F}_{\tau, U_{\theta \rightarrow \phi}}^{\text{mm}}(q_\theta, q_\phi) - \mathcal{J}_\tau^{\text{mm}}(\theta, \phi) = \frac{1}{2}(D_{\text{KL}}(q_\theta\|\tilde{q}_{\phi,\tau}) - D_{\text{KL}}(q_\theta\|q_\phi) + D_{\text{KL}}(q_\phi\|\tilde{q}_{\theta,\tau}) - D_{\text{KL}}(q_\phi\|q_\theta)). \quad (57)$$

Now use the elementary difference formula: for any densities  $p, r_1, r_2$  with  $r_1, r_2 > 0$   $\mu$ -a.e.,

$$D_{\text{KL}}(p\|r_1) - D_{\text{KL}}(p\|r_2) = \int p \log \frac{r_2}{r_1} d\mu.$$

Since  $\kappa_\tau > 0$  and  $q_\theta, q_\phi$  are probability densities by assumption,  $\tilde{q}_{\theta,\tau}, \tilde{q}_{\phi,\tau} > 0$  everywhere. Apply it to  $(p, r_1, r_2) = (q_\theta, \tilde{q}_{\phi,\tau}, q_\phi)$  and  $(q_\phi, \tilde{q}_{\theta,\tau}, q_\theta)$  to obtain

$$\mathcal{F}_{\tau, U_{\theta \rightarrow \phi}}^{\text{mm}}(q_\theta, q_\phi) - \mathcal{J}_\tau^{\text{mm}}(\theta, \phi) = \frac{1}{2} \left( \int q_\theta \log \frac{q_\phi}{\tilde{q}_{\phi,\tau}} d\mu + \int q_\phi \log \frac{q_\theta}{\tilde{q}_{\theta,\tau}} d\mu \right). \quad (58)$$

**Step 2: Nonasymptotic bound by KDE sup-errors.** By the lower bounds  $q_\theta \geq \underline{q}_\theta$  and  $q_\phi \geq \underline{q}_\phi$  and the Lem. C.1 applied separately to  $q_\theta$  and  $q_\phi$ , there exists  $\tau_0(\theta, \phi) > 0$  such that for all  $0 < \tau \leq \tau_0(\theta, \phi)$ ,

$$\varepsilon_{\text{kde}}^{(\theta)}(\tau) = \|\tilde{q}_{\theta,\tau} - q_\theta\|_\infty \leq \frac{\underline{q}_\theta}{2}, \quad \varepsilon_{\text{kde}}^{(\phi)}(\tau) = \|\tilde{q}_{\phi,\tau} - q_\phi\|_\infty \leq \frac{\underline{q}_\phi}{2}.$$

Hence, for all  $\mathbf{z} \in \mathcal{Z}$  and all such  $\tau$ ,

$$\tilde{q}_{\theta,\tau}(\mathbf{z}) \geq \frac{\underline{q}_\theta}{2}, \quad \tilde{q}_{\phi,\tau}(\mathbf{z}) \geq \frac{\underline{q}_\phi}{2}. \quad (59)$$

On  $[\underline{q}_\phi/2, \infty)$ , the map  $\log(\cdot)$  is Lipschitz with constant  $2/\underline{q}_\phi$ ; thus, for all  $\mathbf{z}$ ,

$$|\log q_\phi(\mathbf{z}) - \log \tilde{q}_{\phi,\tau}(\mathbf{z})| \leq \frac{2}{\underline{q}_\phi} |q_\phi(\mathbf{z}) - \tilde{q}_{\phi,\tau}(\mathbf{z})| \leq \frac{2 \varepsilon_{\text{kde}}^{(\phi)}(\tau)}{\underline{q}_\phi}.$$

Equivalently,

$$\left| \log \frac{q_\phi(\mathbf{z})}{\tilde{q}_{\phi,\tau}(\mathbf{z})} \right| \leq \frac{2 \varepsilon_{\text{kde}}^{(\phi)}(\tau)}{\underline{q}_\phi}. \quad (60)$$

Analogously,

$$\left| \log \frac{q_\theta(\mathbf{z})}{\tilde{q}_{\theta,\tau}(\mathbf{z})} \right| \leq \frac{2 \varepsilon_{\text{kde}}^{(\theta)}(\tau)}{\underline{q}_\theta}. \quad (61)$$

Now bound Eq. (58) using  $\int q_\theta \, d\mu = \int q_\phi \, d\mu = 1$ :

$$\begin{aligned}
 |\mathcal{J}_\tau^{\text{mm}}(\theta, \phi) - \mathcal{F}_{\tau, \mathbf{U}_{\theta, \phi}}^{\text{mm}}(q_\theta, q_\phi)| &= |\mathcal{F}_{\tau, \mathbf{U}_{\theta, \phi}}^{\text{mm}}(q_\theta, q_\phi) - \mathcal{J}_\tau^{\text{mm}}(\theta, \phi)| \\
 &\leq \frac{1}{2} \left( \int q_\theta \left| \log \frac{q_\phi}{\tilde{q}_{\phi, \tau}} \right| d\mu + \int q_\phi \left| \log \frac{q_\theta}{\tilde{q}_{\theta, \tau}} \right| d\mu \right) \\
 &\leq \frac{1}{2} \left( \left\| \log \frac{q_\phi}{\tilde{q}_{\phi, \tau}} \right\|_\infty + \left\| \log \frac{q_\theta}{\tilde{q}_{\theta, \tau}} \right\|_\infty \right) \\
 &\leq \frac{1}{2} \left( \frac{2 \varepsilon_{\text{kde}}^{(\phi)}(\tau)}{\underline{q}_\phi} + \frac{2 \varepsilon_{\text{kde}}^{(\theta)}(\tau)}{\underline{q}_\theta} \right) \\
 &\leq \frac{\varepsilon_{\text{kde}}^{(\theta)}(\tau) + \varepsilon_{\text{kde}}^{(\phi)}(\tau)}{\min\{\underline{q}_\theta, \underline{q}_\phi\}}.
 \end{aligned}$$

This proves the claimed nonasymptotic bound for all  $0 < \tau \leq \tau_0(\theta, \phi)$ .

**Step 3: Vanishing discrepancy as  $\tau \downarrow 0^+$ .** By Lemma Lem. C.1 applied to  $q_\theta$  and  $q_\phi$  (using Asm. 3.2),

$$\varepsilon_{\text{kde}}^{(\theta)}(\tau) \xrightarrow{\tau \downarrow 0^+} 0, \quad \varepsilon_{\text{kde}}^{(\phi)}(\tau) \xrightarrow{\tau \downarrow 0^+} 0.$$

Therefore the bound in Step 2 implies

$$|\mathcal{J}_\tau^{\text{mm}}(\theta, \phi) - \mathcal{F}_{\tau, \mathbf{U}_{\theta, \phi}}^{\text{mm}}(q_\theta, q_\phi)| \xrightarrow{\tau \downarrow 0^+} 0,$$

for the fixed pair  $(\theta, \phi)$ . This completes the proof.  $\square$

### C.10. Proof of Prop. 4.2

*Proof.* Fix  $\tau > 0$  and  $\rho_2 \in \mathcal{P}_+(\mathcal{Z})$ . Throughout, we treat  $\rho_2$  as fixed and analyze  $\rho_1$  (while analysis for  $\rho_2$  applies symmetrically) and write the coordinate map as

$$\mathcal{F}_1(\rho_1) := \mathcal{F}_{\tau, \mathbf{U}_{1,2}}^{\text{mm}}(\rho_1, \rho_2), \quad \rho_1 \in \mathcal{P}_+(\mathcal{Z}).$$

**Step 1: Concavity of  $\rho_1 \mapsto \mathcal{F}_\tau$  and its lower bound.** Using  $H(\rho_1) = -\int \rho_1 \log \rho_1 d\mu$ ,  $D_{\text{KL}}(\rho_1 \parallel \rho_2) = \int \rho_1 \log(\rho_1 / \rho_2) d\mu$ , and  $D_{\text{KL}}(\rho_2 \parallel \rho_1) = \int \rho_2 \log(\rho_2 / \rho_1) d\mu$ , expand the  $\rho_1$ -dependent terms in  $\mathcal{F}_1(\rho_1)$ :

$$\mathcal{F}_1(\rho_1) = \frac{1}{2} \int \rho_1(\mathbf{z}) V_{1|2}(\mathbf{z}) d\mu(\mathbf{z}) + \frac{1}{2} \int \rho_2(\mathbf{z}) \log \rho_1(\mathbf{z}) d\mu(\mathbf{z}) + C(\rho_2), \quad (62)$$

where  $V_{1|2}(\mathbf{z}) := \frac{1}{\tau} U_{1+2}(\mathbf{z}) + \log \rho_2(\mathbf{z})$ , and  $C(\rho_2)$  does not depend on  $\rho_1$ . We observe  $\rho_1 \mapsto \int \rho_1 V_{1|2} d\mu$  is linear, and  $\rho_1 \mapsto \int \rho_2 \log \rho_1 d\mu$  is concave on the positive cone since  $\log$  is concave and  $\rho_2 \geq \rho > 0$ . Thus, the coordinate map  $\rho_1 \mapsto \mathcal{F}_1$  is concave on the convex set  $\mathcal{P}_+(\mathcal{Z})$ . Consequently, the infimum over  $\mathcal{P}_+(\mathcal{Z})$  can be approached by a sequence on the boundary.

Now, write any feasible  $\rho_1 \in \mathcal{P}_+(\mathcal{Z})$  as  $\rho_1(\mathbf{z}) = \underline{\rho} + \eta(\mathbf{z})$  so that  $\eta(\mathbf{z}) \geq 0$ . The excess probability mass is strictly positive

$$M_{\text{ex}} = \int \eta(\mathbf{z}) d\mu(\mathbf{z}) > 0.$$

Then, using  $V_{1|2}(\mathbf{z}) \geq \text{ess inf}_\mu V_{1|2} =: v_*$  and  $\log \rho_1(\mathbf{z}) \geq \log \underline{\rho}$   $\mu$ -a.e.,

$$\begin{aligned}
 \int \rho_1 V_{1|2}(\mathbf{z}) d\mu(\mathbf{z}) &= \underline{\rho} \int V_{1|2}(\mathbf{z}) d\mu(\mathbf{z}) + \int \eta(\mathbf{z}) V_{1|2}(\mathbf{z}) d\mu(\mathbf{z}) \\
 &\geq \underline{\rho} \int V_{1|2}(\mathbf{z}) d\mu(\mathbf{z}) + v_* M_{\text{ex}},
 \end{aligned}$$

and

$$\int \rho_2 \log(\rho_1) d\mu(\mathbf{z}) \geq \int \rho_2 \log \underline{\rho} d\mu(\mathbf{z}) = \log \underline{\rho}.$$

Plugging these into Eq. (62) yields the lower bound

$$\mathcal{F}_1(\rho_1) \geq \frac{1}{2} \left( \underline{\rho} \int V_{1|2}(\mathbf{z}) d\mu(\mathbf{z}) + v_* M_{\text{ex}} \right) + \frac{1}{2} \log \underline{\rho} + C(\rho_2) =: \mathcal{F}_*. \quad (63)$$

Hence,  $\inf_{\rho_1 \in \mathcal{P}_+(\mathcal{Z})} \mathcal{F}_1(\rho_1) \geq \mathcal{F}_*$ .

**Step 2: Evaluate  $\mathcal{F}_1$  as  $\rho_1^{(\sigma)}$ .** For each  $\sigma > 0$ , define the sublevel set

$$\mathcal{W}_1^\sigma = \{\mathbf{z} \in \mathcal{Z} : V_{1|2}(\mathbf{z}) \leq v_* + \sigma\}.$$

We have  $\mu(\mathcal{W}_1^\sigma) > 0$ . Further since  $\mu$  is the volume measure on the compact manifold  $\mathcal{Z}$ ,  $\mu$  is non-atomic. Thus, there exist a shrinking subset  $\mathcal{S}_1^\sigma \subseteq \mathcal{W}_1^\sigma$  satisfying  $\mu(\mathcal{S}_1^\sigma) \xrightarrow{\sigma \rightarrow 0} 0$  (when  $\mathcal{W}_1^\sigma$  itself is sharp  $\mu(\mathcal{W}_1^\sigma) \xrightarrow{\sigma \rightarrow 0} 0$ , we simply choose  $\mathcal{S}_1^\sigma = \mathcal{W}_1^\sigma$ ). Defined the density as

$$\rho_1^{(\sigma)}(\mathbf{z}) = \underline{\rho} + \mathbb{1}_{\mathcal{S}_1^\sigma}(\mathbf{z}) \frac{M_{\text{ex}}}{\mu(\mathcal{S}_1^\sigma)}.$$

Since  $\rho_1^{(\sigma)} \geq \underline{\rho}$  and

$$\int \rho_1^{(\sigma)} d\mu(\mathbf{z}) = \underline{\rho} \mu(\mathcal{Z}) + \frac{M_{\text{ex}}}{\mu(\mathcal{S}_1^\sigma)} \mu(\mathcal{S}_1^\sigma) = \underline{\rho} \mu(\mathcal{Z}) + M_{\text{ex}} = 1,$$

we have  $\rho_1^{(\sigma)} \in \mathcal{P}_+(\mathcal{Z})$ . Now, evaluate  $\mathcal{F}_1$  at  $\rho_1^{(\sigma)}$ :

(i) *Linear term.* Since  $\mathcal{S}_1^\sigma \subseteq \mathcal{W}_1^\sigma$ , we have  $V_{1|2}(\mathbf{z}) \leq v_* + \sigma$  on  $\mathcal{S}_1^\sigma$ , hence

$$\begin{aligned} \int \rho_1^{(\sigma)} V_{1|2}(\mathbf{z}) d\mu &= \underline{\rho} \int V_{1|2} d\mu + \frac{M_{\text{ex}}}{\mu(\mathcal{S}_1^\sigma)} \int_{\mathcal{S}_1^\sigma} V_{1|2} d\mu \\ &\leq \underline{\rho} \int V_{1|2} d\mu + M_{\text{ex}}(v_* + \sigma). \end{aligned}$$

(ii) *Log term.* Split the domain  $\mathcal{Z} = (\mathcal{Z} \setminus \mathcal{S}_1^\sigma) \cup \mathcal{S}_1^\sigma$ :

$$\int \rho_2 \log \rho_1^{(\sigma)} d\mu = \int_{\mathcal{Z} \setminus \mathcal{S}_1^\sigma} \rho_2 \log \underline{\rho} d\mu + \int_{\mathcal{S}_1^\sigma} \rho_2 \log \left( \underline{\rho} + \frac{M_{\text{ex}}}{\mu(\mathcal{S}_1^\sigma)} \right) d\mu.$$

Using the mass of the spike  $m_\sigma := \int_{\mathcal{S}_1^\sigma} \rho_2 d\mu$ , the first term is  $(1 - m_\sigma) \log \underline{\rho}$ . Therefore,

$$\int \rho_2 \log \rho_1^{(\sigma)} d\mu = \log \underline{\rho} + m_\sigma \left( \log \left( \underline{\rho} + \frac{M_{\text{ex}}}{\mu(\mathcal{S}_1^\sigma)} \right) - \log \underline{\rho} \right) = \log \underline{\rho} + m_\sigma L_\sigma, \quad \text{where } L_\sigma := \log \left( 1 + \frac{M_{\text{ex}}}{\underline{\rho} \mu(\mathcal{S}_1^\sigma)} \right).$$

Combining terms yields:

$$\mathcal{F}_1(\rho_1^{(\sigma)}) \leq \frac{1}{2} \left( \underline{\rho} \int V_{1|2} d\mu + M_{\text{ex}}(v_* + \sigma) \right) + \frac{1}{2} (\log \underline{\rho} + m_\sigma L_\sigma) + C(\rho_2). \quad (64)$$

**Step 3: Conclude convergence.** We first analyze the limit of the log-penalty  $m_\sigma L_\sigma \rightarrow 0$  as  $\sigma \downarrow 0$ . Since  $\rho_2 \in L^1(\mu)$  and  $\mu(\mathcal{Z}) < \infty$ , the integral is absolutely continuous: for every  $\varepsilon > 0$  there exists  $\delta(\varepsilon) > 0$  such that for any measurable  $\mathcal{A} \subset \mathcal{Z}$  with  $\mu(\mathcal{A}) \leq \delta(\varepsilon)$ ,

$$\int_{\mathcal{A}} \rho_2 d\mu \leq \varepsilon.$$

Define the modulus of absolute continuity

$$\Psi(t) := \sup \left\{ \int_{\mathcal{A}} \rho_2 d\mu : \mathcal{A} \subset \mathcal{Z} \text{ measurable, } \mu(\mathcal{A}) \leq t \right\}.$$

Since  $\rho_2 \in L^1(\mu)$  and  $\mu(\mathcal{Z}) < \infty$ , we have  $\Psi(t) \downarrow 0$  as  $t \downarrow 0$ . Since  $\Psi(t) \rightarrow 0$  as  $t \downarrow 0$  and  $|\log t|^{-2} \rightarrow 0$  as  $t \downarrow 0$ , we may choose a sequence  $\delta_\sigma \downarrow 0$  such that  $\delta_\sigma \leq \mu(\mathcal{W}_1^\sigma)$  and  $\Psi(\delta_\sigma) \leq |\log \delta_\sigma|^{-2}$ .

By non-atomicity of  $\mu$ , choose  $\mathcal{S}_1^\sigma \subseteq \mathcal{W}_1^\sigma$  with  $\mu(\mathcal{S}_1^\sigma) = \delta_\sigma$ . Then

$$m_\sigma := \int_{\mathcal{S}_1^\sigma} \rho_2 \, d\mu \leq \Psi(\delta_\sigma) \leq \frac{1}{|\log \delta_\sigma|^2}.$$

With  $L_\sigma = \log(1 + M_{\text{ex}}/(\underline{\rho} \mu(\mathcal{S}_1^\sigma)))$  and  $\mu(\mathcal{S}_1^\sigma) = \delta_\sigma$ , we have

$$L_\sigma \leq \log\left(1 + M_{\text{ex}}/\underline{\rho}\right) + |\log \delta_\sigma| =: K + |\log \delta_\sigma|.$$

Therefore,

$$0 \leq m_\sigma L_\sigma \leq \frac{1}{|\log \delta_\sigma|^2} (K + |\log \delta_\sigma|) = \frac{K}{|\log \delta_\sigma|^2} + \frac{1}{|\log \delta_\sigma|} \xrightarrow{\sigma \downarrow 0} 0.$$

Thus the additional log-penalty incurred by the spike vanishes.

Now, subtract  $\mathcal{F}_*$  (Eq. (63)) from Eq. (64):

$$\mathcal{F}_1(\rho_1^{(\sigma)}) - \mathcal{F}_* \leq \frac{1}{2}(M_{\text{ex}}\sigma + m_\sigma L_\sigma).$$

Letting  $\sigma \downarrow 0$  gives

$$\limsup_{\sigma \downarrow 0} \mathcal{F}_1(\rho_1^{(\sigma)}) \leq \mathcal{F}_*.$$

But Step 1 showed  $\inf_{\rho_1 \in \mathcal{P}_+(\mathcal{Z})} \mathcal{F}_1(\rho_1) \geq \mathcal{F}_*$ , therefore

$$\inf_{\rho_1 \in \mathcal{P}_+(\mathcal{Z})} \mathcal{F}_1(\rho_1) = \mathcal{F}_* \quad \text{and} \quad \lim_{\sigma \downarrow 0} \mathcal{F}_1(\rho_1^{(\sigma)}) = \inf_{\rho_1 \in \mathcal{P}_+(\mathcal{Z})} \mathcal{F}_1(\rho_1).$$

This concludes that the infimum approached by the boundary solutions concentrating on the minima of  $V_{1|2}$ . The  $\rho_2$ -coordinate statement is identical after swapping indices and using  $V_{2|1} = \frac{1}{\tau} U_{2 \rightarrow 1} + \log \rho_1$ .  $\square$

### C.11. Proof of Cor. 4.1

*Proof.* We provide the derivation for the modality  $\mathcal{X}$  with parameter  $\theta \in \Theta$ . The corresponding result for  $\phi \in \Phi$  follows by interchanging modalities and notation.

Fix  $\phi \in \Phi$  and  $\tau > 0$ , and let  $\theta^* \in \arg \min_{\theta \in \Theta} \mathcal{J}_\tau^{\text{mm}}(\theta, \phi)$ . Since  $q_{\theta^*} \geq \underline{q}_{\theta^*} \mu\text{-a.e.}$ ,  $M_{\text{ex}}^{(\theta^*)} = 1 - \underline{q}_{\theta^*} \mu(\mathcal{Z}) > 0$ , and  $\int q_{\theta^*} \, d\mu = 1$ , we have  $\bar{q}_{\theta^*} \geq 0 \mu\text{-a.e.}$  and  $\int \bar{q}_{\theta^*} \, d\mu = (1 - \underline{q}_{\theta^*} \mu(\mathcal{Z}))/M_{\text{ex}}^{(\theta^*)} = 1$ , hence  $\bar{q}_{\theta^*} \mu$  is a probability measure.

Define the effective potential field and its essential infimum

$$V_{\theta^*|\phi}(\mathbf{z}) = \frac{1}{\tau} U_{\theta^* \rightarrow \phi}(\mathbf{z}) + \log q_\phi(\mathbf{z}), \quad v_* := \text{ess inf}_\mu V_{\theta^*|\phi},$$

and for  $\sigma > 0$  the sublevel set is  $\mathcal{W}_{\theta^*}^\sigma = \{\mathbf{z} \in \mathcal{Z} : V_{\theta^*|\phi}(\mathbf{z}) \leq v_* + \sigma\}$ .

**Step 1: A quantitative implication of near-optimality.** Consider the coordinate functional with the peer encoder  $\phi$  fixed

$$\mathcal{F}_\tau(\rho) := \mathcal{F}_{\tau, \mathbf{U}_{\theta^*, \phi}}^{\text{mm}}(\rho, q_\phi), \quad \rho \in \mathcal{P}_+^{(\theta^*)}(\mathcal{Z}).$$

As made explicit in the proof of Prop. 4.2 by expanding  $\mathcal{F}_{\tau, \mathbf{U}_{\theta^*, \phi}}^{\text{mm}}$  and collecting  $\rho$ -dependent terms,  $\mathcal{F}_\tau$  can be written in the form

$$\mathcal{F}_\tau(\rho) = \frac{1}{2} \int V_{\theta^*|\phi}(\mathbf{z}) \rho(\mathbf{z}) \, d\mu(\mathbf{z}) + \frac{1}{2} \int q_\phi(\mathbf{z}) \log \rho(\mathbf{z}) \, d\mu(\mathbf{z}) + \text{const}_\tau(\phi), \quad (65)$$

where  $\text{const}_\tau(\phi)$  is independent of  $\rho$ . By the floor constraint  $\rho \geq \underline{q}_{\theta^*} \mu\text{-a.e.}$  and  $\int q_\phi \, d\mu = 1$ ,

$$\int q_\phi \log \rho \, d\mu \geq \log \underline{q}_{\theta^*}.$$

Hence, for any  $\rho \in \mathcal{P}_+^{(\theta^*)}(\mathcal{Z})$ ,

$$\mathcal{F}_\tau(\rho) \geq \frac{1}{2} \int V_{\theta^*|\phi} \rho \, d\mu + \frac{1}{2} \log \underline{q}_{\theta^*} + \text{const}_\tau(\phi). \quad (66)$$

Let

$$\mathcal{F}_\tau^* := \inf_{\rho \in \mathcal{P}_+^{(\theta^*)}(\mathcal{Z})} \mathcal{F}_\tau(\rho).$$

Applying Prop. 4.2 (with floor  $\underline{q}_{\theta^*}$ ) to  $\mathcal{F}_\tau$  yields, for each  $\delta > 0$ , a boundary competitor  $\rho^{(\delta)} \in \mathcal{P}_+^{(\theta^*)}(\mathcal{Z})$  whose excess mass is supported on a shrinking set  $\mathcal{S}^\delta \subseteq \mathcal{W}_{\theta^*}^\delta$  with  $\mu(\mathcal{S}^\delta) \xrightarrow{\delta \downarrow 0} 0$ , such that  $\mathcal{F}_\tau(\rho^{(\delta)}) \downarrow \mathcal{F}_\tau^*$  as  $\delta \downarrow 0$ .

Moreover, since  $\rho^{(\delta)} = \underline{q}_{\theta^*}$  on  $\mathcal{Z} \setminus \mathcal{S}^\delta$  and  $q_\phi$  is continuous on compact  $\mathcal{Z}$ , hence

$$\begin{aligned} \int q_\phi \log \rho^{(\delta)} \, d\mu &= \log \underline{q}_{\theta^*} + \int_{\mathcal{S}^\delta} q_\phi \log \left(1 + \frac{M_{\text{ex}}^{(\theta^*)}}{\underline{q}_{\theta^*} \mu(\mathcal{S}^\delta)}\right) \, d\mu \\ &\leq \log \underline{q}_{\theta^*} + \|q_\phi\|_\infty \mu(\mathcal{S}^\delta) \log \left(1 + \frac{c}{\mu(\mathcal{S}^\delta)}\right) \\ &= \log \underline{q}_{\theta^*} + o_\delta(1), \end{aligned}$$

where  $o_\delta(1) \rightarrow 0$  as  $\delta \downarrow 0$  because  $\mu(\mathcal{S}^\delta) \log(1/\mu(\mathcal{S}^\delta)) \rightarrow 0$ . In addition, since  $\rho^{(\delta)} - \underline{q}_{\theta^*}$  places all excess mass inside  $\{\mathbf{z} \in \mathcal{Z} : V_{\theta^*|\phi}(\mathbf{z}) \leq v_* + \delta\}$ ,

$$\begin{aligned} \int V_{\theta^*|\phi} \rho^{(\delta)} \, d\mu &= \underline{q}_{\theta^*} \int V_{\theta^*|\phi} \, d\mu + M_{\text{ex}}^{(\theta^*)} \int V_{\theta^*|\phi} \bar{\rho}^{(\delta)} \, d\mu \\ &\leq \underline{q}_{\theta^*} \int V_{\theta^*|\phi} \, d\mu + M_{\text{ex}}^{(\theta^*)}(v_* + \delta), \end{aligned}$$

where  $\bar{\rho}^{(\delta)} := (\rho^{(\delta)} - \underline{q}_{\theta^*})/M_{\text{ex}}^{(\theta^*)}$ .

Plugging these bounds into Eq. (65) and letting  $\delta \downarrow 0$  yields the upper bound

$$\mathcal{F}_\tau^* \leq \frac{1}{2} \left( \underline{q}_{\theta^*} \int V_{\theta^*|\phi} \, d\mu + M_{\text{ex}}^{(\theta^*)} v_* \right) + \frac{1}{2} \log \underline{q}_{\theta^*} + \text{const}_\tau(\phi). \quad (67)$$

Now apply Eq. (66) to  $\rho = q_{\theta^*}$  and subtract Eq. (67). Using

$$\int V_{\theta^*|\phi} q_{\theta^*} \, d\mu = \underline{q}_{\theta^*} \int V_{\theta^*|\phi} \, d\mu + M_{\text{ex}}^{(\theta^*)} \int V_{\theta^*|\phi} \bar{q}_{\theta^*} \, d\mu.$$

we obtain

$$\mathcal{F}_\tau(q_{\theta^*}) - \mathcal{F}_\tau^* \geq \frac{M_{\text{ex}}^{(\theta^*)}}{2} \int (V_{\theta^*|\phi}(\mathbf{z}) - v_*) \bar{q}_{\theta^*}(\mathbf{z}) \, d\mu(\mathbf{z}). \quad (68)$$

**Step 2: Use realizability and convert to leakage.** By the encoder-expressiveness assumption in Eq. (13),

$$\mathcal{F}_\tau(q_{\theta^*}) \leq \mathcal{F}_\tau^* + \varepsilon_{\text{real}}(\tau).$$

Combining with Eq. (68) gives

$$\int (V_{\theta^*|\phi} - v_*) \bar{q}_{\theta^*} \, d\mu \leq \frac{2 \varepsilon_{\text{real}}(\tau)}{M_{\text{ex}}^{(\theta^*)}}. \quad (69)$$

Finally, since  $V_{\theta^*|\phi}(\mathbf{z}) - v_* \geq \sigma$   $\mu$ -a.e. on  $\mathcal{Z} \setminus \mathcal{W}_{\theta^*}^\sigma$ , we have

$$\int (V_{\theta^*|\phi} - v_*) \bar{q}_{\theta^*} \, d\mu \geq \int_{\mathcal{Z} \setminus \mathcal{W}_{\theta^*}^\sigma} (V_{\theta^*|\phi} - v_*) \bar{q}_{\theta^*} \, d\mu \geq \sigma \int_{\mathcal{Z} \setminus \mathcal{W}_{\theta^*}^\sigma} \bar{q}_{\theta^*} \, d\mu = \sigma (\bar{q}_{\theta^*} \mu)(\mathcal{Z} \setminus \mathcal{W}_{\theta^*}^\sigma),$$

and therefore, by Eq. (69),

$$(\bar{q}_{\theta^*} \mu)(\mathcal{Z} \setminus \mathcal{W}_{\theta^*}^\sigma) \leq \frac{2 \varepsilon_{\text{real}}(\tau)}{M_{\text{ex}}^{(\theta^*)} \sigma},$$

which is exactly Eq. (14). The concluding asymptotic statement follows immediately: if  $\sigma \downarrow 0$  with  $\varepsilon_{\text{real}}(\tau)/\sigma \rightarrow 0$ , then the right-hand side vanishes and  $(\bar{q}_{\theta^*} \mu)(\mathcal{Z} \setminus \mathcal{W}_{\theta^*}^\sigma) \rightarrow 0$  as  $\tau \downarrow 0^+$ .  $\square$

## D. Numerical Validations

This section provides controlled experiments that complement the theoretical analysis by probing the *mechanistic signatures* predicted by our large-batch and intrinsic-functional limits. Our goal is to sanity-check that (i) finite-batch InfoNCE gradients approach the deterministic energy gradients as the number of negatives grows, (ii) unimodal training exhibits the expected Gibbs-shaped concentration/spread behavior under sharp kernels and low temperature, and (iii) in multimodal settings, controlled conditional heterogeneity induces a persistent population-level marginal gap consistent with the predicted negative symmetric divergence mechanism. All experiments are intentionally designed to isolate each phenomenon with as few confounders as possible.<sup>9</sup>

### D.1. Large-Batch Gradient Consistency Across Critics

This experiment provides an numerical validation of the large-batch consistency established in Thm. 3.1. We verify that as the number of negatives  $N$  increases, the stochastic InfoNCE descent direction aligns increasingly well with the deterministic energy gradient. Crucially, since the multimodal symmetric objective (Eq. (2)) is the sum of two directional terms, establishing consistency for the unimodal gradient implies consistency for the full multimodal objective by linearity.

**Data and pairing.** We construct a synthetic unimodal dataset in  $\mathbb{R}^m$  ( $m = 64$ ) from a mixture of  $K = 4$  Gaussians:  $\mathbf{x} \sim \sum_{k=1}^K \pi_k \mathcal{N}(\boldsymbol{\mu}_k, \sigma^2 \mathbf{I})$ . The component means  $\{\boldsymbol{\mu}_k\}$  are random directions scaled by a separation factor of 4, with  $\sigma = 1$ . Positive pairs are generated via additive noise  $\tilde{\mathbf{x}} = \mathbf{x} + \boldsymbol{\varepsilon}$ , where  $\boldsymbol{\varepsilon} \sim \mathcal{N}(\mathbf{0}, \sigma_{\text{aug}}^2 \mathbf{I})$ . Negatives  $\{\mathbf{x}_j^-\}_{j=1}^N$  are i.i.d. draws from the same mixture.

**Encoder and regimes.** We employ a linear encoder  $f_{\mathbf{W}}(\mathbf{x})$  with parameters  $\mathbf{W} \in \mathbb{R}^{d \times m}$  ( $d = 128$ ) under two distinct geometric regimes:

$$\mathbf{z} = f_{\mathbf{W}}(\mathbf{x}) = \begin{cases} \text{normalize}(\mathbf{W}\mathbf{x}) \in \mathbb{S}^{d-1}, & \text{(Spherical regime)} \\ \tanh(\mathbf{W}\mathbf{x}) \in [-1, 1]^d, & \text{(Compact Euclidean regime).} \end{cases}$$

The spherical case corresponds to the standard feature-normalized setting, while the compact Euclidean case mirrors our theoretical assumption of a compact  $\mathcal{Z}$  without enforcing explicit normalization, allowing for distance-based critics.

**Critics and kernels.** We evaluate the exponential kernel defined in § 2 with the two canonical critics: the cosine critic  $s_{\text{cos}}(\mathbf{z}, \mathbf{w}) = \langle \mathbf{z}, \mathbf{w} \rangle$  and the RBF critic  $s_{\text{rbf}}(\mathbf{z}, \mathbf{w}) = -\frac{1}{d} \|\mathbf{z} - \mathbf{w}\|^2$ , with temperatures  $\tau_{\text{cos}} = 0.1$  and  $\tau_{\text{rbf}} = 1.0$ , respectively. The RBF critic includes  $1/d$  scaling to maintain  $O(1)$  logits. We set augmentation noise  $\sigma_{\text{aug}} = 0.05$  for the cosine regime and  $\sigma_{\text{aug}} = 0.2$  for the RBF regime.

**Loss and gradients.** For each seed, we sample a fixed batch of  $B = 64$  anchors/positives and a large ‘‘reference’’ pool of  $N_{\text{ref}} = 4096$  negatives. For a given  $N$ , we compute the loss  $\hat{\ell}_{B,N}(\mathbf{W})$  using the first  $N$  negatives from this pool:

$$\hat{\ell}_{B,N}(\mathbf{W}) = \frac{1}{B} \sum_{i=1}^B \left[ -\frac{1}{\tau} s(\mathbf{z}_i, \tilde{\mathbf{z}}_i) + \log \left( \exp(s(\mathbf{z}_i, \tilde{\mathbf{z}}_i)/\tau) + \sum_{j=1}^N \exp(s(\mathbf{z}_i, \mathbf{w}_j^-)/\tau) \right) \right].$$

Let  $\mathbf{g}_N := \nabla_{\mathbf{W}} \hat{\ell}_{B,N}(\mathbf{W})$  denote the gradient estimate using  $N$  negatives, and  $\mathbf{g}_{\text{ref}} := \mathbf{g}_{N_{\text{ref}}}$  denote the high-fidelity reference gradient. Fixing the negative pool ensures that variations in  $\mathbf{g}_N$  are attributable solely to the sample size  $N$ .

**Metrics.** We sweep  $N \in \{4, 8, 16, 32, 64, 128, 256, 512, 1024\}$  and report two metrics: (1) *gradient alignment*  $\cos(\mathbf{g}_N, \mathbf{g}_{\text{ref}})$ , measuring directional accuracy; and (2) *relative error*  $\|\mathbf{g}_N - \mathbf{g}_{\text{ref}}\|/\|\mathbf{g}_{\text{ref}}\|$ , measuring magnitude deviation. Results are averaged over 20 random seeds; error bars indicate  $\pm 1$  standard deviation across seeds.

**Results.** As shown in Fig. 2, across both the spherical/cosine and compact/RBF regimes, the gradient alignment score increases monotonically with  $N$  while the relative error decreases. This confirms our theoretical claims: as the denominator concentrates, the stochastic InfoNCE gradient converges to the deterministic energy gradient. The rapid convergence (alignment  $> 0.95$  at  $N = 256$ ) suggests that the large-batch energy landscape is a faithful proxy for practical training dynamics even at moderate batch sizes.

<sup>9</sup>Code is available at [https://github.com/YichaoCai1/InfoNCE\\_Geometry](https://github.com/YichaoCai1/InfoNCE_Geometry).

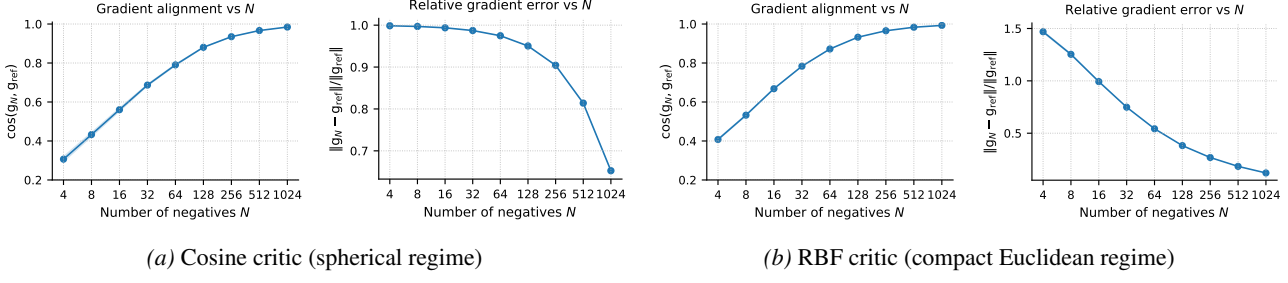


**Figure 2. Large-batch gradient consistency.** Comparison of batch gradients against the large-batch reference across various  $N$ . Left: Cosine alignment (higher is better). Right: Relative gradient error (lower is better). Results are mean  $\pm$  standard error over 20 seeds.

## D.2. Unimodal Gibbs Equilibrium and Low-Temperature Concentration

This experiment provides a direct numerical verification of the intrinsic unimodal geometry characterized in § 3. Specifically, we validate the variational perspective by demonstrating that: (i) for fixed  $\tau > 0$ , the functional  $\mathcal{F}_{\tau,U}$  admits a unique Gibbs-type equilibrium (Prop. 3.2); and (ii) as  $\tau \downarrow 0^+$ , this equilibrium concentrates exponentially around the minimizers of  $U$ , confirming the ground-state convergence predicted in Prop. 3.3.

**Representation space and potential field.** We define the domain as the unit sphere  $\mathcal{Z} = \mathbb{S}^2 \subset \mathbb{R}^3$  equipped with surface measure  $\mu$  and geodesic distance  $d_{\mathbb{S}^2}$ . We construct a smooth, non-isotropic potential  $U(\mathbf{z})$  using a log-sum-exp mixture of two von-Mises–Fisher-like modes:

$$U(\mathbf{z}) := -\frac{1}{\gamma} \log(w \exp(\kappa \langle \mathbf{z}, \mathbf{m}_1 \rangle) + (1-w) \exp(\kappa \langle \mathbf{z}, \mathbf{m}_2 \rangle)), \quad \mathbf{z} \in \mathbb{S}^2, \quad (70)$$

with  $\gamma = 12$ , concentration  $\kappa = 12$ , and mixture weight  $w = 0.5$ . The modes are centered at  $\mathbf{m}_1 = (0, 0, 1)$  and a separated direction  $\mathbf{m}_2 = (0.85, 0.15, -0.50)/\|(0.85, 0.15, -0.50)\|$ , creating two distinct low-energy basins (Fig. 3, left).

**Particle training objective (intrinsic functional surrogate).** To emulate minimization of  $\mathcal{F}_{\tau,U}(\rho) = \frac{1}{\tau} \int U \rho \, d\mu - H(\rho)$  (Def. 3.3) without committing to a parametric encoder, we represent  $\rho$  by  $M$  particles  $\{\mathbf{z}_i\}_{i=1}^M \subset \mathbb{S}^2$  and optimize a standard particle/KDE surrogate. We parameterize unconstrained variables  $\{\mathbf{v}_i\}_{i=1}^M \subset \mathbb{R}^3$  and project to the sphere  $\mathbf{z}_i = \mathbf{v}_i / \|\mathbf{v}_i\|$  at each iteration. We approximate the density at particle locations by a wrapped Gaussian kernel on the sphere,

$$\hat{\rho}_h(\mathbf{z}_i) := \frac{1}{M} \sum_{j=1}^M \exp\left(-\frac{d_{\mathbb{S}^2}(\mathbf{z}_i, \mathbf{z}_j)^2}{2h^2}\right), \quad (71)$$

with bandwidth  $h = 0.35$ . The optimized objective is the particle approximation

$$\hat{\mathcal{F}}_{\tau,U}(\{\mathbf{z}_i\}) := \frac{1}{\tau} \cdot \frac{1}{M} \sum_{i=1}^M U(\mathbf{z}_i) + \frac{1}{M} \sum_{i=1}^M \log \hat{\rho}_h(\mathbf{z}_i), \quad (72)$$

where the second term is the usual KDE-based surrogate for  $-H(\rho)$  up to an additive constant. We minimize (72) using Adam (Kingma & Ba, 2015) for 5000 steps with learning rate  $5 \times 10^{-2}$ , while injecting Gaussian noise sampled from  $\mathcal{N}(\mathbf{0}, \sigma^2 \mathbf{I})$  with  $\sigma = 0.06$  at each iteration. This injection approximates a Langevin diffusion process (Welling & Teh, 2011), ensuring that the particles maintain active exploration of the energy landscape to escape shallow local traps, while the gradient of the entropy term drives the global dispersion.

**Temperatures and Gibbs baseline.** We sweep  $\tau \in \{10, 5.0, 2.5, 1.0, 0.5, 0.2, 0.1\}$  and run 20 seeds. As a reference, we estimate the Gibbs equilibrium  $\rho_{\tau}^*(\mathbf{z}) \propto \exp(-U(\mathbf{z})/\tau)$  (Prop. 3.2) by importance sampling: we draw  $n_{\text{mc}} = 120,000$  uniform points on  $\mathbb{S}^2$ , weight by  $\exp(-U/\tau)$ , and compute weighted expectations. For visualization, we use a separate pool of 24,000 uniform points and perform weighted sampling without replacement to draw 2400 Gibbs points per  $\tau$ .

**Evaluation metric.** To quantify low- $\tau$  concentration, we report the *cap mass* within geodesic radius  $\varepsilon = 0.50$  around either potential well:  $\text{CapMass}_{\varepsilon}(\rho) := (\rho \mu)(\mathcal{C}_{\varepsilon}(\mathbf{m}_1) \cup \mathcal{C}_{\varepsilon}(\mathbf{m}_2))$ , where  $\mathcal{C}_{\varepsilon}(\mathbf{m}) := \{\mathbf{z} \in \mathbb{S}^2 : d_{\mathbb{S}^2}(\mathbf{z}, \mathbf{m}) \leq \varepsilon\}$ . For the trained particles, this is simply the fraction of particles whose distance to  $\{\mathbf{m}_1, \mathbf{m}_2\}$  is at most  $\varepsilon$ . For the Gibbs baseline, we compute the same quantity as a weighted Monte Carlo estimate. We report mean  $\pm$  std over the 20 seeds.

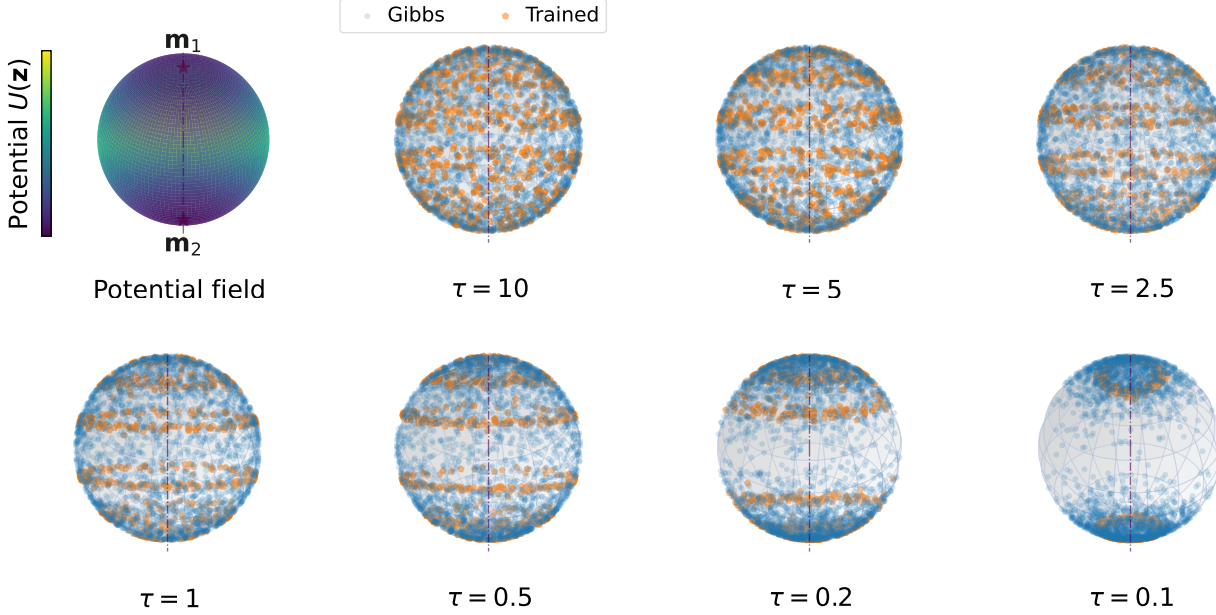


**Figure 3. Unimodal potential landscape on  $\mathbb{S}^2$  and equilibria across temperature  $\tau$ .** Left: the two-well potential  $U$  in Eq. (70) (colored by value), with minima centers  $\mathbf{m}_1, \mathbf{m}_2$  marked. Right: Gibbs samples (blue; importance-resampled) and trained particles (orange; minimizing Eq. (72)) across various temperatures. As  $\tau$  decreases, both distributions concentrate around the low-energy wells.

**Results.** Fig. 3 visualizes the potential landscape and the learned equilibria across temperatures. At high temperature (e.g.,  $\tau = 10$ ), both the Gibbs samples and the trained particles spread broadly over the sphere: the entropy term in  $\mathcal{F}_{\tau, U}$  is comparatively strong, producing a diffuse equilibrium consistent with the ‘‘entropic expansion’’ force in Rem. 3.6. As  $\tau$  decreases (e.g.,  $\tau = 0.2, \tau = 0.1$ ), the potential term  $\frac{1}{\tau} \int U \rho d\mu$  dominates and both distributions increasingly concentrate near the two low-energy basins. Notably, the trained particles exhibit semi-regular lattice-like bands, in contrast to the purely random scatter of the Gibbs samples. This micro-structure is an intrinsic consequence of the optimization: the KDE entropy term induces a repulsive force between particles, causing them to self-organize into low-discrepancy packing configurations to maximize mutual separation. This behavior is a known feature of particle-based variational inference, where it effectively yields a variance-reduced discretization of the target density (Liu & Wang, 2016). Crucially, this microscopic regularity does not violate the macroscopic prediction: at  $\tau = 0.1$ , the global mass is visibly localized around the wells, matching the qualitative prediction of ground-state concentration (Prop. 3.3).

This trend is quantified in Fig. 4: the cap mass  $\text{CapMass}_\varepsilon(\rho)$  increases as  $\tau$  decreases for both the Gibbs baseline and the trained particles. The trained curve closely tracks the trend, with small deviations attributable to finite particle count  $M$ , finite optimization time, and the fixed KDE bandwidth  $h$  which imposes a smoothing scale on the entropy surrogate. Overall, the experiment supports the intrinsic unimodal message: minimizing the free-energy functional produces a unique Gibbs-type equilibrium at each  $\tau$ , and the equilibrium exhibits systematic low-temperature concentration near minimizers of  $U$ , thereby validating the mechanistic picture used to analyze the unimodal parametric energy in § 3.

### D.3. Multimodal Structural Gap under Controlled Misalignment

This experiment provides a controlled empirical validation of the *multimodal* mechanism developed in § 4, grounded in the well-documented *modality gap* phenomenon observed in CLIP-style training (Liang et al., 2022). Our theory explains this gap as an objective-induced geometric necessity: although symmetric multimodal InfoNCE admits a stable large-batch

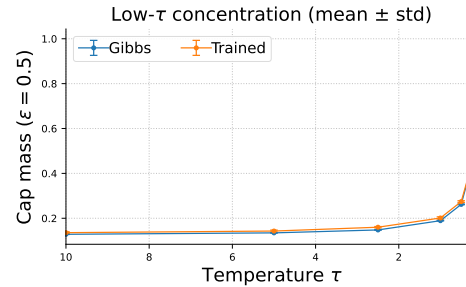


**Figure 4. Low- $\tau$  concentration on  $\mathbb{S}^2$  (mean  $\pm$  std over 20 seeds).** Cap mass  $\text{CapMass}_\varepsilon$  with  $\varepsilon = 0.50$  around potential wells  $\{\mathbf{m}_1, \mathbf{m}_2\}$  increases as  $\tau$  decreases, quantifying the ground-state trend.

deterministic limit, its intrinsic landscape is inherently *cross-coupled*, with equilibrium determined by the interplay of two directional alignment fields. When the two modalities exhibit heterogeneous conditional laws—arising from noise, distinct semantic density, or mismatched semantic structure—these fields generically fail to share a common potential, yielding a persistent negative symmetric divergence. We test this mechanism in a controlled setting by showing that exact marginal matching is a *knife-edge* condition: even mild, structured misalignment introduces a structural wedge that forces the population-level marginals apart.

**Latent variables and paired observations.** We generate paired observations from a shared latent angle  $\theta \in (-\pi, \pi]$ . To strictly rule out the trivial solution where marginals are uniform (and thus trivially match regardless of noise), we sample  $\theta$  from a *non-uniform* (multi-peaked) mixture of von Mises–Fisher distributions:

$$\theta \sim w \text{vM}(\mu_1, k) + (1 - w) \text{vM}(\mu_2, k), \quad (w = 0.7, \mu_1 = 0, \mu_2 = \pi, k = 6).$$

Modality 1 observes  $\theta$  directly, while Modality 2 observes a *misaligned* latent  $\theta_2 := \text{wrap}(\theta + \eta)$  with  $\eta \sim \mathcal{N}(0, \sigma_{\text{mis}}^2)$ . Given an angle  $\alpha$ , the raw observation is a noisy point on the unit circle:

$$\mathbf{x}(\alpha) := [\cos \alpha, \sin \alpha]^\top + \boldsymbol{\xi}, \quad \boldsymbol{\xi} \sim \mathcal{N}(\mathbf{0}, \sigma_{\text{obs}}^2 \mathbf{I}), \quad \sigma_{\text{obs}} = 0.02.$$

Thus, increasing  $\sigma_{\text{mis}}$  continuously increases the *cross-modal conditional mismatch* while keeping the marginal complexity of both modalities comparable.

**Encoders, objective, and protocol.** We use linear encoders  $f, g : \mathbb{R}^2 \rightarrow \mathbb{R}^2$  (bias-free) and project outputs to the unit circle:

$$\tilde{\mathbf{z}}_1 = f(\mathbf{x}_1), \quad \tilde{\mathbf{z}}_2 = g(\mathbf{x}_2), \quad \mathbf{z}_1 = \frac{\tilde{\mathbf{z}}_1}{\|\tilde{\mathbf{z}}_1\|}, \quad \mathbf{z}_2 = \frac{\tilde{\mathbf{z}}_2}{\|\tilde{\mathbf{z}}_2\|} \in \mathbb{S}^1.$$

We adopt the cosine critic and exponential kernel:

$$s(\mathbf{z}, \mathbf{w}) = \langle \mathbf{z}, \mathbf{w} \rangle, \quad \kappa_\tau(\mathbf{z}, \mathbf{w}) = \exp(s(\mathbf{z}, \mathbf{w})/\tau), \quad \tau = 0.07,$$

matching the CLIP-style symmetric objective analyzed in the multimodal analysis. Training uses the symmetric CLIP loss

$$\mathcal{L}_{\text{CLIP}}(f, g) = \frac{1}{2} (\text{CE}(S/\tau, \text{diag}) + \text{CE}(S^\top/\tau, \text{diag})), \quad \text{with } S_{ij} := \langle z_{1,i}, z_{2,j} \rangle,$$

where  $\text{CE}(\cdot, \cdot)$  is the cross-entropy loss. using Adam with learning rate  $5 \times 10^{-3}$  for 2000 steps and batch size as 256. We sweep eight misalignment scales  $\sigma_{\text{mis}} \in \{0, 0.1, 0.2, 0.3, 0.4, 0.5, 0.6, 0.7\}$ ; larger scales induce progressively more severe cross-modal misalignment, yet all settings retain a meaningful statistical dependence between positive pairs. For each  $\sigma_{\text{mis}}$ , we repeat training over 20 random seeds (seeds 0–19). The large batch size makes the training dynamics closer to the large-batch deterministic regime in Thm. 4.1, whose proof follows the same Monte-Carlo concentration logic as the asymmetric case but applied to the bidirectional symmetric normalization.

**Evaluation metrics.** After training, we evaluate on  $n_{\text{eval}} = 8000$  fresh paired samples and compute the embedding angles  $a_1 = \text{atan}2(z_{1,y}, z_{1,x})$  and  $a_2 = \text{atan}2(z_{2,y}, z_{2,x})$  from the unit-normalized representations  $\mathbf{z}_1, \mathbf{z}_2 \in \mathbb{S}^1$ . The following visual diagnostics are considered:

(i) *Marginal gap.* We discretize  $a_1$  and  $a_2$  into 60 bins on  $(-\pi, \pi]$  and estimate the two empirical angle marginals  $\hat{q}_\theta$  and  $\hat{q}_\phi$ . As a scalar summary of marginal mismatch, we report the symmetric KL divergence

$$D_{\text{KL}}^{\text{sym}}(\hat{q}_\theta, \hat{q}_\phi) := D_{\text{KL}}(\hat{q}_\theta \parallel \hat{q}_\phi) + D_{\text{KL}}(\hat{q}_\phi \parallel \hat{q}_\theta),$$

averaged over 20 random seeds (seeds 0–19), with error bars (shadow areas) showing  $\pm$  standard error (the *gap curve*).

(ii) *Polar marginals.* To visualize *where* the mismatch occurs on the circle, we plot the two estimated angle marginals as polar density curves for each misalignment scale  $\sigma_{\text{mis}}$ .

(iii) *Joint-angle heatmaps.* To visualize the learned *cross-modal coupling* (beyond marginals), we plot a 2D histogram of the joint distribution of  $(a_1, a_2)$ . Diagonal concentration indicates near-deterministic alignment  $a_2 \approx a_1$ ; off-diagonal spread indicates systematic cross-modal mismatch.

(iv) *Angle-shift density.* Finally, we compute the wrapped angular difference  $\Delta a := \text{wrap}(a_2 - a_1) \in (-\pi, \pi]$  and plot its empirical density. This directly measures the distribution of residual misalignment in embedding space.

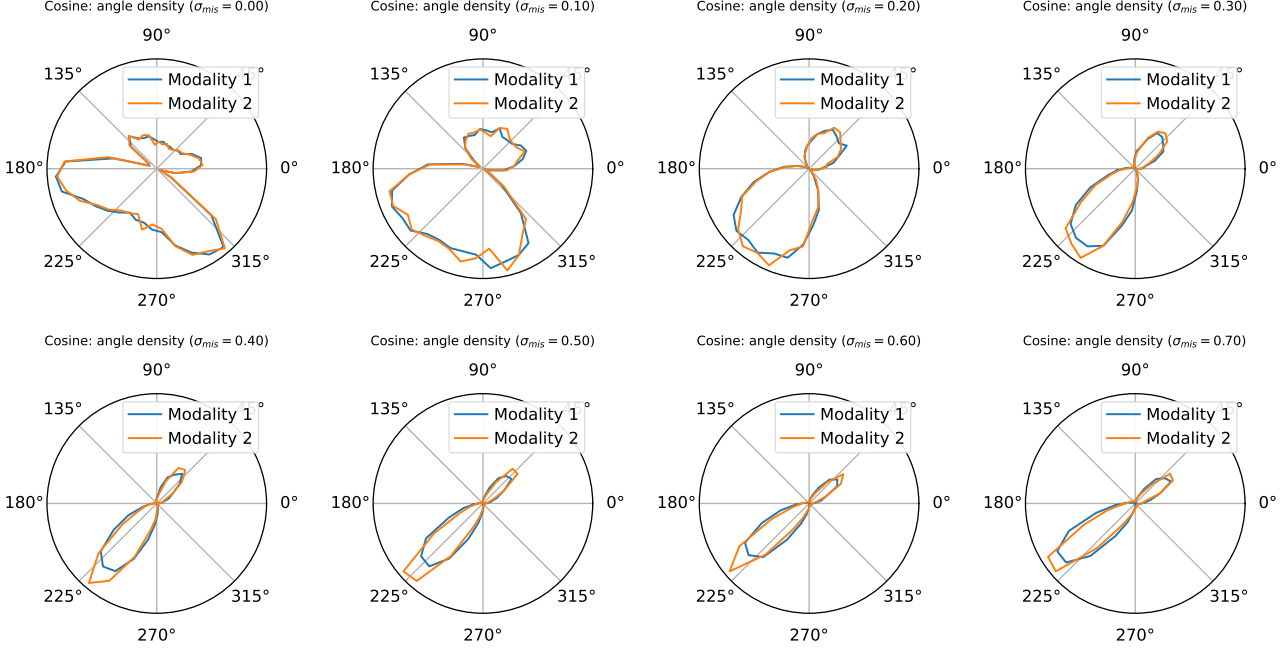


**Figure 6. Polar angle marginals across misalignment.** Estimated angle marginals of the two modalities on  $S^1$  (polar density plots). The mismatch becomes visually apparent for  $\sigma_{\text{mis}} > 0$  and grows with  $\sigma_{\text{mis}}$ .

**Results.** Fig. 5 shows that the marginal discrepancy  $D_{\text{KL}}^{\text{sym}}(\hat{q}_\theta, \hat{q}_\phi)$  increases as the latent misalignment scale  $\sigma_{\text{mis}}$  grows. Since the encoder architecture, critic function, and optimization protocol remain fixed across all runs, this result isolates the conditional mismatch  $\sigma_{\text{mis}}$  as the primary driver of the gap. It confirms that as the two modalities become less conditionally compatible, the symmetric InfoNCE objective is forced to sacrifice marginal alignment, inducing a persistent modality separation that cannot be resolved by optimization alone.

The polar marginals in Fig. 6 provide a structural view of *how* this separation manifests geometrically. First, across all settings ( $\sigma_{\text{mis}} \geq 0$ ), the learned angular marginals are clearly *multi-peaked* rather than uniform. The density concentrates in specific angular regions, reflecting the underlying non-uniform latent law (a two-component von Mises–Fisher mixture) and confirming that the encoders successfully recover the latent structure up to a global rotation. Second, the evolution of these peaks reveals the gap mechanism. At  $\sigma_{\text{mis}} = 0$ , the polar curves for the two modalities nearly overlap, consistent with a compatible pairing law where symmetric InfoNCE can simultaneously achieve alignment and marginal coincidence. However, for any  $\sigma_{\text{mis}} > 0$ , the curves begin to diverge within the same modal regions: the peaks shift relative to each other and their probability masses differ. This mismatch becomes visually more pronounced as  $\sigma_{\text{mis}}$  increases, tracking the quantitative rise in the gap curve.

The joint-angle heatmaps in Fig. 7 elucidate the mechanism behind this separation. At  $\sigma_{\text{mis}} = 0$ , probability mass concentrates sharply along the diagonal  $a_2 \approx a_1$ , indicating a near-deterministic coupling. Because the latent distribution is bimodal, this diagonal concentration is not uniform but forms distinct “bright spots” (high-density clusters) corresponding to the latent modes. As  $\sigma_{\text{mis}}$  increases, these clusters persist—indicating the model still captures the coarse latent semantics—but they deform into thickened, elongated ellipses. The diagonal band broadens significantly, reflecting that the conditional law of  $a_2$  given  $a_1$  has become intrinsically noisy. Crucially, this is not merely a symmetric “blur” around the diagonal; the deformation is accompanied by the shifts in marginal occupancy observed in Fig. 6. This confirms that under the symmetric objective, broadening conditional alignment structurally necessitates a shift in the marginal supports.

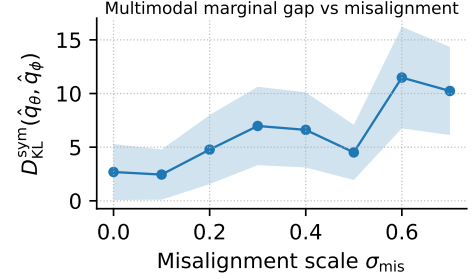


**Figure 5. Marginal gap vs. misalignment (mean  $\pm$  standard error).** Symmetric KL divergence  $D_{\text{KL}}^{\text{sym}}$  increases as latent misalignment  $\sigma_{\text{mis}}$  grows.

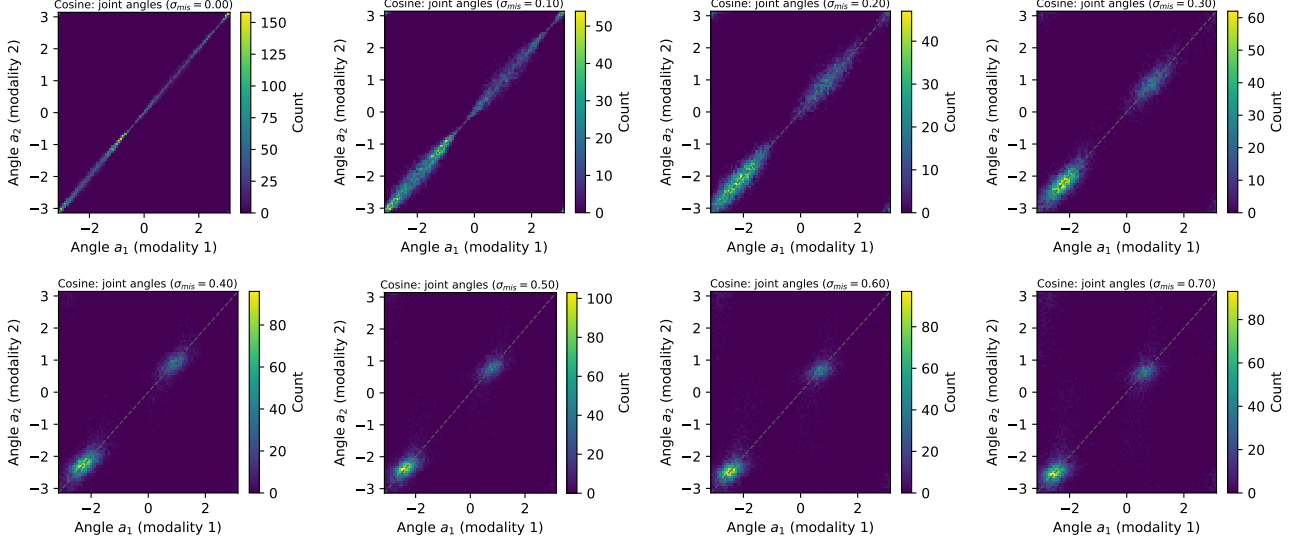


**Figure 7. Joint-angle coupling across misalignment.** 2D histograms of  $(a_1, a_2)$  from  $\sigma_{\text{mis}} = 0.0$  to  $\sigma_{\text{mis}} = 0.7$ . Diagonal concentration (small  $\sigma_{\text{mis}}$ ) indicates near-deterministic alignment; increasing off-diagonal spread (large  $\sigma_{\text{mis}}$ ) indicates intrinsically noisy coupling.

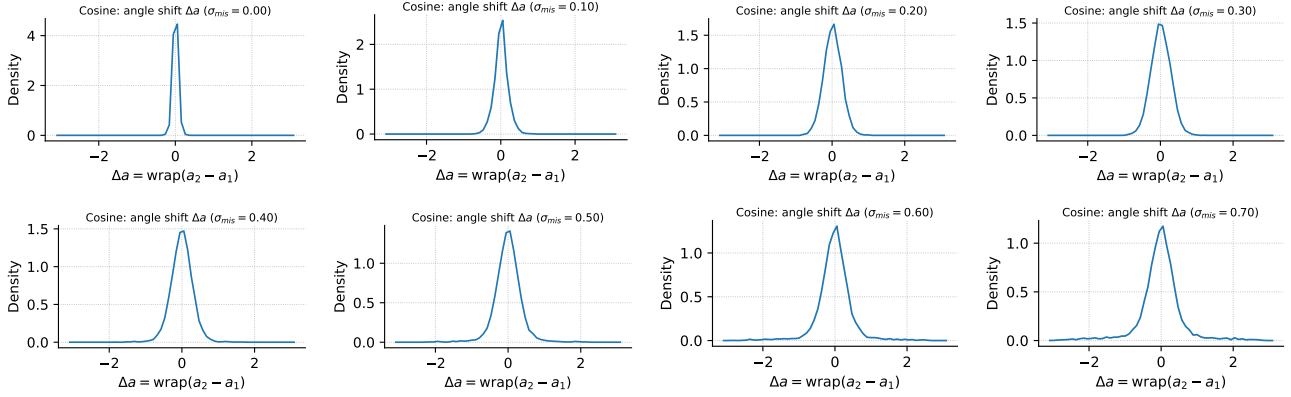


**Figure 8. Residual embedding-space misalignment.** Densities of  $\Delta a = \text{wrap}(a_2 - a_1)$  from  $\sigma_{\text{mis}} = 0.0$  to  $\sigma_{\text{mis}} = 0.7$ . The distribution broadens as  $\sigma_{\text{mis}}$  increases, indicating larger and more variable residual misalignment in representation space.

Finally, the angle-shift densities in Fig. 8 quantify the residual embedding misalignment  $\Delta a = \text{wrap}(a_2 - a_1)$ . As  $\sigma_{\text{mis}}$  increases, the distribution of  $\Delta a$  transitions from a sharp peak at zero to a progressively wider distribution with heavy tails. The residual shift becomes both larger in magnitude and more variable, matching the signature expected from the injection of additive latent noise  $\eta \sim \mathcal{N}(0, \sigma_{\text{mis}}^2)$ .

In summary, these empirical patterns provide direct validation for the multimodal mechanism characterized in Thm. 4.2. Our theoretical analysis posits that the symmetric objective is composed of two directional alignment fields that are coupled via the marginals. In this experiment, the controlled perturbation  $\theta_2 = \text{wrap}(\theta + \eta)$  creates heterogeneous conditional laws: the optimal alignment from Modality 1 to 2 is not the inverse of the alignment from Modality 2 to 1. Consequently, the two directions of the symmetric objective do not share a single potential function. Empirically, this manifests as a “tug-of-war” between the two modalities. *Intrinsically noisy coupling*: the broadening diagonal band in Fig. 7 reflects the necessary rise in conditional entropy due to the mismatched conditionals. *Structural modality gap*: the widening marginal separation in Fig. 5 and Fig. 6 matches our prediction that marginal coincidence is a knife-edge property and becomes unstable once misalignment is introduced. Together, these observations show that the population-level gap is not a finite-sample artifact or a symptom of under-training, but a consequence of the objective’s geometry: when the knife-edge pairwise compatibility is violated (here, for any  $\sigma_{\text{mis}} > 0$ ), the symmetric InfoNCE equilibrium cannot maintain identical marginals.

## E. Broader Implications and Discussion

A recurring lesson from the history of contrastive learning theory is that pointwise similarity is an incomplete proxy for the objective being optimized. Early analyses emphasized geometric regularities, such as alignment and the spread of the induced feature distribution on the hypersphere (Wang & Isola, 2020). Our measure-theoretic viewpoint extends this further: in the large-batch regime, training dynamics are governed by induced *fields* and *landscapes* over  $\mathcal{Z}$ , acting directly on the laws of the learned representations. As a result, two models may exhibit strong pointwise alignment (e.g., high retrieval accuracy) while maintaining persistent population-level discrepancies between modalities, consistent with the modality-gap phenomenon observed in CLIP-like systems (Liang et al., 2022; Shi et al., 2023).

This shift suggests that evaluation and debugging should treat population geometry as a first-class concern. Concretely, in addition to retrieval metrics, one can report distributional diagnostics that capture global mismatches: symmetric divergences (when densities are well-defined), as well as sample-based two-sample measures such as kernel two-sample tests (Gretton et al., 2012) or energy statistics (Székely & Rizzo, 2013). These metrics belong to the broader family of integral probability metrics (IPMs), which quantify distributional discrepancies via function classes and thus offer a principled suite of geometry-aware probes (Sriperumbudur et al., 2009). In practice, such diagnostics can be complemented with representation-comparison tools designed to assess feature geometry across runs or components, beyond marginal distributional similarity (Kornblith et al., 2019).

Our multimodal decomposition further yields a concrete, testable prediction: interventions that improve pointwise matching without reshaping the induced fields over  $\mathcal{Z}$  need not reduce population-level mismatch. Specifically, we predict that (i) retrieval performance can improve even as a gap proxy (e.g.,  $D_S(q_\theta, q_\phi)$ ) remains essentially unchanged; and (ii) mechanisms that explicitly attenuate the  $\log q$  barriers in the lifted landscape should reduce boundary-seeking co-adaptation, even when retrieval performance is held constant. These hypotheses can be evaluated using lightweight diagnostics over held-out embeddings, and they clarify why “closing the gap” can interact non-trivially with other desiderata, such as representational spread and downstream transferability.

From the standpoint of objective design, the key takeaway is to regularize *geometry*, not just similarity. Since each modality enters the other’s effective field via population terms, mitigating extremal dynamics requires shaping the induced functional itself. This may involve directly penalizing population mismatch (e.g., by adding  $D_S$  or an IPM-style discrepancy term), replacing cross-entropy against the other modality’s KDE with a shared reference field (e.g., barycentric or tempered mixtures), or modifying the loss to convexify the induced landscape and suppress boundary solutions. The appropriate evaluation criterion for such interventions is not merely pairwise similarity, but the extent to which they reshape the induced fields over  $\mathcal{Z}$ , as revealed by the diagnostics discussed above.

A related implication is that directionality is structural in heterogeneous modalities. Prior studies have already shown that modality-gap dynamics depend on initialization, temperature, and training dynamics (Liang et al., 2022; Shi et al., 2023). Our framework explains why, beyond these factors, the two disintegrations of  $\pi_{\theta\phi}$  generically induce distinct directional potentials. Treating multimodal alignment as governed by a single shared potential therefore implicitly assumes symmetry in the conditional structure, a condition that is rarely satisfied in real-world data. Practically, this implies that architectures, temperature schedules, and negative sampling strategies should be evaluated direction-by-direction, rather than via a single aggregated alignment metric. This perspective also clarifies the role of data curation: it influences not only marginal noise but also the conditional laws that define the optimization fields. Underspecification, many-to-many pairing, and systematic annotation artifacts reshape  $U_{\theta+\phi}$  and  $U_{\phi+\theta}$ , the fields that guide optimization, and thereby account for performance differences that are not captured by pointwise metrics alone.

Finally, the scope and limitations of our analysis warrant emphasis. Our conclusions are sharpest in the large-batch, compact-kernel regime, where the induced energies are well-approximated and density-based diagnostics are meaningful. Extending this analysis to settings involving heterogeneous volumes, unnormalized spaces, or singular and boundary-supported measures remains an important direction for future work. More broadly, this separation of concerns delineates a clean interface with identifiability: while the objective determines the geometry (i.e., the fields and landscapes over  $\mathcal{Z}$ ), establishing whether this geometry reflects meaningful latent structure requires further assumptions—typically about the generative process, the data distribution, or structural constraints on the model.